ERDC/GSL TR-06-15

Geotechnical and Structures Laboratory

US Army Corps of Engineers®
Engineer Research and Development Center

Laboratory Characterization of SAM-35 Concrete

Erin M. Williams, Stephen A. Akers, and Paul A. Reed

September 2006

ERDC/GSL TR-06-15
September 2006

Laboratory Characterization of SAM-35 Concrete

Erin M. Williams, Stephen A. Akers, and Paul A. Reed

Geotechnical and Structures Laboratory
U.S. Army Engineer Research and Development Center
3909 Halls Ferry Road
Vicksburg, MS 39180-6199

Final report

Approved for public release; distribution is unlimited

Prepared for Headquarters, U.S. Army Corps of Engineers
Washington, DC 20314-1000

Under Work Unit AT40-SA-006, Dynamic Behavior of Urban Materials

ABSTRACT: Personnel of the Geotechnical and Structures Laboratory, U.S. Army Engineer Research and Development Center, conducted a laboratory investigation to characterize the strength and constitutive property behavior of a SAM-35 concrete. Forty-four mechanical property tests consisting of two hydrostatic compression tests, four unconfined compression (UC) tests, 18 triaxial compression (TXC) tests, two uniaxial strain tests, four uniaxial strain load/biaxial unload (UX/BX) tests, three uniaxial strain load/constant volume tests, two uniaxial strain load/constant strain ratio tests, five direct pull (DP) tests, and four reduced triaxial extension (RTE) tests were successfully completed. In addition to the mechanical property tests, nondestructive pulse-velocity measurements were performed on each specimen. The TXC tests exhibited a continuous increase in principal stress difference with increasing confining stress. A recommended compression failure surface was developed from the TXC and UC test results. Test data from the RTE and DP tests were used to develop a recommended extension failure surface for SAM-35. Results from the stress paths of the strain path tests and the recommended compression failure surface exhibited good agreement except for the UX/BX tests.

Contents

List of Figures

Preface

This laboratory mechanical property investigation of SAM-35 concrete was conducted by personnel of the U.S. Army Engineer Research and Development Center (ERDC). The study was conducted with funds provided by the Directorate of Military Programs, Headquarters, U.S. Army Corps of Engineers, under the Research, Development, Test, and Evaluation (RDT&E) Program. The investigation reported herein was accomplished under the Military RDT&E Work Package AT40, Scalable and Adaptable Lethality Versus Personnel, Platforms, and Structures; Work Unit AT40-SA-006, Dynamic Behavior of Urban Materials.

This study was conducted during March 2003 to August 2003 by staff members of the Impact and Explosion Effects Branch (IEEB), Engineering Systems and Materials Division (ESMD), Geotechnical and Structures Laboratory (GSL), ERDC, under the general direction of Henry S. McDevitt, Jr., Chief, IEEB; Dr. Albert J. Bush III, Chief, ESMD; Dr. William P. Grogan, Deputy Director, GSL; and Dr. David W. Pittman, Director, GSL.

The Principal Investigator for this project was Dr. Stephen A. Akers, IEEB. Material property data were processed by Erin M. Williams, IEEB, Co-Investigator for this project. The laboratory characterization tests were performed by Paul A. Reed, IEEB, under the technical direction of Dr. Akers. Instrumentation support was provided by A. Leroy Peeples, formerly of the Data Acquisition and Integration Branch, Engineering and Informatic Systems Division, Information Technology Laboratory, ERDC. The SAM-35 material was designed and developed by Brian H. Green and coworkers in the Concrete and Materials Branch, ESMD, GSL. This report was prepared by Ms. Williams, under the direction of Dr. Akers.

COL Richard B. Jenkins was Commander and Executive Director of ERDC. Dr. James R. Houston was Director.

1 Introduction

Background

Personnel of the Geotechnical and Structures Laboratory, U.S. Army Engineer Research and Development Center, at the Waterways Experiment Station (WES) conducted a laboratory investigation to characterize the strength and constitutive property behavior of SAM-35 concrete for the Dynamic Behavior of Urban Materials Work Unit of the AT40-SA-006 Scalable and Adaptable Lethality Versus Personnel, Platforms, and Structures Work Package. WES personnel conducted a total of 45 mechanical property tests of which 44 were successfully completed. The 44 successfully completed mechanical property tests consisted of two hydrostatic compression tests, four unconfined compression tests, 18 triaxial compression tests, two uniaxial strain tests, four uniaxial strain/biaxial unloading tests, three uniaxial strain/constant volume tests, two uniaxial strain/constant strain ratio tests, five direct-pull tests, and four reduced triaxial extension tests. In addition to the mechanical property tests, nondestructive pulse-velocity measurements were performed on each specimen.

Purpose and Scope

The primary purpose of this report is to document the results from the laboratory mechanical property tests conducted on the SAM-35 specimens. In addition, results from the nondestructive pulse-velocity measurements are documented. The physical and composition properties, test procedures, and test results are documented in Chapter 2. Comparative plots and analyses of the experimental results are presented in Chapter 3. A summary is provided in Chapter 4.

2 Laboratory Tests

Material Description

The test specimens used in this investigation were cut from samples cored from discs of SAM-35 concrete. The discs were cast during the placement of SAM-35 for projectile penetration targets. The form used to cast each disc was a section of a 55-gal drum. Typically, each section of core was of sufficient length to obtain two test specimens. Table 1 (presented at the end of this chapter) displays the mix design for SAM-35. Additional details are documented in the "Specimen preparation" section of this chapter.

Composition Property Tests

Prior to performing the mechanical property tests, the height, diameter, and mass of each test specimen were determined. These measurements were used to compute the specimen's wet, bulk, or "as-tested" density. Results from these determinations are provided in Table 2. Measurements of posttest water content[1] were conducted in accordance with procedures given in American Society for Testing and Materials (ASTM) D 2216 (ASTM 2002e). Based on the appropriate values of posttest water content, wet density, and an assumed grain density of 2.7 Mg/m^3, values of dry density, porosity, degree of saturation, and volumes of air, water, and solids were calculated (Table 2). Also listed in the table are maximum, minimum, and mean values and the standard deviation about the mean for each quantity. The SAM-35 specimens had a mean wet density of 2.163 Mg/m^3, a mean water content of 3.39 percent, and a mean dry density of 2.092 Mg/m^3 based on data from 44 specimens.

Ultrasonic Pulse-Velocity Determinations

Prior to performing a mechanical property test, ultrasonic pulse-velocity measurements were collected on each test specimen. This involved measuring the transit distance and time for each P (compressional) or S (shear) pulse to propagate through a given specimen. The velocity was then computed by dividing the transit distance by the transit time. A matching pair of 1-MHz

[1] Water content is defined as the mass of water removed during drying in a standard oven divided by the mass of dry solids.

piezoelectric transducers was used to transmit and receive the ultrasonic P waves. A pair of 2.25-MHz piezoelectric transducers was used to transmit and receive the ultrasonic S waves. The transit time was measured with a 100-MHz digital oscilloscope and the transit distance with a digital micrometer. All of these wave-velocity determinations were made under atmospheric conditions; i.e., no prestress of any kind was applied to the specimens. The tests were conducted in accordance with procedures given in ASTM C 597 (ASTM 2002c).

One compressional-wave (P-wave) and one shear-wave (S-wave) velocity were determined axially through each specimen. Six radial P-wave velocities were determined, i.e., two transverse to each other at elevations of one-quarter, one-half, and three-quarters of the specimen height. Two radial S-wave velocities were measured; both of these determinations were made at the mid-height of the specimen, transverse to each other. The various P- and S-wave velocities determined for the test specimens are provided in Table 2; the radial velocities listed in Table 2 are the average values.

Mechanical Property Tests

Forty-four mechanical property tests were successfully performed on the SAM-35 specimens to characterize the strength and composition properties of the material. All of the mechanical property tests were conducted quasi-statically with axial strain rates on the order of 10^{-4} to 10^{-5} per second and times to peak load on the order of 5 to 30 min. Mechanical property data were obtained from several different stress and strain paths. Undrained bulk compressibility data were obtained during the hydrostatic loading phase of the triaxial compression (TXC) tests and from two hydrostatic compression (HC) tests. Shear and failure data were obtained from unconfined compression (UC) tests, unconsolidated-undrained TXC tests, direct-pull (DP) tests, and unconsolidated-undrained reduced triaxial extension (RTE) tests. One-dimensional compressibility data were obtained from undrained uniaxial strain (UX) tests with lateral stress measurements, or K_o tests. Three types of undrained strain-path tests were conducted during the test program. All of the strain-path tests were initially loaded under uniaxial strain boundary conditions to some prescribed level of stress or strain. At the end of the UX loading, constant axial to radial strain ratios (ARSR) of 0, -1.33, and -2.0 were applied. The ARSR = 0 path is a constant axial strain unloading path and produces a forced state of volumetric expansion; these tests will be referred to as UX/BX tests. The UX/SR tests had an ARSR = -1.33, which produced a path that has a constant strain ratio when loaded. The ARSR = -2.0 path is a constant volume strain loading path, and these paths will be referred to as UX/CV tests. The terms undrained and unconsolidated signify that no pore fluid (liquid or gas) was allowed to escape or drain from the membrane-enclosed specimens. The completed test matrix is presented in Table 3, which lists the types of tests conducted, the number of tests, the test numbers for each group, the test numbers of the specimens that had cyclic loading, and the nominal peak radial stress applied to specimens prior to shear loading or during the HC, UX, or strain-path loading.

Specimen preparation

The mechanical-property test specimens were cut from sections of SAM-35 that were obtained using a diamond-bit core barrel by following the procedures provided in ASTM C 42 (ASTM 2002b). The ends of all test specimens were cut to the correct length and then ground flat and parallel to each other and perpendicular to the sides of the core in accordance with procedures in ASTM D 4543 (ASTM 2002f). Prior to testing, the prepared specimens were measured for height, diameter, and mass and were ultrasonically pulsed. This information was used to calculate the composition properties and wave velocities of the specimens. The prepared test specimens had a nominal height of 110 mm and a diameter of 50 mm.

Prior to testing, each specimen was placed between hardened steel top and base caps. With the exception of the unconfined compression (UC) and the direct-pull (DP) test specimens, two 0.6-mm-thick synthetic latex membranes and an Aquaseal® membrane were placed around the specimen, and the exterior of the outside membrane was coated with a liquid synthetic rubber to inhibit deterioration caused by the confining-pressure fluid (Figure 1). The fluid was a mixture of kerosene and hydraulic oil. Finally, the specimen, along with its top cap and base cap assembly, was placed on the instrumentation stand of the test apparatus, and the instrumentation setup was initiated.

Test devices

Four different sets of test devices were used in this test program. The axial load for all of the UC tests was provided by a 3.3-MN (750,000-lb, force) loading machine. The application of load was manually controlled with this test device. No pressure vessel was required for the UC tests; only a base, load cell, and vertical and radial deformeters were necessary.

Direct-pull tests were performed by using the direct-pull apparatus, in which end caps were attached to the specimens with a high-modulus high-strength epoxy. A manual hydraulic pump was used to pressurize the direct-pull chamber. When the direct-pull chamber was pressurized, a piston rose and produced tensile loading on the test specimen. Measurements for the tensile loading of the specimen were recorded with an 89-kN load cell.

To perform an RTE test, a static high-pressure triaxial test device (HPTX) was used (Figure 2). This device was manually controlled and can be pressurized up to 100 MPa. The pumping equipment that was used during the operation of this device limited the peak pressure that was achieved to 70 MPa. When the triaxial extension top cap was used with the HPTX device, independent control of the vertical and lateral stresses was permitted. The specimen top cap was bolted to the extension loading piston, and the surface on top of the piston was pressurized. During an RTE test, the confining pressure (or radial stress) was kept constant while the vertical stress was reduced (Akers et al. 1986).

All of the remaining tests were conducted in a 600-MPa-capacity pressure vessel, and the axial load was provided by an 8.9-MN (2 million-lb, force) loader. With the 8.9-MN loader, the application of load, pressure, and axial displacement was regulated by a servo-controlled data acquisition system. This servo-controlled system allowed the user to program rates of load, pressure, and

axial displacement in order to achieve the desired stress or strain path. Confining pressure was measured external to the pressure vessel by a pressure transducer mounted in the confining fluid line. A load cell mounted in the base of the specimen pedestal was used to measure the applied axial loads inside the pressure vessel (Figure 1).

Outputs from the various instrumentation sensors were electronically amplified and filtered, and the conditioned signals were recorded by computer-controlled 16-bit analog-to-digital converters. The data acquisition systems were programmed to sample the data channels every 1 to 5 sec. They converted the measured voltages to engineering units and stored the data for further posttest processing.

Test instrumentation

The vertical deflection measurement system in all the test areas except the DP test area consisted of two linear variable differential transformers (LVDTs) mounted vertically on the instrumentation stands and positioned 180 deg apart. They were oriented to measure the displacement between the top and base caps, thus providing a measure of the axial deformations of the specimen. For the confined tests, a linear potentiometer was mounted external to the pressure vessel so as to measure the displacement of the piston through which axial loads were applied. This provided a backup to the vertical LVDTs in case they exceeded their calibrated range.

Two radial deflection measurement systems were used in this test program. The output of each deformeter was calibrated to the radial displacement of the two footings that were glued to the sides of the test specimen (Figure 1). These two small steel footings were mounted 180 deg apart at the specimen's mid-height. The footing faces were machined to match the curvature of the test specimen. A threaded post extended from the outside of each footing and protruded through the membrane. The footings must be mounted to the specimen prior to placement of the membrane. Once the membranes were in place, steel caps were screwed onto the threaded posts to seal the membrane to the footing. The lateral deformeter ring is attached to these steel caps with set screws (Figure 3).

One type of lateral deformeter consisted of an LVDT mounted on a hinged ring; the LVDT measured the expansion or contraction of the ring. This lateral deformeter was used over smaller ranges of radial deformation when the greatest measurement accuracy was required. This lateral deformeter was used for all of the HC, UC, UX, and strain-path tests and for the TXC tests at confining pressures less than 50 MPa. This design is similar to the radial-deformeter design provided by Bishop and Henkel (1962). When the specimen expanded (or contracted), the hinged-deformeter ring opened up (or closed) causing a change in the electrical output of the horizontally mounted LVDT.

The second type of lateral deformeter, which was used for all of the TXC tests at confining pressures of 50 MPa and above, consisted of two strain-gauged spring-steel arms mounted on a double-hinged ring; the strain-gauged arms deflected as the ring expanded or contracted. This lateral deformeter was used when the greatest radial deformation range was required and, therefore, was less precise than the LVDT deformeter. With this deformeter, when the specimen expanded or contracted, the rigid deformeter ring flexed about its hinge causing

a change in the electrical output of the strain-gauged spring-arm. The output of the spring-arms was calibrated to the specimen's deformation. Radial measurements were not performed during the DP tests.

Test descriptions

The UC and TXC tests were performed in accordance with ASTM C 39 (ASTM 2002a) and ASTM C 801 (ASTM 2002d). A TXC test was conducted in two phases. During the first phase, the hydrostatic compression phase, the cylindrical test specimen was subjected to an increase in hydrostatic pressure while measurements of the specimen's height and diameter changes were made. The data are typically plotted as pressure versus volumetric strain, the slope of which, assuming elastic theory, is the bulk modulus, *K*. The second phase of the TXC test, the shear phase, was conducted after the desired confining pressure was applied during the HC phase. While holding the desired confining pressure constant, axial load was increased, and measurements of the changes in the specimen's height and diameter were made. The compressive axial load was increased until the specimen failed. The shear data are generally plotted as principal stress difference versus axial strain, the slope of which is Young's modulus, *E*. The maximum principal stress difference that a given specimen can support, or the principal stress difference at 15 percent axial strain during the shear loading, whichever occurs first, is defined as the peak strength.

Note that the UC test is a TXC test in which no confining pressure is applied. The maximum principal stress difference observed during a UC test is defined as the unconfined compressive strength of the material.

Extension data were obtained for SAM-35 by performing DP and RTE tests. The DP tests have no confining pressure during the tests. To conduct the DP tests, end caps were attached with epoxy to the specimen. The end caps were screwed into the direct-pull apparatus, and the specimen was pulled apart vertically when pressure was applied to the piston. The RTE tests were conducted with the HPTX device and the TXE top cap (Figure 2). To begin the RTE test, the specimen was loaded hydrostatically to a desired confining pressure. After the hydrostatic loading was applied and while the radial stress was held constant, the vertical stress was reduced until the specimen failed (Akers et al. 1986). Throughout the RTE test, the specimen's height and diameter changes were recorded. Extension shear data for the material are generally plotted as principal stress difference versus axial strain.

A UX test was conducted by simultaneously applying axial load and confining pressure so that, as the cylindrical specimen shortened, its diameter remained unchanged, i.e., zero radial strain boundary conditions were maintained. The data are generally plotted as axial stress versus axial strain, the slope of which is the constrained modulus, *M*. The data are also plotted as principal stress difference versus mean normal stress, the slope of which is twice the shear modulus *G* divided by the bulk modulus *K* , i.e., $2G/K$, or, in terms of Poisson's ratio ν , $3(1-2\nu)/(1+\nu)$.

The strain-path tests in this test program were conducted in two phases. Initially, the specimen was subjected to a uniaxial-strain loading up to a desired level of mean normal, radial, or axial stress. At the end of the UX loading, constant axial to radial strain ratios of 0, -1.33, or -2.0 were applied; these tests

were identified earlier as UX/BX, UX/SR, and UX/CV tests, respectively. To conduct these tests, the software controlling the servo-controls had to correct the measured inputs for system compressibility and for the nonlinear calibrations of specific transducers.

Definition of stresses and strains

During the mechanical property tests, measurements were typically made of the axial and radial deformations of the specimen as confining pressure and/or axial load was applied or removed. These measurements along with the pretest measurements of the initial height and diameter of the specimen were used to convert the measured test data to true stresses and engineering strains.[1]

Axial strain, ε_a, was computed by dividing the measured axial deformation, Δh (change in height), by the original height h_o, i.e., $\varepsilon_a = \Delta h/h_o$. Similarly, radial strain, ε_r, was computed by dividing the measured radial deformation, Δd (change in diameter), by the original diameter d_o, i.e., $\varepsilon_r = \Delta d/d_o$. For this report, the volumetric strain was assumed to be the sum of the axial strain and twice the radial strain, $\varepsilon_v = \varepsilon_a + 2\varepsilon_r$.

The principal stress difference q was calculated by dividing the axial load by the cross-sectional area of the specimen A, which is equal to the original cross-sectional area A_o multiplied by $(1 - \varepsilon_r)^2$. In equation form,

$$q = (\sigma_a - \sigma_r) = \frac{Axial\ Load}{A_o(1-\varepsilon_r)^2} \tag{1}$$

where σ_a is the axial stress. The axial stress is related to the confining pressure and the principal stress difference by

$$\sigma_a = q + \sigma_r \tag{2}$$

The mean normal stress, p, is the average of the applied principal stresses. In cylindrical geometry,

$$p = \frac{(\sigma_a + 2\sigma_r)}{3} \tag{3}$$

[1] Compressive stresses and strains are positive in this report.

Results

Results from all mechanical property tests, except the direct-pull tests, are presented in Plates 1-35. One data plate is presented for each test with reliable results. Results from the HC tests are presented on the plates in four plots, i.e., (a) mean normal stress versus volumetric strain, (b) mean normal stress versus axial strain, (c) radial versus axial strain, and (d) mean normal stress versus radial strain. Each plate for the UC, TXC, UX, strain-paths, and RTE tests displays four plots, i.e., (a) principal stress difference versus mean normal stress, (b) principal stress difference versus axial strain, (c) volumetric strain versus mean normal stress, and (d) volumetric strain versus axial strain.

Table 1
SAM-35 Mix Design

Materials	Mass per cubic meter batch
Portland cement Type I/II	190.2 kg
Fine aggregate: Natural river sand	738.2 kg
Coarse aggregate: 9.5mm crushed limestone	650.3 kg
200 N (water-reducing admixture)	496 mL
AE 90 (air-entraining admixture)	57.1 mL
Water	120 kg

Table 2
Physical and composition properties of SAM-35

Test Number	Type of Test	Plate Number	Wet Density Mg/m^3	Posttest Water Content %	Dry Density Mg/m^3	Porosity %	Degree of Saturation %	Volume of Air %	Volume of Water %	Volume of Solids %	Axial P Wave Velocity km/s	Radial P Wave Velocity km/s	Axial S Wave Velocity km/s	Radial S Wave Velocity km/s
1	UC	3	2.152	3.84	2.073	20.58	38.67	12.62	7.96	79.42	4.240	4.348	2.531	2.625
2	UC	4	2.185	3.78	2.105	19.35	41.12	11.39	7.96	80.65	4.478	4.473	2.616	2.685
3	UC	5	2.169	3.79	2.090	19.94	39.72	12.02	7.92	80.06	4.419	4.444	2.592	2.635
4	UC	6	2.172	3.95	2.090	19.93	41.41	11.68	8.25	80.07	4.443	4.351	2.643	2.605
5	HC	1	2.157	3.86	2.076	20.44	39.21	12.43	8.02	79.56	4.351	4.385	2.582	2.568
6	HC	2	2.180	3.70	2.102	19.46	39.97	11.68	7.78	80.54	4.452	4.412	2.594	2.588
7	TXC/5	7	2.164	3.66	2.088	20.02	38.17	12.38	7.64	79.98	4.417	4.404	2.603	2.621
8	TXC/5	8	2.168	3.98	2.085	20.12	41.25	11.82	8.30	79.88	4.444	4.486	2.587	2.595
9	TXC/10	9	2.195	3.64	2.118	18.86	40.87	11.15	7.71	81.14	4.505	4.444	2.652	2.737
10	TXC/10	10	2.175	3.69	2.097	19.65	39.39	11.91	7.74	80.35	4.391	4.400	2.618	2.619
11	TXC/20	11	2.164	3.91	2.083	20.19	40.33	12.05	8.14	79.81	4.282	4.469	2.566	2.652
12	TXC/20	12	2.163	3.83	2.083	20.18	39.54	12.20	7.98	79.82	4.329	4.435	2.526	2.621
13	TXC/50	13	2.19	3.74	2.111	19.12	41.30	11.22	7.90	80.88	4.457	4.518	2.632	2.628
14	TXC/50	14	2.141	3.72	2.064	20.93	36.68	13.25	7.68	79.07	4.298	4.429	2.500	2.598
15	TXC/100	15	2.148	3.66	2.072	20.60	36.82	13.02	7.58	79.40	4.349	4.452	2.558	2.551
16	TXC/100	16	2.164	3.69	2.087	20.03	38.46	12.33	7.70	79.97	4.282	4.459	2.542	2.628
17	TXC/200	17	2.156	3.65	2.080	20.32	37.36	12.73	7.59	79.68	4.351	4.380	2.559	2.638
18	TXC/200	18	2.170	3.53	2.096	19.70	37.55	12.31	7.40	80.30	4.509	4.376	2.637	2.640
19	TXC/300	19	2.179	3.57	2.104	19.38	38.77	11.86	7.51	80.62	4.525	4.422	2.651	2.632
20	TXC/300	20	2.159	3.50	2.086	20.06	36.40	12.76	7.30	79.94	4.392	4.403	2.576	2.595
21	TXC/400	21	2.175	3.65	2.098	19.61	39.06	11.95	7.66	80.39	4.441	4.500	2.647	2.645
22	TXC/400	22	2.162	3.41	2.091	19.89	35.84	12.76	7.13	80.11	4.261	4.435	2.559	2.566
23	UX	29	2.158	3.54	2.084	20.14	36.64	12.76	7.38	79.86	4.422	4.480	2.600	2.612
24	UX	30	2.182	3.51	2.108	19.25	38.44	11.85	7.40	80.75	4.449	4.441	2.626	2.661
26	UX/BX	31	2.186	3.50	2.112	19.07	38.78	11.67	7.39	80.93	4.563	4.455	2.661	2.691
27	UX/BX	32	2.156	3.47	2.084	20.15	35.89	12.92	7.23	79.85	4.493	4.350	2.550	2.609
28	UX/BX	33	2.159	3.41	2.087	20.02	35.55	12.91	7.12	79.98	4.362	4.504	2.590	2.626

(*continued*)

Table 2 (Concluded)

Test Number	Type of Test	Plate Number	Wet Density Mg/m^3	Posttest Water Content %	Dry Density Mg/m^3	Porosity %	Degree of Saturation %	Volume of Air %	Volume of Water %	Volume of Solids %	Axial P Wave Velocity km/s	Radial P Wave Velocity km/s	Axial S Wave Velocity km/s	Radial S Wave Velocity km/s
29	UX/BX	34	2.174	3.49	2.101	19.51	37.59	12.17	7.33	80.49	4.500	4.425	2.621	2.625
30	UX/CV	35	2.177	3.29	2.107	19.26	36.00	12.32	6.93	80.74	4.383	4.435	2.602	2.625
31	UX/CV	36	2.183	3.43	2.111	19.14	37.83	11.90	7.24	80.86	4.425	4.438	2.671	2.621
32	UX/CV	37	2.164	3.41	2.092	19.84	35.97	12.70	7.13	80.16	4.569	4.401	2.604	2.604
33	UX/SR	38	2.171	3.35	2.101	19.51	36.06	12.48	7.04	80.49	4.390	4.485	2.640	2.608
34	UX/SR	39	2.154	3.47	2.081	22.91	31.52	15.69	7.22	77.09	4.358	4.493	2.582	2.588
35	TXC/400	23	2.167	3.37	2.096	22.37	31.57	15.31	7.06	77.63	4.473	4.322	2.576	2.619
36	TXC/400	24	2.174	3.01	2.110	21.85	29.07	15.50	6.35	78.15	4.434	4.428	2.619	2.635
37	RTE	25	2.157	3.33	2.087	22.69	30.64	15.74	6.95	77.31	4.311	4.386	2.554	2.548
38	RTE	26	2.156	3.34	2.087	22.72	30.68	15.75	6.97	77.28	4.348	4.473	2.574	2.639
39	RTE	27	2.166	3.38	2.095	22.41	31.60	15.33	7.08	77.59	4.474	4.484	2.656	2.614
40	RTE	28	2.151	3.23	2.084	22.82	29.50	16.09	6.73	77.18	4.349	4.389	2.539	2.619
41	DP		2.184	2.72	2.126	21.26	27.20	15.48	5.78	78.74	4.424	4.398	2.593	2.622
42	DP		2.154	2.70	2.097	22.32	25.37	16.66	5.66	77.68	4.315	4.382	2.545	2.586
43	DP		2.129	2.75	2.072	23.25	24.51	17.56	5.70	76.75	4.451	4.471	2.566	2.560
44	DP		2.133	2.71	2.077	23.07	24.39	17.45	5.63	76.93	4.452	4.412	2.594	2.588
45	DP		2.137	2.67	2.081	22.92	24.25	17.36	5.56	77.08	4.452	4.449	2.624	2.609
N			44	44	44	44	44	44	44	44	44	44	44	44
Mean			2.163	3.39	2.092	20.75	34.47	13.65	7.09	79.25	4.407	4.434	2.593	2.615
Stdv			0.015	0.343	0.013	1.331	4.996	1.88	0.712	1.331	0.079	0.047	0.041	0.036
Max			2.195	3.98	2.126	23.25	41.41	17.56	8.3	81.14	4.569	4.518	2.671	2.737
Min			2.129	2.67	2.064	18.86	24.25	11.15	5.56	76.75	4.240	4.322	2.500	2.548

Table 3
Completed SAM-35 Test Matrix

Type of Test	No. of Tests	Test No.	Tests with Cycles Test No.	Nominal Peak Radial Stress, MPa
Hydrostatic Compression	2	5, 6	5	509
Triaxial Compression	4	1, 2, 3, 4		0
	2	7, 8		5
	2	9, 10	10	10
	2	11, 12	12	20
	2	13, 14	14	50
	2	15, 16	16	100
	2	17, 18	17	200
	2	19, 20		300
	4	21, 22, 35, 36	21, 35, 36	400
UX Strain	2	23, 24	23	509
UX/BX	2	28, 29		100
	2	26, 27		200
UX/CV	1	32		60
	2	30, 31		110
UX/SR	2	33, 34		50
Reduced Triaxial Extension	1	39		35
	1	40		42
	2	37, 38		65
Direct-Pull	5	41, 42, 43, 44, 45		0
Total No. Tests:	44			

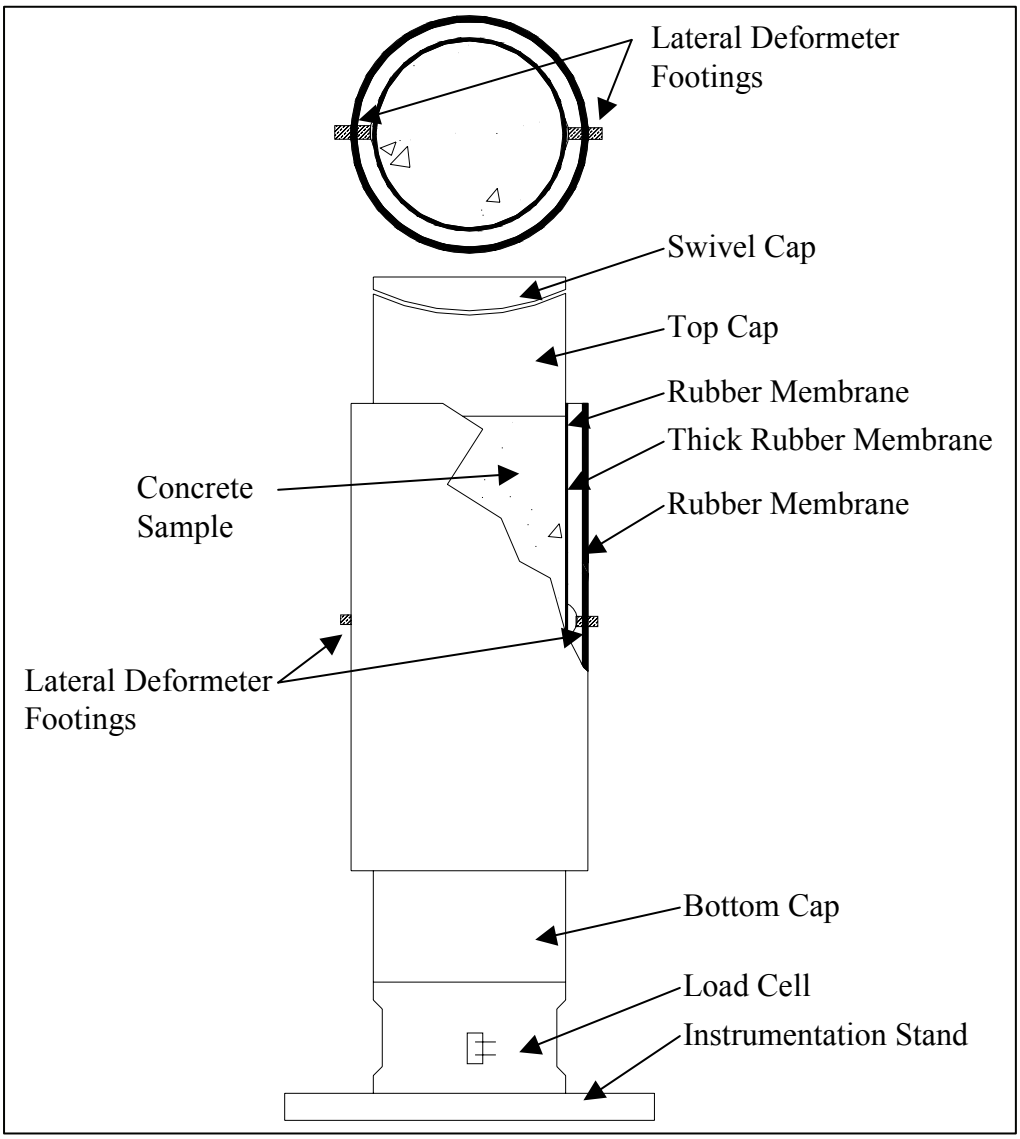

Figure 1. Typical test specimen setup

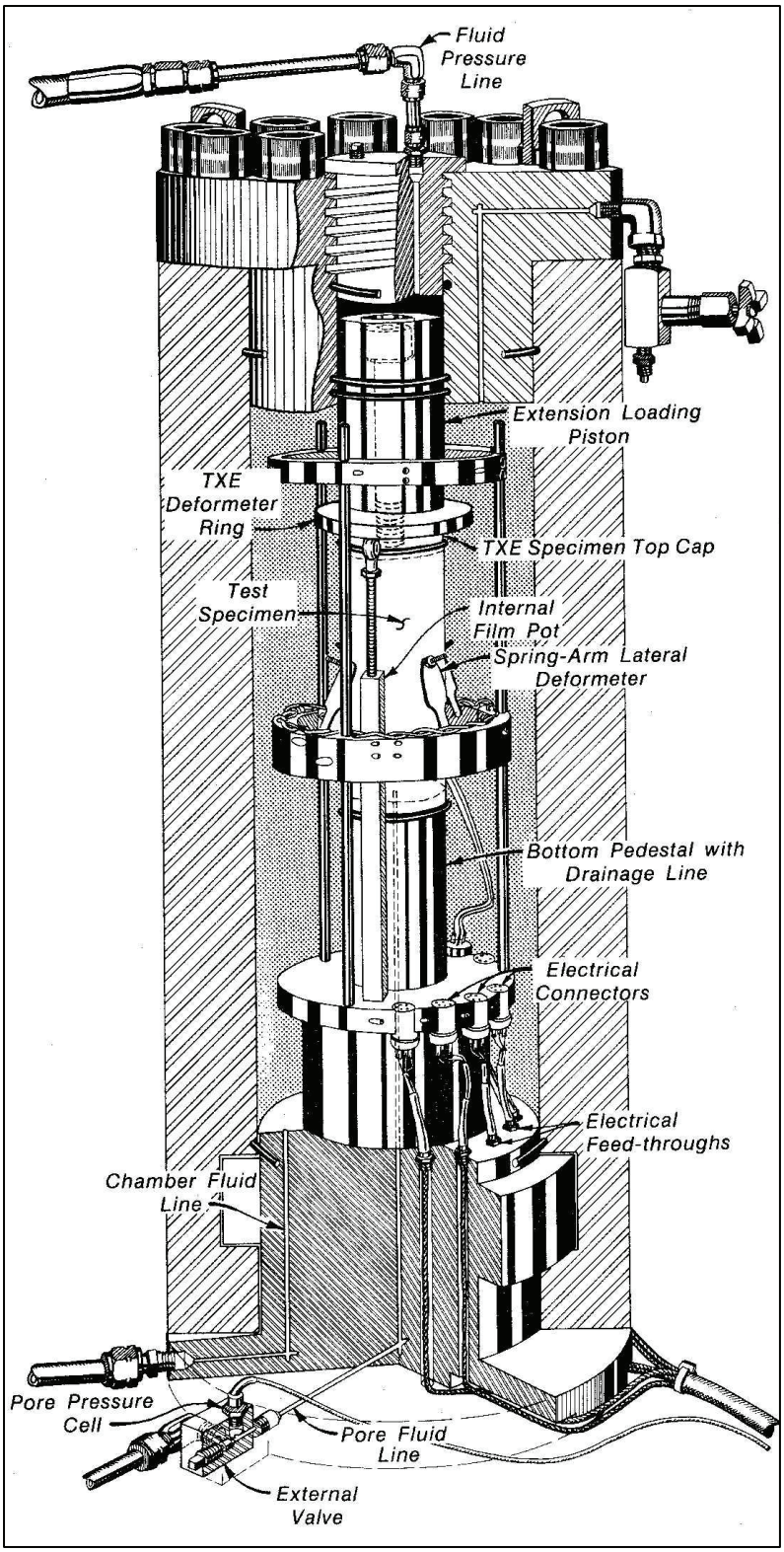

Figure 2. HPTX test device with TXE top cap

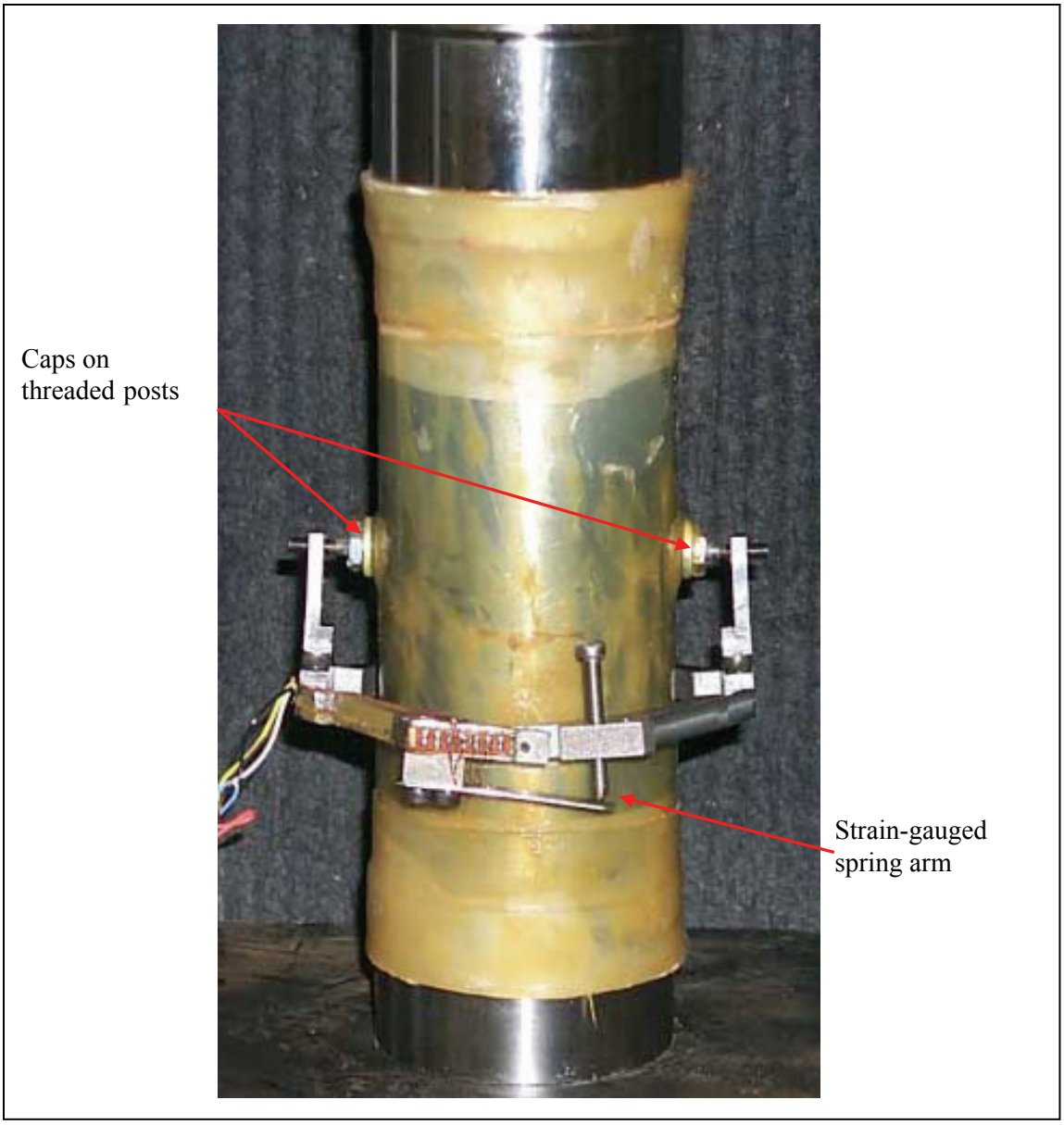

Figure 3. Spring-arm lateral deformeter mounted on test specimen

3 Analysis of Test Results

An analysis of the results from laboratory tests conducted on SAM-35 concrete is presented in this chapter. The purpose of the investigation was to characterize the strength and constitutive property behavior of the material. As described in Chapter 2, a total of 45 mechanical property tests were conducted in this investigation, and 44 tests were successfully completed. The analysis in this chapter is based on the results from two HC tests, four UC tests, 18 TXC tests, two UX tests, four UX/BX tests, three UX/CV tests, two UX/SR tests, five DP tests, and four RTE tests.

Hydrostatic Compression Test Results

Undrained compressibility data were obtained from two HC tests and during the hydrostatic loading phases of the 18 TXC tests. The pressure-volume data from the HC tests are plotted in Figure 4. Unload-reload cycles were applied to HC test specimen 05 to obtain unload-reload data at an intermediate level of confining stress. The initial dry densities of the specimens for HC tests 05 and 06 were 2.076 and 2.102 Mg/m^3, respectively. The HC compressibility is affected by the initial dry density, i.e., increased compressibility with decreased dry density. Figure 5 presents the pressure time-histories for the HC tests. During the HC tests, the pressure was intentionally held constant for a period of time prior to the unloading cycles. During each hold in pressure, the volume strains continued to increase, indicating that SAM-35 is susceptible to creep at high pressures (Figure 4). At the peak of the first cycle, specimen 05 was held at 255 MPa for 342 sec, while a volume strain of 0.49 percent was measured. At the start of the second cycle the specimen was held at 255 MPa for 175 sec, causing a volume strain of 0.11 percent. During the peak of the second cycle, the pressure was held at 510 MPa for 410 sec, and a volume strain of 0.42 percent was measured. The pressure was held at 510 MPa for 600 sec for test specimen 06, during which time a volume strain of 0.55 percent was measured.

Pressure-volume data were also obtained during the hydrostatic loading phases of the TXC tests (Figure 6). Pressure-volume data from all of the TXC tests conducted at confining pressures of 100 MPa and above, in addition to the HC data from Figure 4, are plotted in Figure 7. There is no significant scatter in the pressure-volume data, although the pressure-volume curve from test 06 is stiffer at pressures above approximately 25 MPa. The results plotted in Figure 7 indicate that SAM-35 begins to exhibit inelastic strains at a pressure level of

approximately 22 MPa and at a volumetric strain of approximately 0.25 percent. These are the pressure and strain levels at which the pressure-volume response and the initial bulk modulus begin to soften appreciably. Based on the data from the HC and TXC tests, the initial elastic bulk modulus (K) for SAM-35 is approximately 8.9 GPa.

Triaxial Compression Test Results

Shear and failure data were successfully obtained from four unconfined compression tests and 18 unconsolidated-undrained TXC tests. Recall from Chapter 2 that the second phase of the TXC test, the shear phase, is conducted after the desired confining pressure was applied during the HC phase. The UC tests are a special type of TXC test without the application of confining pressure. Results from the UC tests are plotted in Figures 8 and 9, and results from the TXC tests are plotted in Figures 10 through 25. In these latter figures, the axial and volumetric strains at the beginning of the shear phase were set to zero, i.e., only the strains during shear were plotted.

Stress-strain data from the four UC tests in Figures 8 and 9 are plotted as principal stress difference versus axial strain during shear and as principal stress difference versus volumetric strain during shear, respectively. Deformeters instead of strain gauges were used to measure the axial and radial strains of the UC test specimens. During the UC tests, no attempt was made to capture the post-peak (or softening) stress-strain behavior of this material. The mean unconfined strength of SAM-35 determined from specimens 02, 03, and 04 was 33.6 MPa. Specimen 01 was not included in the determination of the unconfined strength since the data for 01 are considered an outlying result. The unconfined strength for test 01 was lower than the other tests because the specimen's initial dry density (2.073 Mg/m^3) was lower than the average dry density (2.092 Mg/m^3). The initial dry densities of test specimens 02, 03, and 04 were 2.105, 2.090, and 2.090 Mg/m^3, respectively.

Figures 10 through 25 present the results from the TXC tests conducted at nominal confining pressures of 5, 10, 20, 50, 100, 200, 300, and 400 MPa. The TXC results are plotted as principal stress difference versus axial strain during shear and as principal stress difference versus volumetric strain during shear. The results are very good considering the inherent variability of the initial wet and dry densities and water contents of the specimens. The wet densities of the specimens ranged from 2.141 to 2.195 Mg/m^3, the dry densities ranged from 2.064 to 2.118 Mg/m^3, and the water contents ranged from 3.41 to 3.98 percent.

The dry density of the SAM-35 specimens affects the specimen's strength, i.e., a specimen with a higher dry density has higher strength at a given confining pressure. A few comments should also be made concerning the unloading results in general. The final unloading stress-strain responses at axial strains approaching 15 percent are less reliable than the unloadings at axial strains less than 11 percent. The vertical deformeters go out of range at axial strains of approximately 11 percent. After that, an external deformeter with less resolution was used to measure axial displacement. During the initial unloadings, the creep strains are greater in magnitude than the recovered elastic strains. This behavior

results in a net increase in axial strain (for example) during the initial unloading, rather than an expected decrease in axial strain.

Results of TXC tests conducted at a constant confining pressure of 5 MPa are shown in Figures 10 and 11. The stress-strain plot (Figure 10) displays minimal post-peak softening stress-strain behavior. At 5 MPa confining pressure, SAM-35 is still brittle. The volumetric response in Figure 11 indicates that the material initially compacts until just below the peak principal stress difference and then starts to dilate. Little compressive volume strain occurs at 5 MPa because the material is still in the elastic region, i.e., the initial cementitious bonds are intact.

Figures 12 and 13 display the results of TXC tests conducted at 10 MPa confining pressure. Both figures for the tests at 10 MPa exhibit increasing peak principal stress difference with increasing dry density. The post-peak data for the test specimens are not displayed because of the brittle response of the material. The volumetric response (Figure 13) for the specimens tested at 10 MPa confining pressure was similar to the volumetric response of the specimens tested at 5 MPa confining pressure.

Results for TXC tests conducted at a confining pressure of 20 MPa are shown in Figures 14 and 15. Both of the specimens tested at 20 MPa had the same initial dry density. Since the dry densities are the same, the data in both figures are very similar with the exception being that test 12 had an unload-reload cycle. Limited amounts of post-peak data were obtained for the test specimens, and the material compacted prior to reaching peak principal stress difference, then started to dilate.

Figures 16 and 17 display the results of TXC tests conducted at 50 MPa confining pressure. Figure 16 displays a more ductile shear response, i.e., the stress-strain curves exhibit some strain hardening. Since the tests at 20 MPa displayed brittle behavior (the material strain softens and minimal amounts of post-peak stress or strain data are acquired), the brittle-to-ductile transition is between 20 and 50 MPa. The brittle-to-ductile transition occurs when the material flows at a near constant value of principal stress difference.

Results of TXC tests conducted at confining pressures of 100, 200, and 300 MPa are shown in Figures 18-19, 20-21, and 22-23, respectively. The qualitative responses at these three levels of confining pressure are essentially the same. The shear responses were predominantly ductile, peak strength increases with increased level of confining pressure, and volumetric dilation occurs just prior to peak strength.

Figures 24 and 25 display the results of TXC tests conducted at 400 MPa confining pressure. With the exception of the sample used in test 36, which had an initial dry density of 2.110 Mg/m^3, the samples used in tests 19 and 20 at a confining pressure of 300 MPa (Figure 22) and the TXC tests at 400 MPa specimens 21, 22, and 35 (Figure 24) had similar values of initial dry density (between 2.086 and 2.104 Mg/m^3). The peak strengths at 400 MPa (Figure 24) are only slightly greater than those at 300 MPa (Figure 22), with the exception of the 400-MPa confining pressure of test 36. This is evidence that this material is approaching full saturation after which strength remains essentially constant with increases in confining pressure.

For comparison purposes, stress-strain curves from selected TXC tests at confining pressures equal to or less than 50 MPa are plotted in Figure 26, and selected tests at confining pressures greater than 50 MPa are plotted in Figure 27. Stress-strain data from all of the TXC tests in Figures 26 and 27 are plotted in Figures 28 and 29, respectively, as principal stress difference versus volumetric strain during shear. As confining pressure increases, the initial loading moduli of the material soften as the stress state moves into the crush regime of the pressure-volume curve, and then stiffen again as the material approaches void closure, i.e., the point at which all of the specimen's air-porosity is crushed out (Figures 26 and 27). At confining pressures of 5 and 10 MPa, the specimens' initial volume changes are basically within the elastic regime of the pressure-volume curve and exhibit stiff initial loading of the stress-strain curves. The TXC tests conducted at confining pressures of 20 and 50 MPa had a softer response (lower moduli) during the initial shear loading than the tests at 5 and 10 MPa (Figure 26). The tests conducted at a confining pressure of 100 MPa had the softest initial loading results in stress difference-axial strain space (Figures 26, 27, and 30). The test specimens at 100 MPa also had the softest response in stress difference-volume strain space (see Figures 28, 29, and 31). The TXC tests conducted at 200, 300, and 400 MPa exhibited increasingly stiffer initial loading moduli. The subsequent increase in initial loading with increasing confining pressure during shear is directly related to the increasing stiffness in the pressure-volume response of the concrete.

Results from TXC tests at confining pressures from 5 to 400 MPa are plotted in Figure 32 as radial strain during shear versus axial strain during shear. A contour of zero volumetric strain during shear is also plotted on this figure. When the instantaneous slope of the curve is shallower than the contour of zero volumetric strain, the specimen is in a state of volume expansion. Data points plotting below the contour signify that a test specimen has dilated, and the current volume of the specimen is greater than the volume at the start of shear.

The failure data from all of the shear tests, i.e., UC and TXC tests, are plotted in Figure 33 as principal stress difference versus mean normal stress; one stress path at each confining stress is also plotted. In Figure 34, a recommended failure surface is plotted with the failure points. The quality of the failure data is good; it exhibits little scatter with the exception of the 400-MPa confining pressure. It is important to note that the failure points exhibit a continuous increase in principal stress difference with increasing values of mean normal stress. The rate of increase is somewhat reduced after reaching a mean normal stress of approximately 320 MPa. The specimens tested below 100 MPa have significant air porosity that can be compressed during shear. The tests above 100 MPa have less air porosity, causing the rate of increase of the principal stress difference to reduce. Void closure is approached during the 400 MPa TXC tests at a mean normal stress of approximately 550 MPa. Concrete will not continue to gain strength with increasing pressure when all of the air porosity in the concrete has been crushed out, i.e., when void closure is reached. It is important to recognize that void closure can be attained during the shear loading phase of the TXC tests as well as under hydrostatic loading conditions. At levels of mean normal stress above void closure, the failure surface will have a minimal slope.

Reduced Triaxial Extension Test Results

Extension stress-strain and failure data were successfully obtained from five direct-pull tests and three unconsolidated-undrained RTE tests. The DP tests are a special type of RTE test without the application of confining pressure. Results from the DP tests are plotted in Figure 35, results from the RTE tests are plotted in Figures 36-38, and the recommended failure surfaces from the triaxial test results are plotted in Figure 39. Data from the DP tests exhibit some scatter but, when examined, the difference for the principal stress difference is only 0.51 MPa. The stress-strain data in Figure 36 display the RTE test results conducted at confining pressures of 35, 42, and 65 MPa. All of the specimens fractured. The RTE tests exhibit slight variations during loading caused by the manual operation of the equipment. Only the DP, RTE, and UC tests included in this test program used a manual operation rather than a servo-controlled system to control the load and confining pressure. The confining pressure for RTE specimen 39 was increased to cause the specimen to fail after reaching zero axial stress. The extension failure surface developed from the DP and RTE tests is shown in Figure 38 with the RTE stress paths. Figure 39 displays data from the UC and selected TXC tests, the results from the DP and RTE tests, and the recommended compression and extension failure surfaces for SAM-35. Comparing the failure surfaces for SAM-35 shows that the slope of the extension failure surface is less then the slope of the compression surface; consequently, SAM-35 has a nonsymmetric failure surface about the mean normal stress axis.

Uniaxial Strain Test Results

One-dimensional compressibility data were obtained from two undrained UX tests with lateral stress measurements. Data from the two tests are plotted in Figures 40-42. The stress-strain data from the UX tests are plotted in Figure 40, the pressure-volume data in Figure 41, and the stress paths with the recommended TXC failure surface in Figure 42. The UX responses in Figure 40 are initially very stiff because the specimens are being loaded in the elastic regime. After the specimens begin to crush, the compressibility responses soften and the material starts to compact significantly. The UX responses become stiff again, once the air porosity is crushed out and the specimens approach full saturation.

From the UX stress-strain loading data (Figure 40), an initial constrained modulus (M) of 16.5 GPa was calculated. UX data may also be plotted as principal stress difference versus mean normal stress; the slope of an elastic material in this space is $2G/K$. A shear modulus (G) of 5.7 GPa was calculated from the constrained modulus and the elastic bulk modulus, K (8.9 GPa), determined from the HC tests and the HC portions of the TXC tests. These two values may be used to calculate any of the other elastic constants. For example, the Young's modulus (E) is 14.0 GPa, and Poisson's ratio (ν) is 0.24.

The UX stress paths in Figure 42 have a steep initial stress path heading toward the recommended TXC failure surface. The stress paths soften after the material is crushed, causing the data to plot well below the failure surface. The

pressure-volume responses from the HC and UX tests are compared in Figure 43. The HC test data display stiffer responses than the UX test data. This implies that the UX state of stress is providing additional shear-induced compaction to the specimens. The differences in these responses for each type of test are caused by the differences in the dry density of the test specimens.

Strain Path Test Results

Three types of strain-path tests were conducted in this test program. UX/BX refers to tests with uniaxial strain loading followed by constant axial strain unloading. UX/CV refers to tests with uniaxial strain loading followed by constant volume strain loading. UX/SR refers to tests with a uniaxial strain loading then continued loading along a constant ratio of axial strain to radial strain of -1.33.

Data were obtained from two UX/BX tests that were loaded to a radial stress of 100 MPa and two UX/BX tests that were loaded to a radial stress of 200 MPa during the initial UX phase. Data from the tests are plotted in Figures 44-47. The stress-strain data from the UX/BX tests are plotted in Figure 44, the pressure-volume data in Figure 45, the strain path data in Figure 46, and the stress paths with the failure surface in Figure 47. The stress-strain response of the material (Figure 44) displays variations during the UX loading that are a function the test specimens' initial properties. The dry densities of the specimens were determined to affect the loading responses during the TXC tests, i.e., stiffer loading responses resulted from specimens with higher dry densities. The initial UX loadings are also affected by the specimens' dry densities; however, it appears that other material properties are affecting the UX loading, since specimens 27 and 28 have almost the same dry density (2.084 and 2.080 Mg/m^3, relatively) but specimen 27 has a much stiffer slope than specimen 28. In addition, the stress-strain curves illustrate that all of the specimens were allowed to creep under zero-radial-strain boundary conditions prior to initiating the BX unloading.

The pressure-volume data presented in Figure 45 illustrate the large amount of volume recovery that occurs during the BX unloading. Most of the specimens recover more than one-half of their peak compressive volume strain. Recall that the BX unloadings are under a forced state of volumetric expansion. Figure 46 shows the strain paths that were followed during the four tests. The stress paths plotted in Figure 47 are typical of most concretes. At the end of the UX loading and prior to the BX unloading, some stress relaxation occurs in the system, hence the slight unload just after the peak stress (Figure 47). During the unloading, the stress paths show a small increase in principal stress difference followed by significant decrease in stress difference with decreasing mean normal stress. This unloading appears to follow a limiting surface, which is normally the material's failure relation (the TXC recommended failure surface, in most cases). In this case, the BX unloading exceeds the failure relation. The reason the failure relation exceeds the limiting surface is that the test specimen density is increased during the UX loading. When the BX loading initiates, the specimen is too dense to follow along the failure surface determined from the TXC test specimens.

Results from three UX/CV tests conducted to two different levels of peak axial stress during the initial UX phase are shown in Figures 48-51. The stress-strain data from the UX/CV tests are plotted in Figure 48, the pressure-volume data in Figure 49, the strain path data in Figure 50, and the stress paths with the failure surface in Figure 51. The CV portions of the stress path data in Figure 51 initially exhibit an increase in stress difference with a slight decrease in mean normal stress and then follow along the failure relation. For this series of tests, the CV portions of the data provide an excellent confirmation of the failure relation by following along the recommended TXC failure surface.

Data were obtained from two UX/SR tests that were loaded to approximately the same nominal peak axial stress during the initial UX phase. Data from the tests are plotted in Figures 52-55. The stress-strain data from the UX/SR tests are plotted in Figure 52, the pressure-volume data in Figure 53, the strain path data in Figure 54, and the stress paths with the failure surface in Figure 55. The plotted stress paths (Figure 55) exhibit increasing values of principal stress difference and decreasing values of mean normal stress after the strain-ratio loading initiates. After reaching the material's limiting surface, both the principal stress difference and the mean normal stress increase, generally following the failure surface. The plot in Figure 55 confirms that the limiting surface for the UX/SR tests is similar to the recommended TXC failure surface.

Comparison plots of selected UX, UX/BX, UX/CV, and UX/SR test results are plotted in Figures 56-59. The stress-strain data are plotted in Figure 56, the pressure-volume data are plotted in Figure 57, the strain paths are plotted in Figure 58, and the stress-paths with the failure surface in Figure 59. The dry density values of the specimens were very similar (ranged from 2.101 to 2.112 Mg/m^3); therefore, the UX loading portions in Figures 56, 57, and 59 are essentially the same.

The following provides an interpretation of the measured pressure-volume data (Figure 57) during the strain paths. When loading along the constant volume strain path, the specimens want to increase in volume because of the material's inherent shear-induced dilation characteristics. Increasing levels of pressure are required to maintain constant volume boundary conditions. The material's behavior while loading along a constant strain ratio path displays decreasing pressure and decreasing volumetric strain. The specimen does not want to expand faster than the boundary conditions permit, unlike the specimens loaded along the constant-volume strain path. To maintain the boundary conditions during the UX/SR tests, the pressure is increased. The boundary conditions applied during the BX unloading require significant amounts of volume expansion. To maintain the boundary conditions, pressure must be reduced. In Figure 59, one stress path for each of the strain path tests and the TXC failure surface are overlaid to illustrate the merger of the data in the vicinity of a failure surface. The convergence of the data from the UX/CV and the UX/SR tests validates the recommended TXC failure surface.

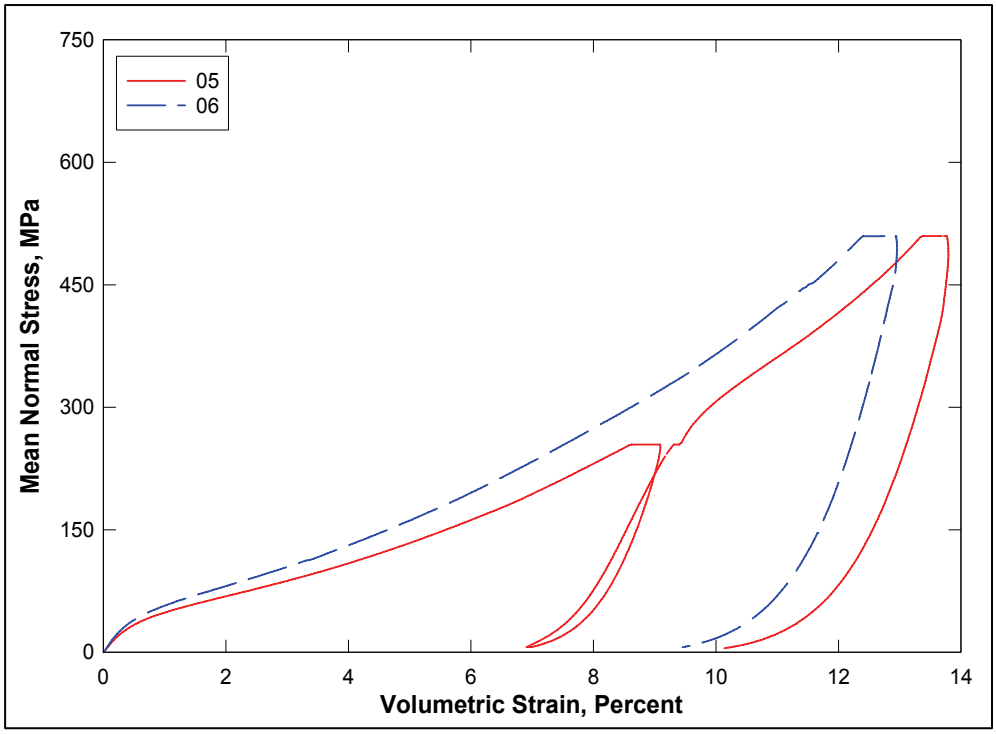

Figure 4. Pressure-volume responses from the HC tests

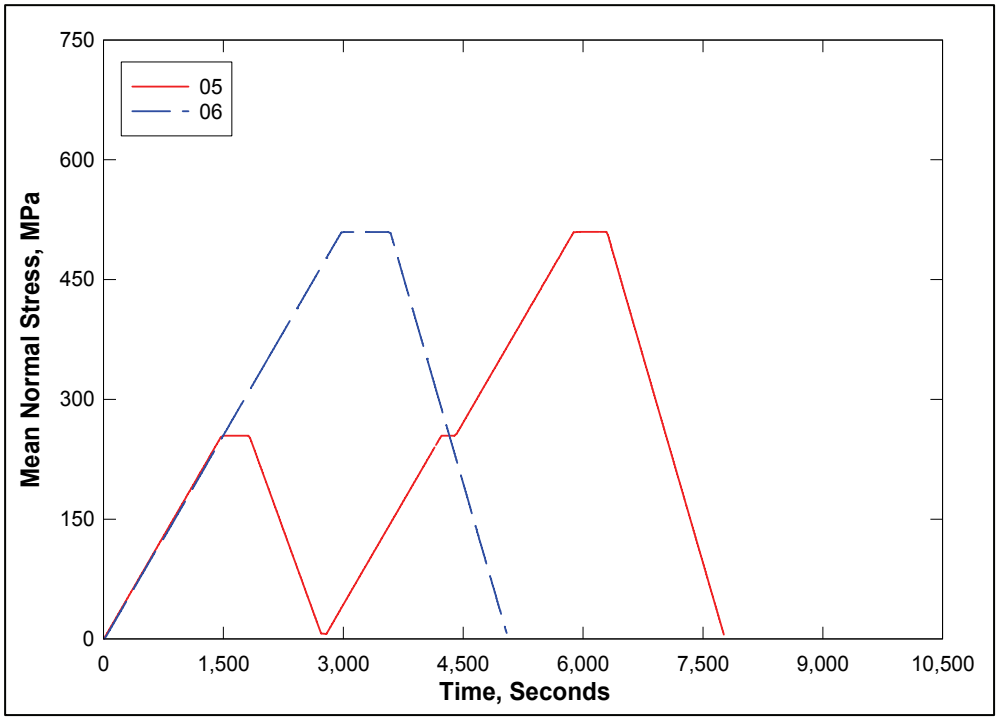

Figure 5. Pressure-time histories from the HC tests

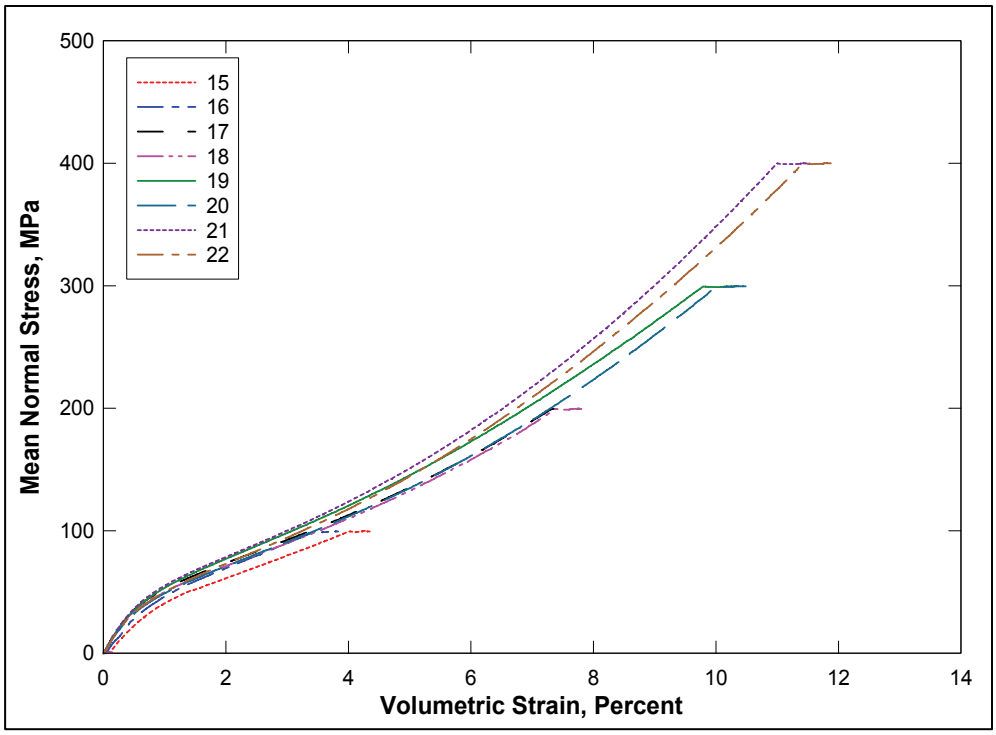

Figure 6. Pressure-volume responses from selected TXC tests

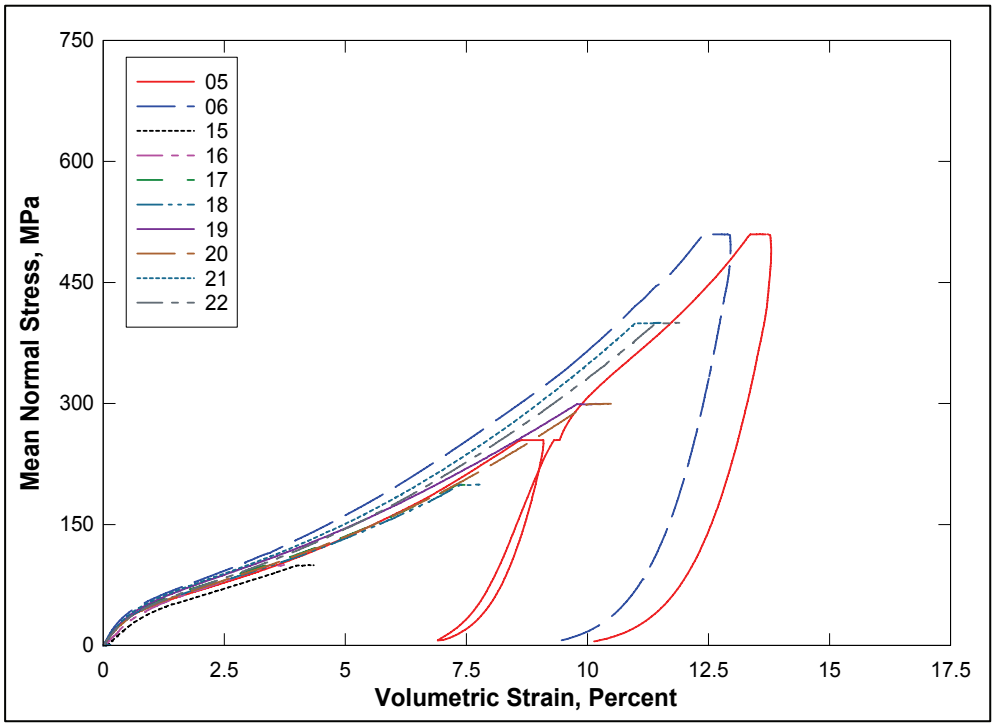

Figure 7. Pressure-volume responses from HC and selected TXC tests

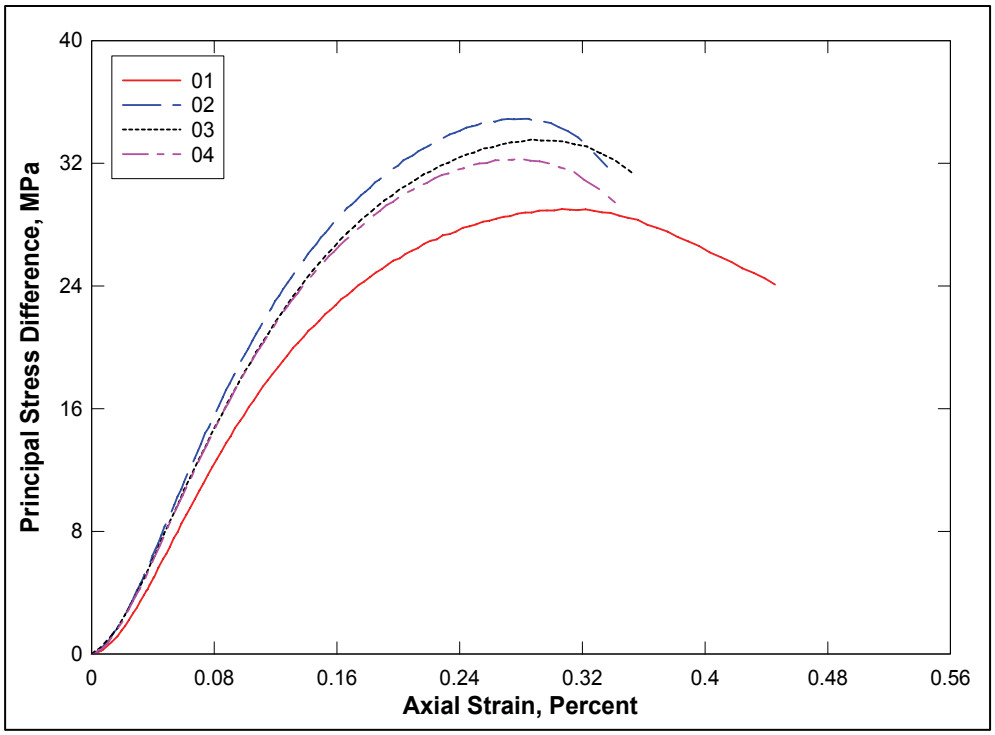

Figure 8. Stress-strain curves from UC tests

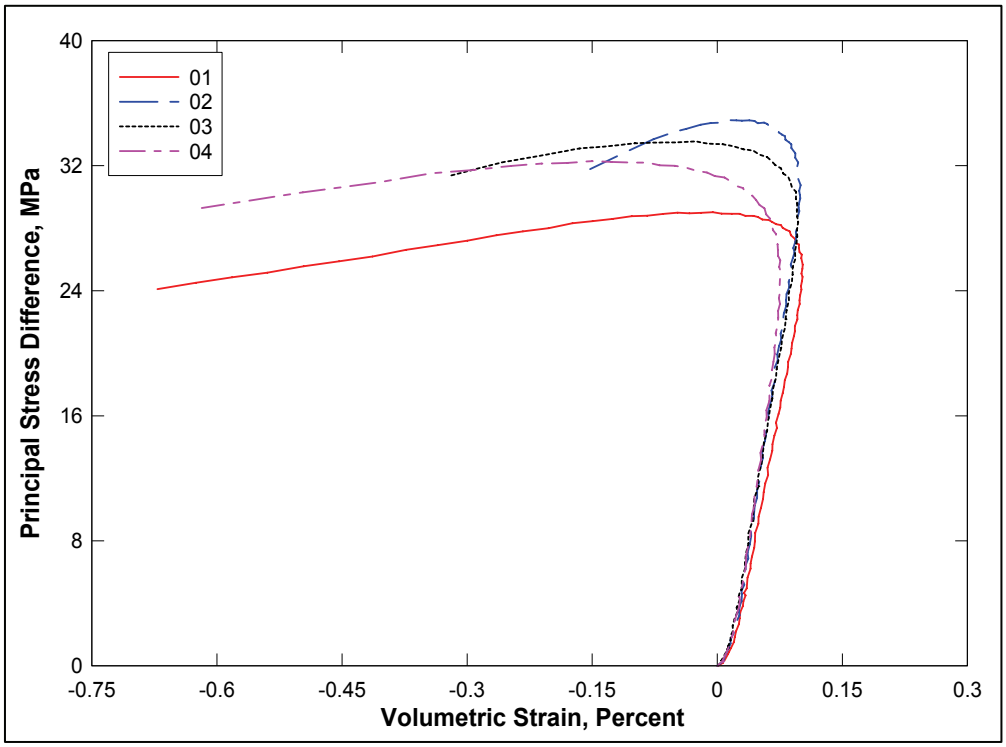

Figure 9. Stress difference-volume strain during shear from UC tests

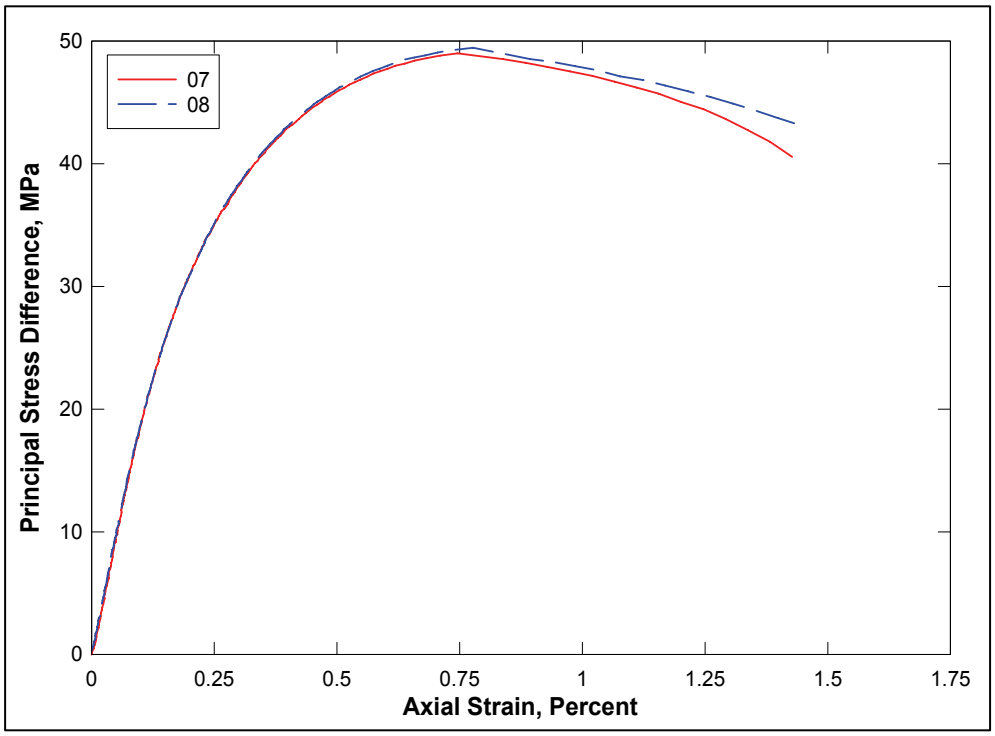

Figure 10. Stress-strain curves from TXC tests at a confining pressure of 5 MPa

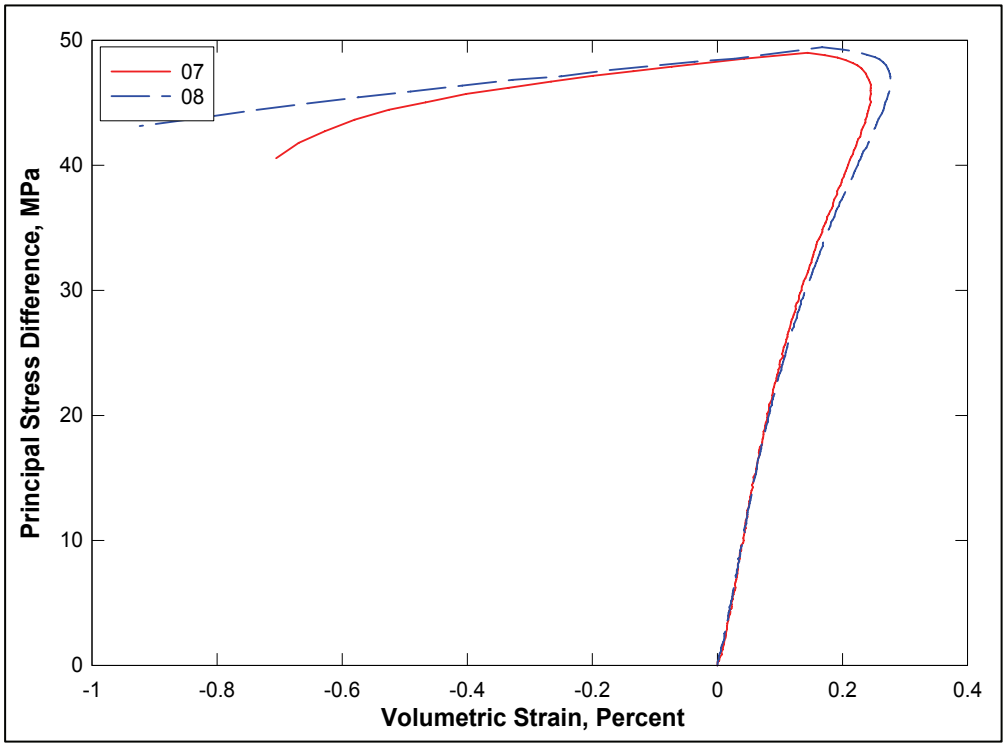

Figure 11. Stress difference-volume strain during shear from TXC tests at a confining pressure of 5 MPa

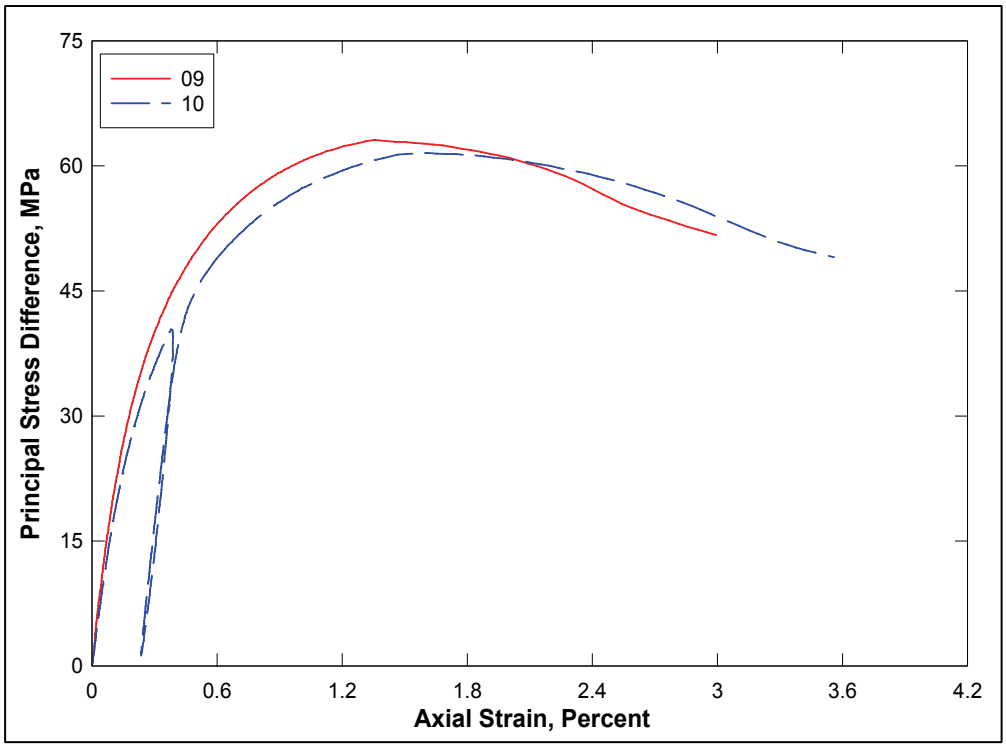

Figure 12. Stress-strain curves from TXC tests at a confining pressure of 10 MPa

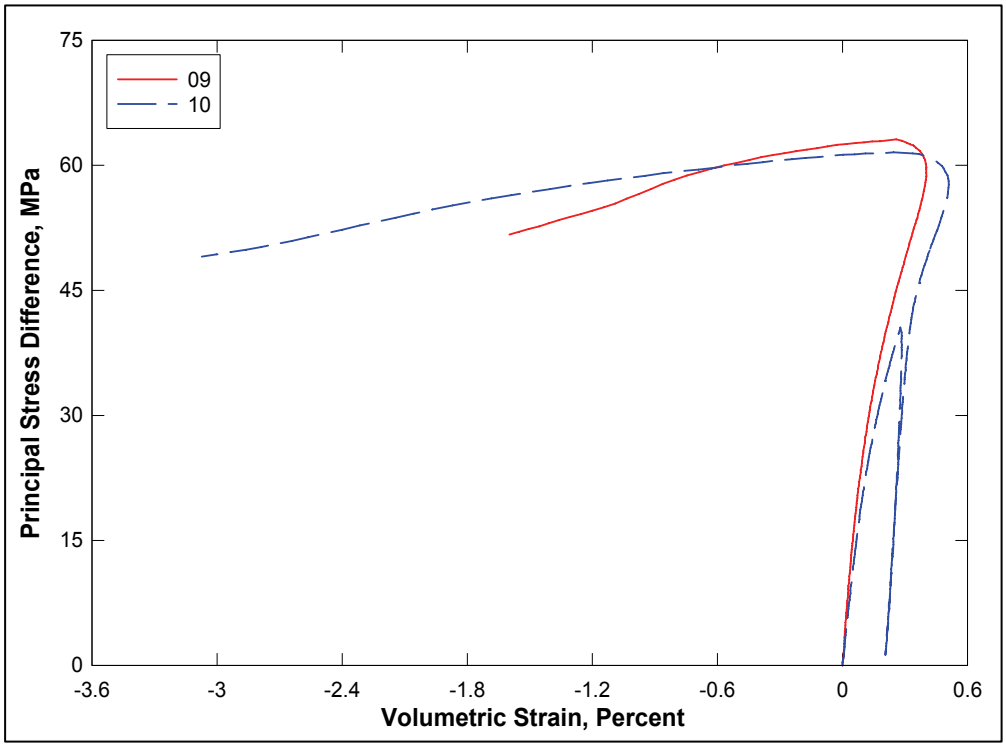

Figure 13. Stress difference-volume strain during shear from TXC tests at a confining pressure of 10 MPa

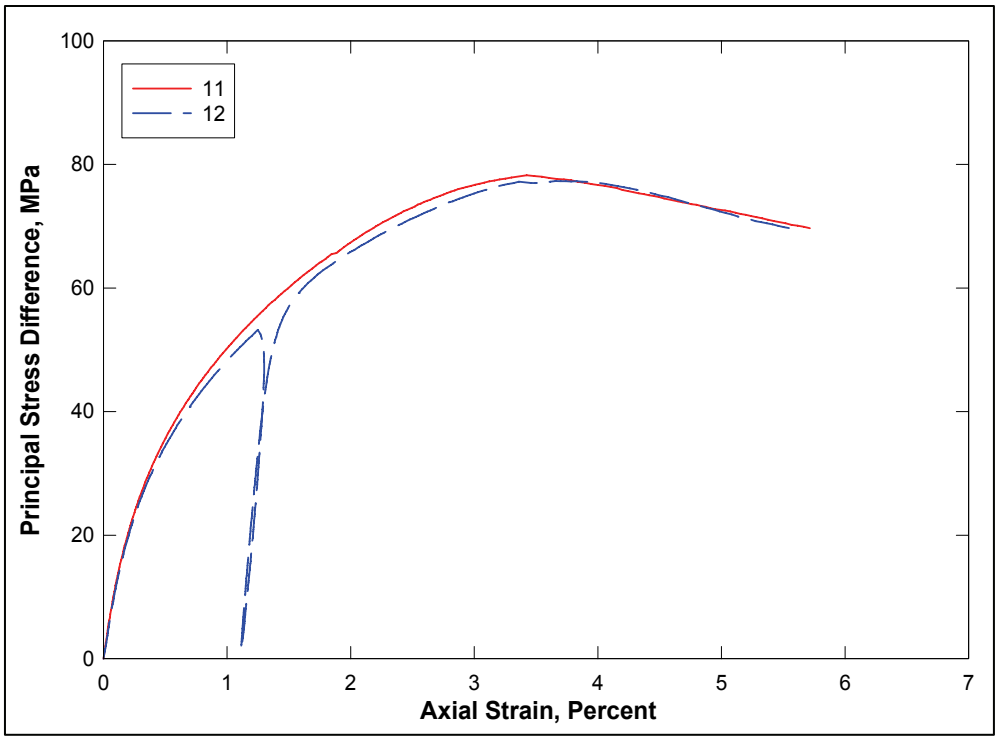

Figure 14. Stress-strain curves from TXC tests at a confining pressure of 20 MPa

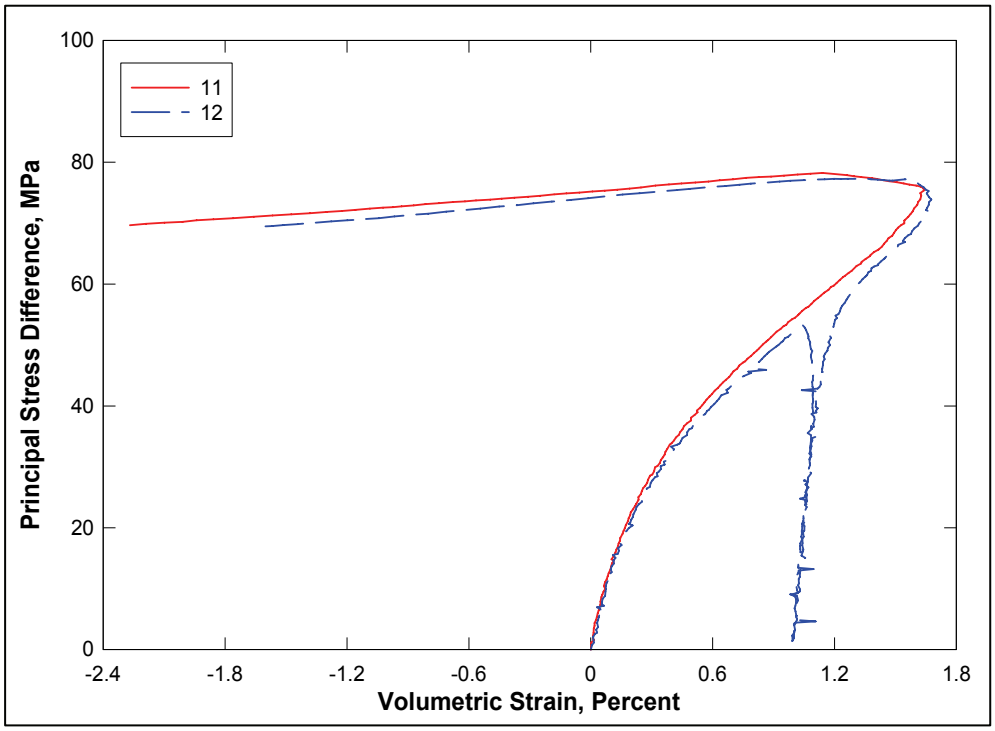

Figure 15. Stress difference-volume strain during shear from TXC tests at a confining pressure of 20 MPa

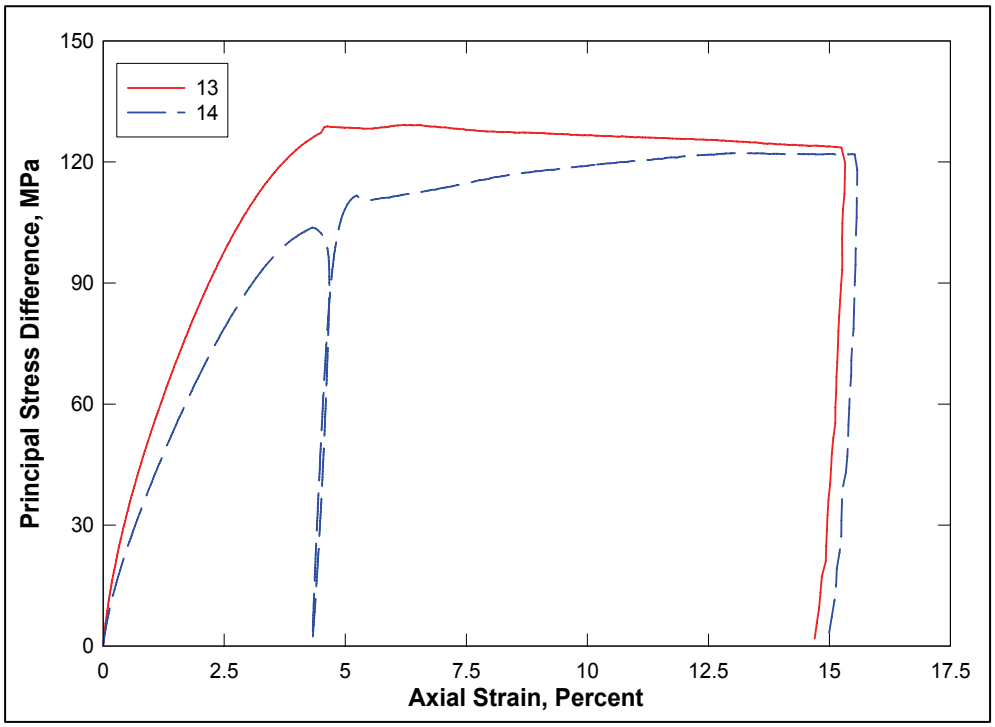

Figure 16. Stress-strain curves from TXC tests at a confining pressure of 50 MPa

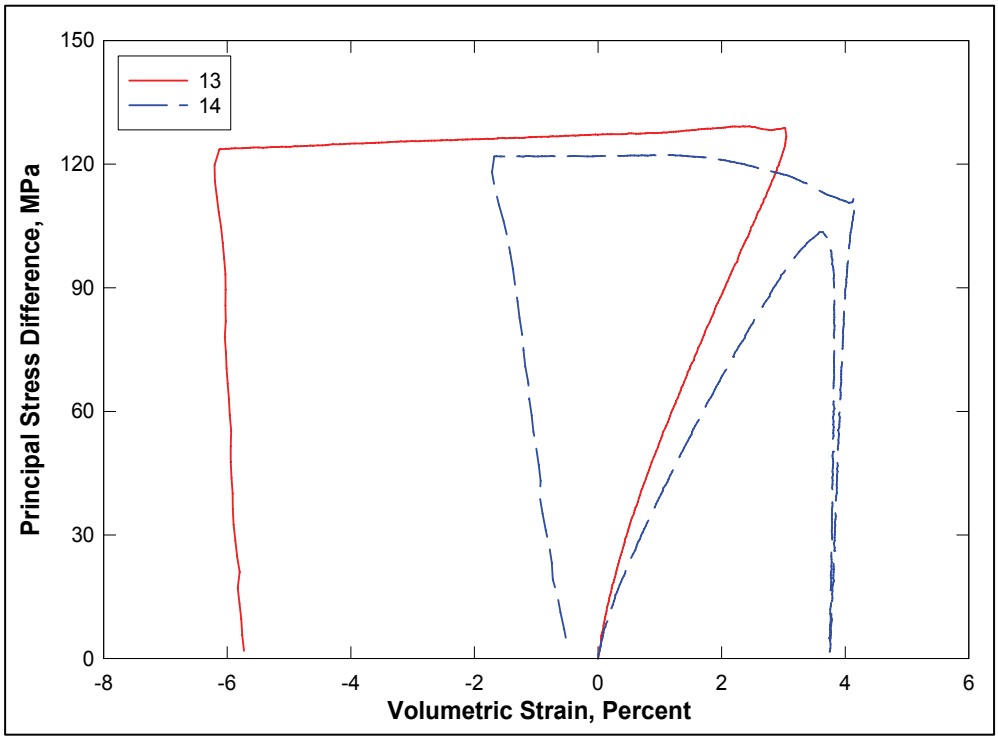

Figure 17. Stress difference-volume strain during shear from TXC tests at a confining pressure of 50 MPa

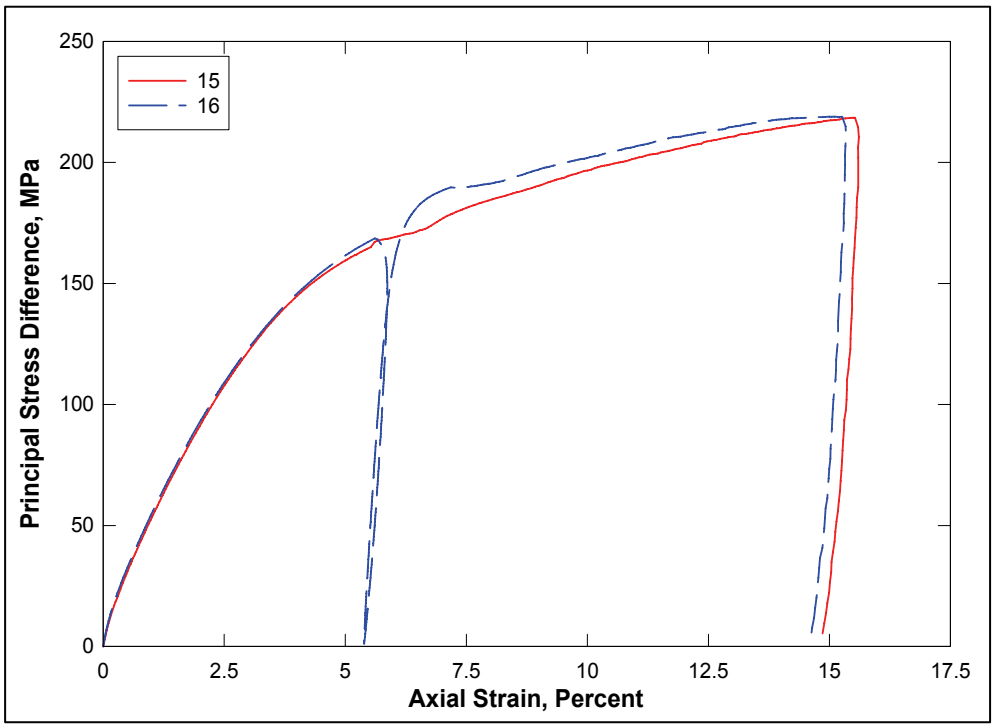

Figure 18. Stress-strain curves from TXC tests at a confining pressure of 100 MPa

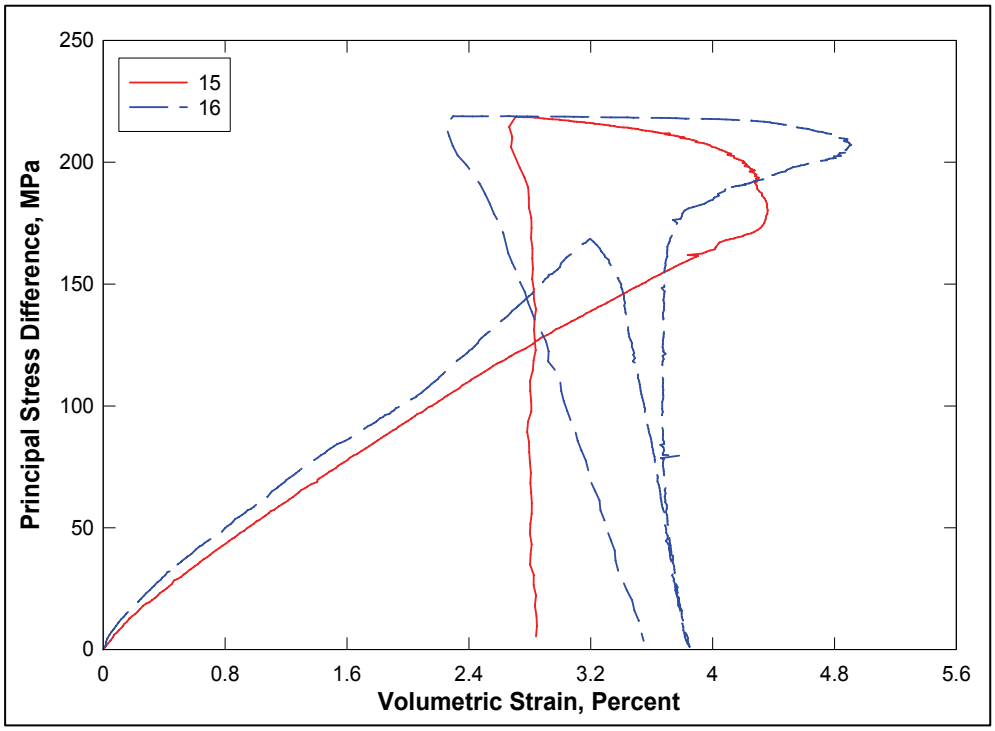

Figure 19. Stress difference-volume strain during shear from TXC tests at a confining pressure of 100 MPa

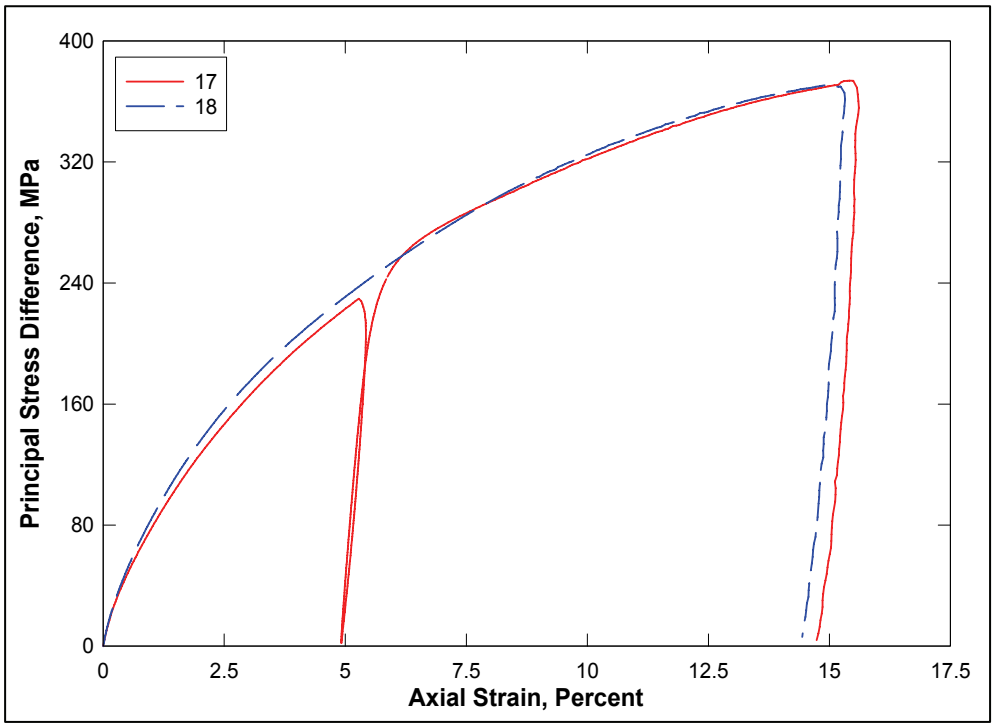

Figure 20. Stress-strain curves from TXC tests at a confining pressure of 200 MPa

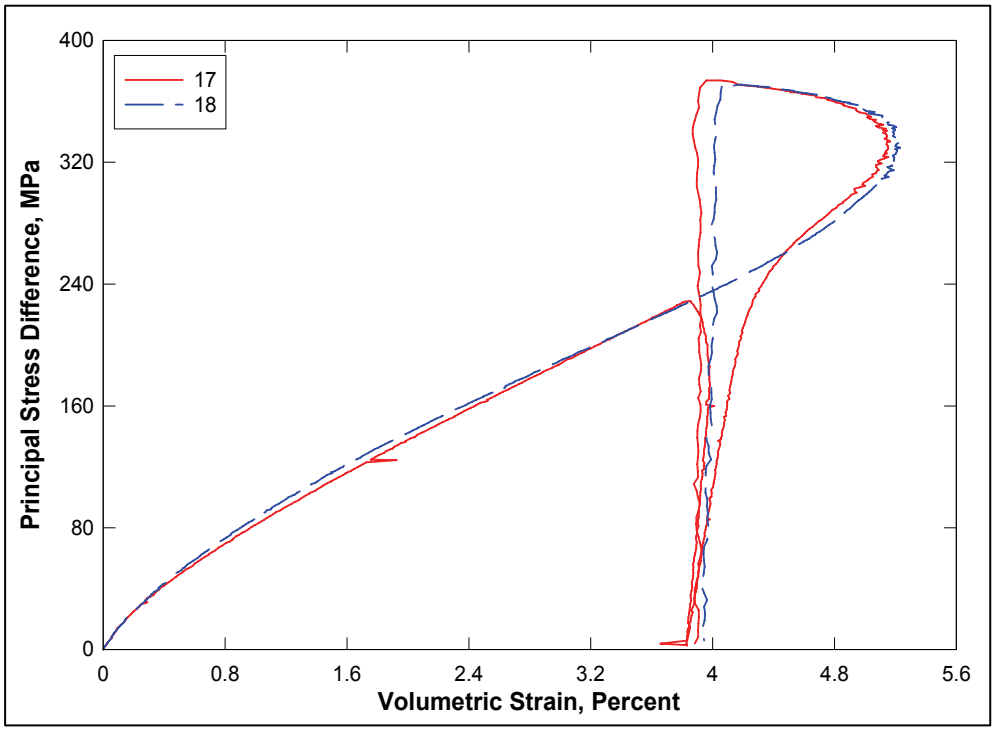

Figure 21. Stress difference-volume strain during shear from TXC tests at a confining pressure of 200 MPa

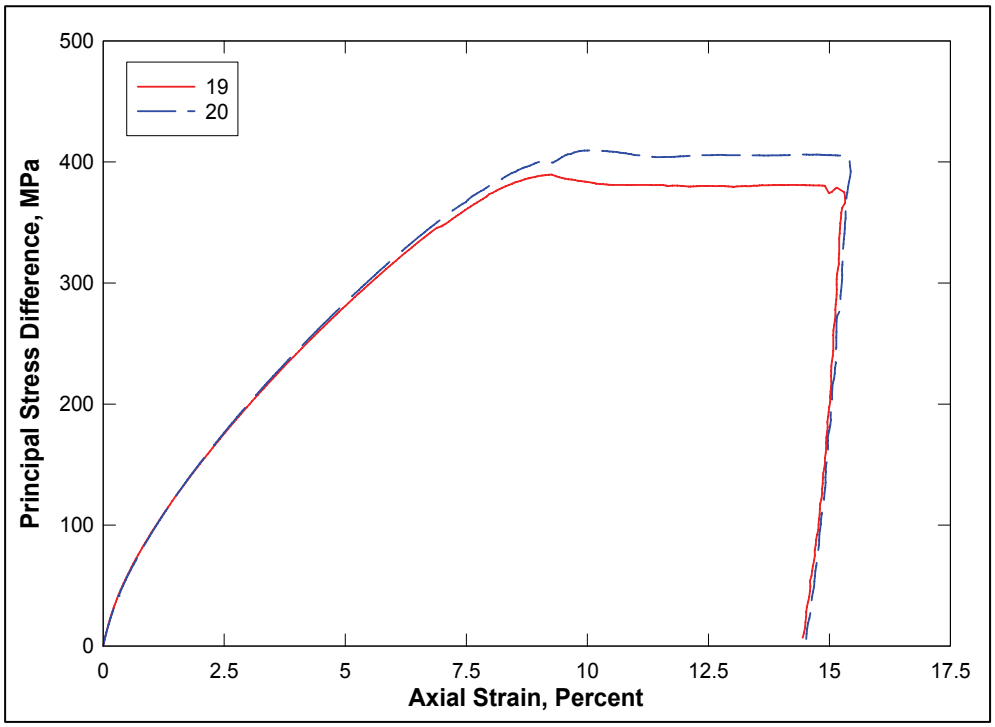

Figure 22. Stress-strain curves from TXC tests at a confining pressure of 300 MPa

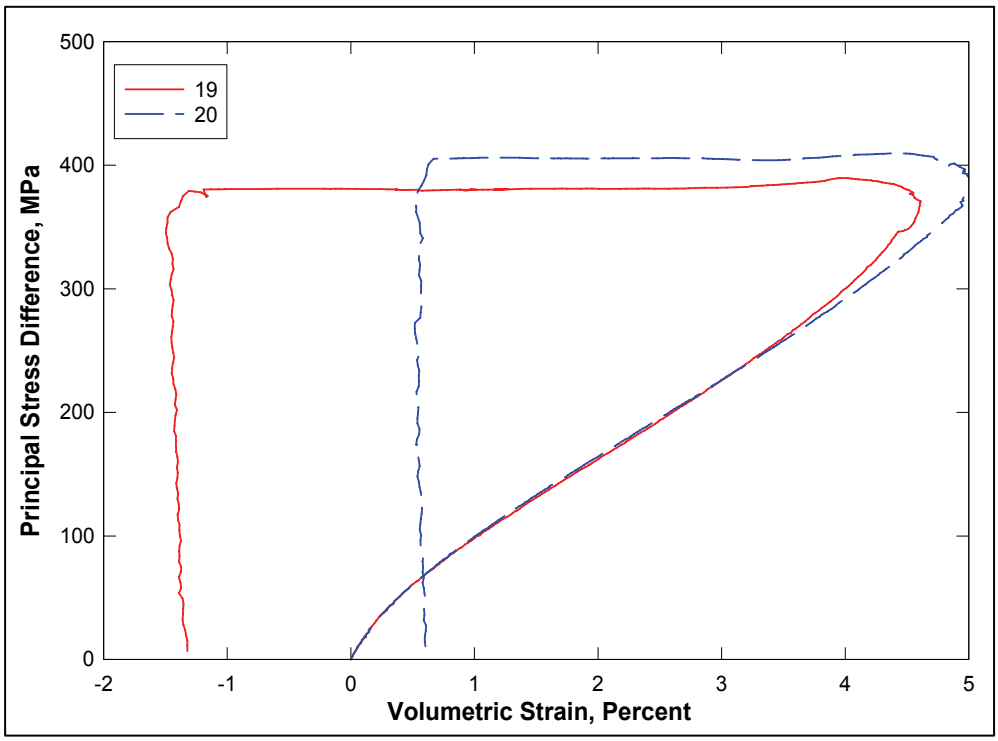

Figure 23. Stress difference-volume strain during shear from TXC tests at a confining pressure of 300 MPa

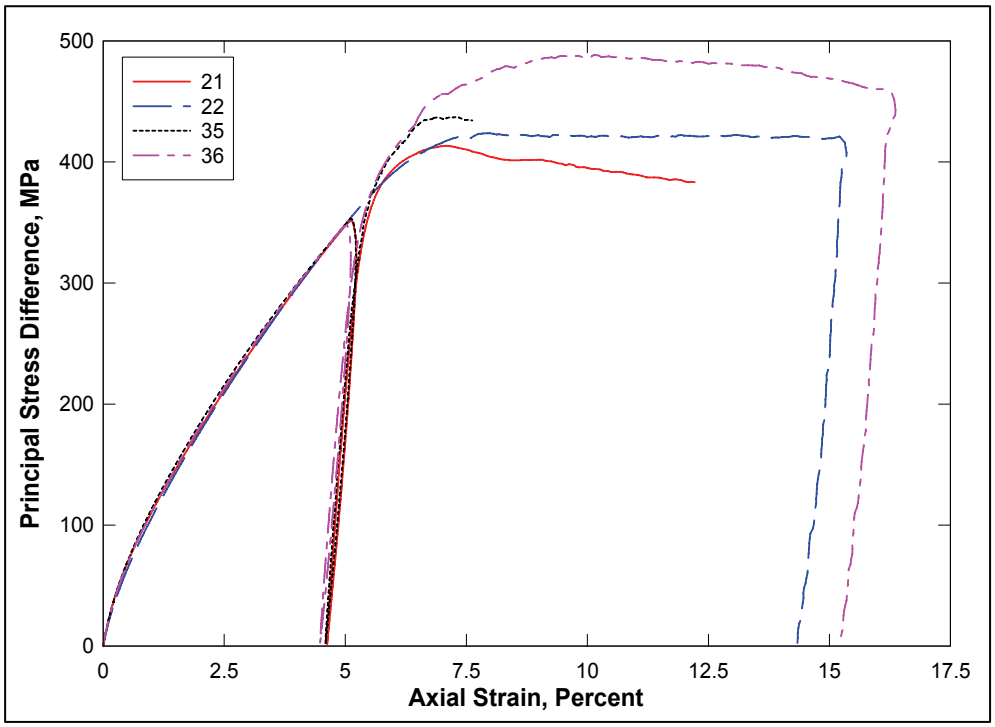

Figure 24. Stress-strain curves from TXC tests at a confining pressure of 400 MPa

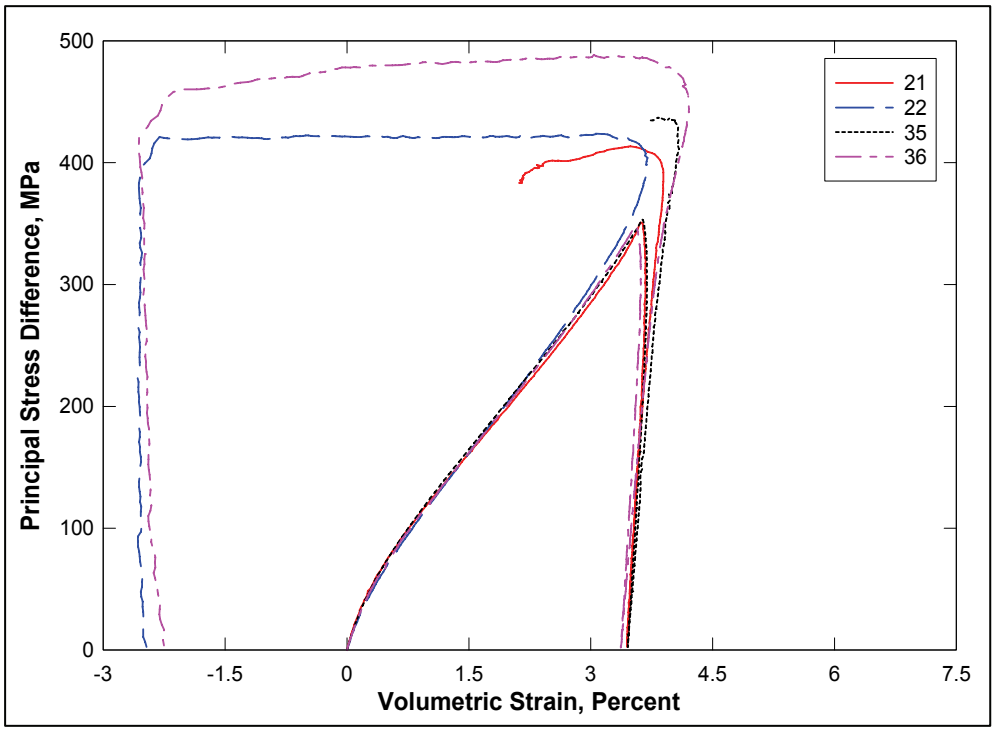

Figure 25. Stress difference-volume strain during shear from TXC tests at a confining pressure of 400 MPa

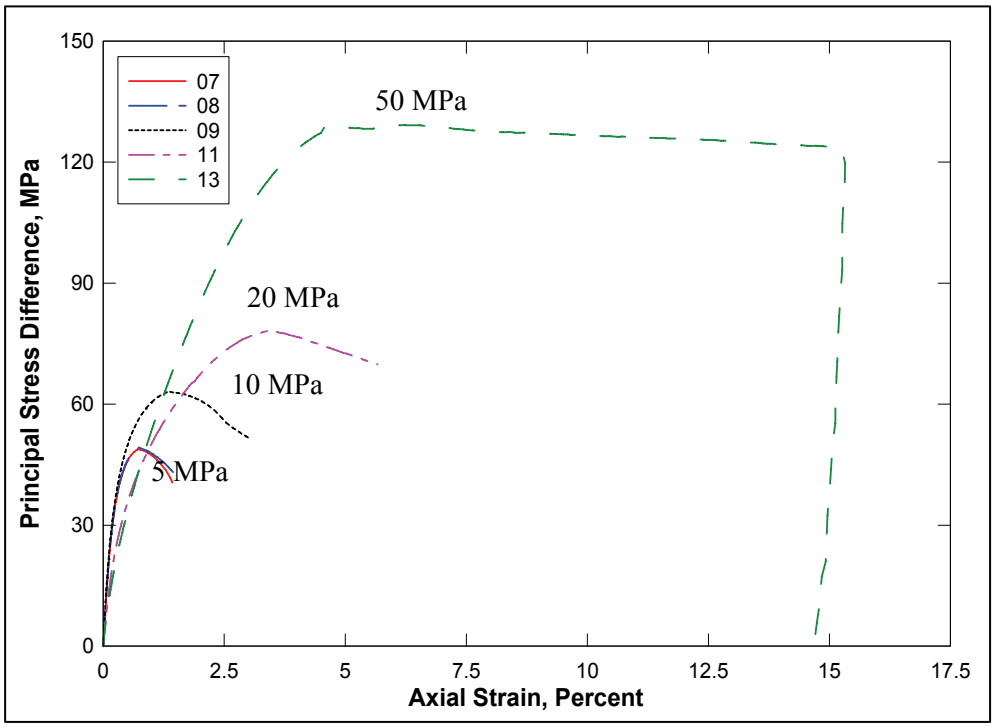

Figure 26. Stress-strain data from TXC non-cyclic tests at confining pressures between 5 and 50 MPa

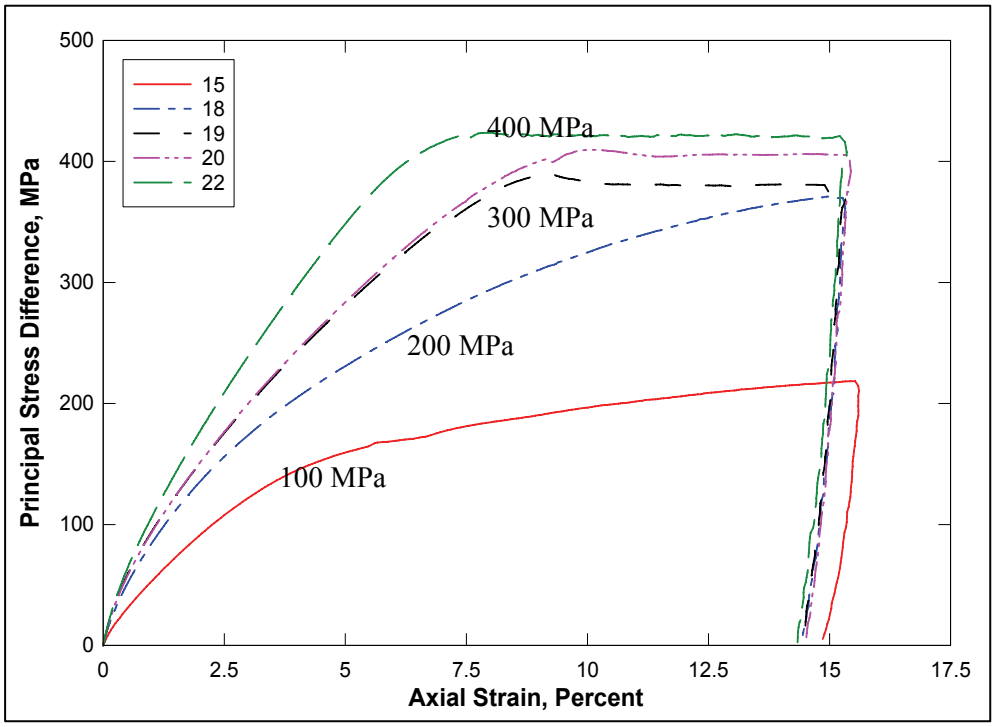

Figure 27. Stress-strain data from TXC non-cyclic tests at confining pressures between 100 and 400 MPa

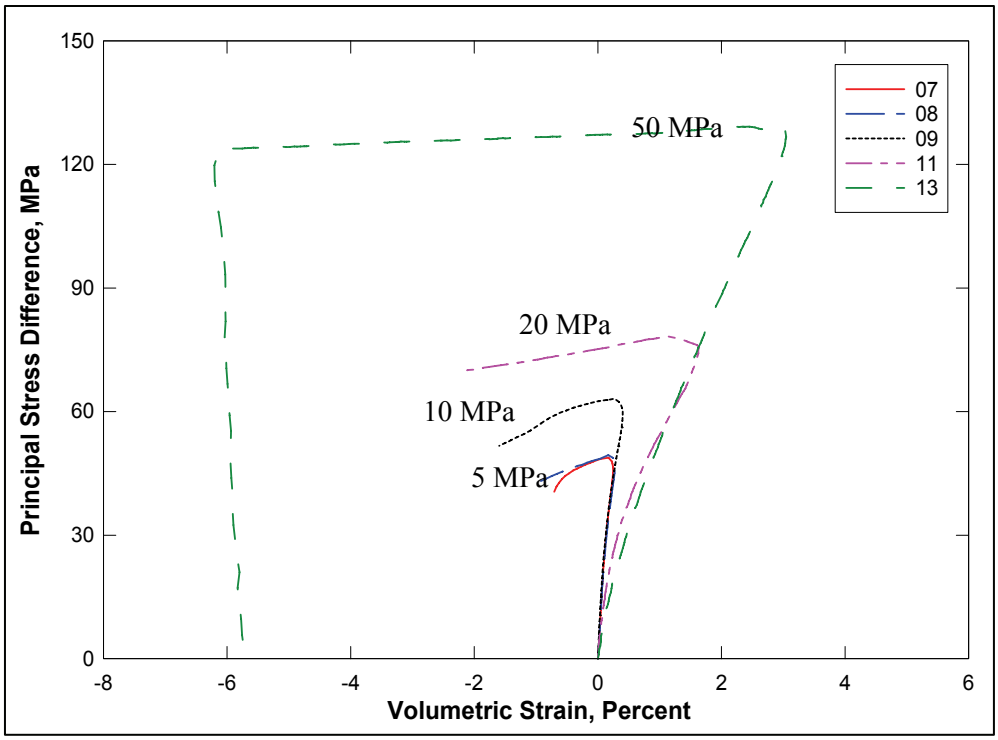

Figure 28. Stress difference-volume strain during shear from TXC non-cyclic tests at confining pressures between 5 and 50 MPa

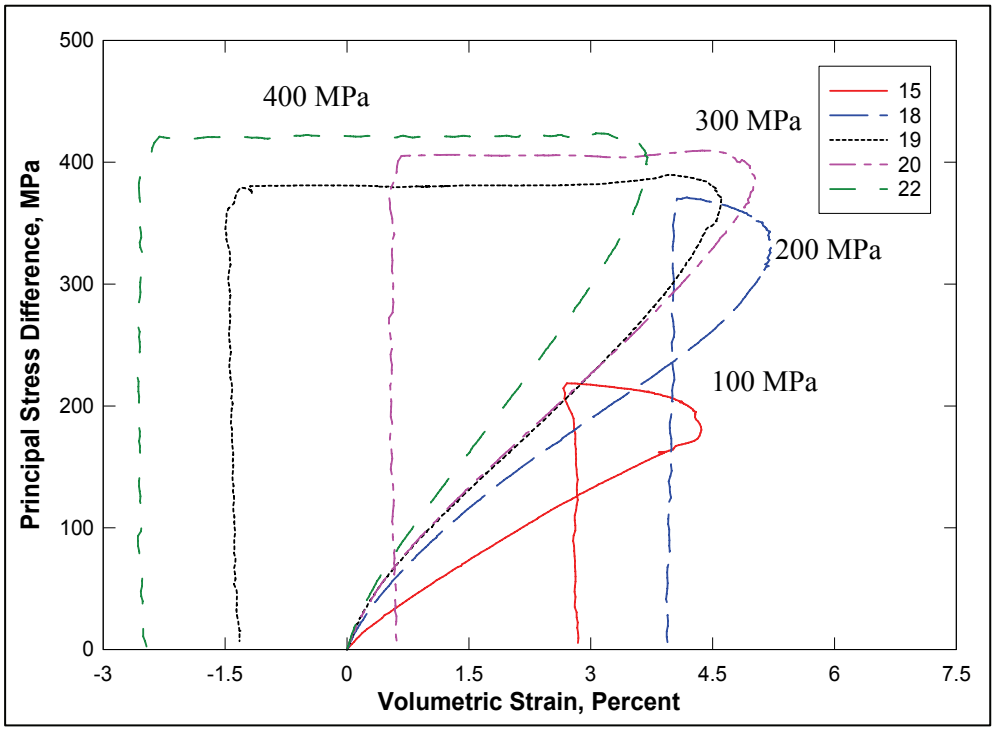

Figure 29. Stress difference-volume strain during shear from TXC non-cyclic tests at confining pressures between 50 and 400 MPa

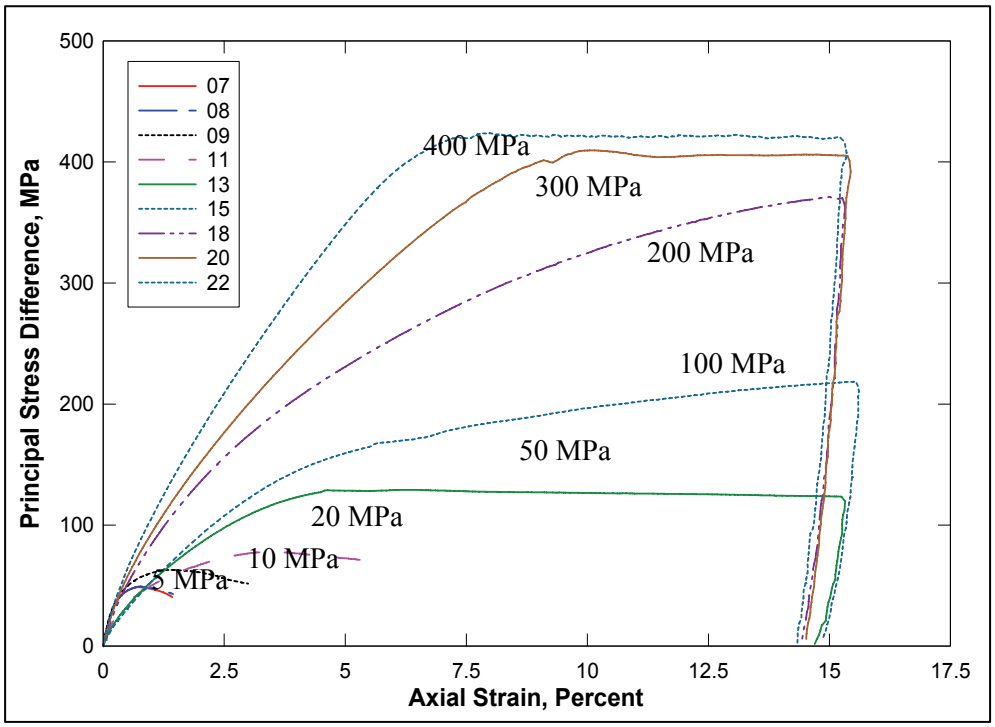

Figure 30. Stress-strain data from TXC non-cyclic tests at confining pressures between 5 and 400 MPa

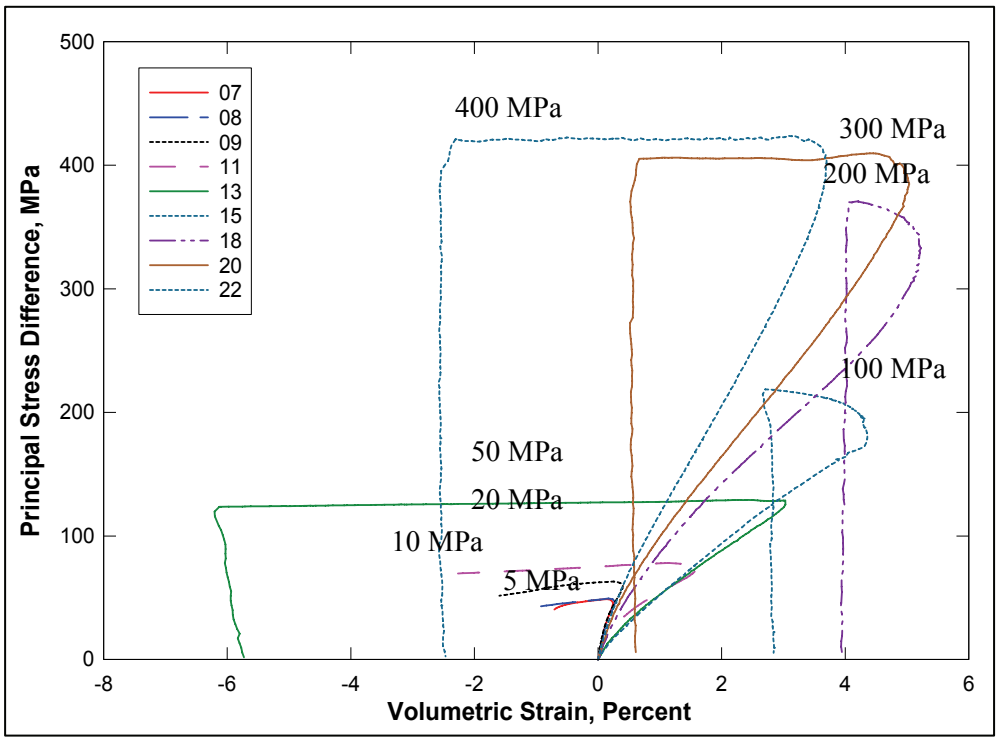

Figure 31. Stress difference-volume strain during shear from TXC non-cyclic tests at confining pressures between 5 and 400 MPa

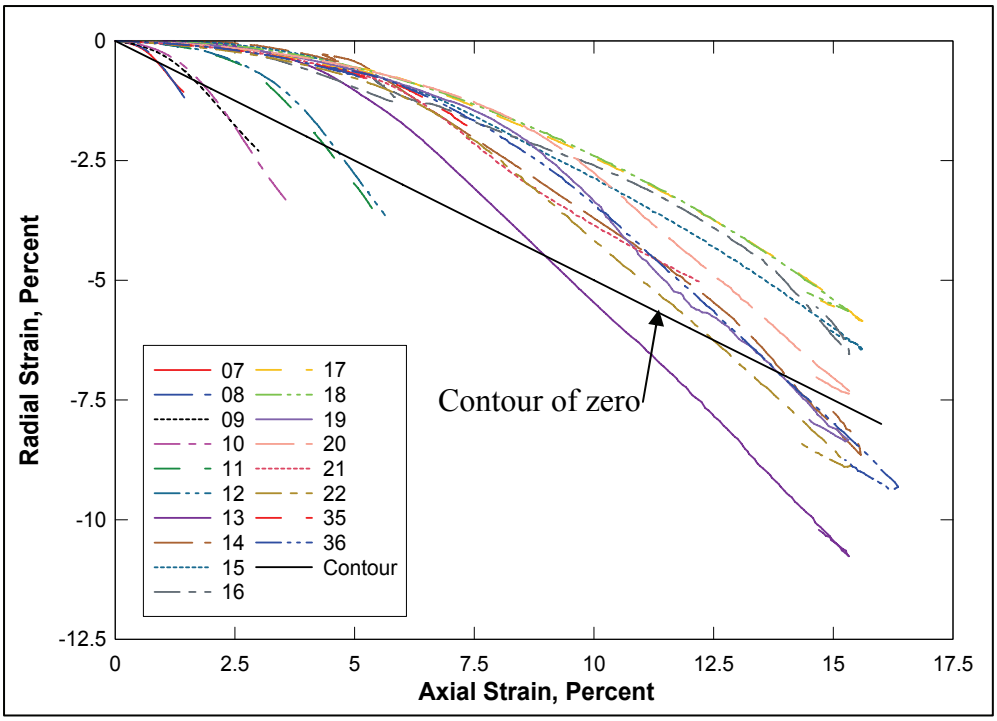

Figure 32. Radial strain-axial strain data during shear from TXC tests at confining pressures between 5 and 400 MPa

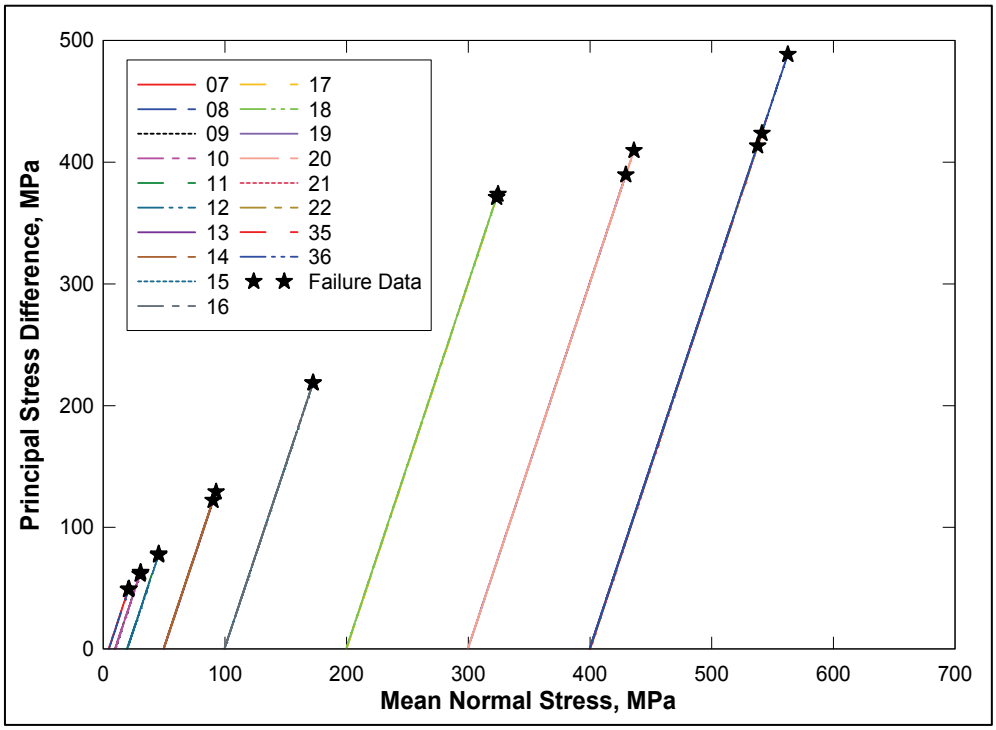

Figure 33. Stress paths from TXC tests at confining pressures between 5 and 400 MPa

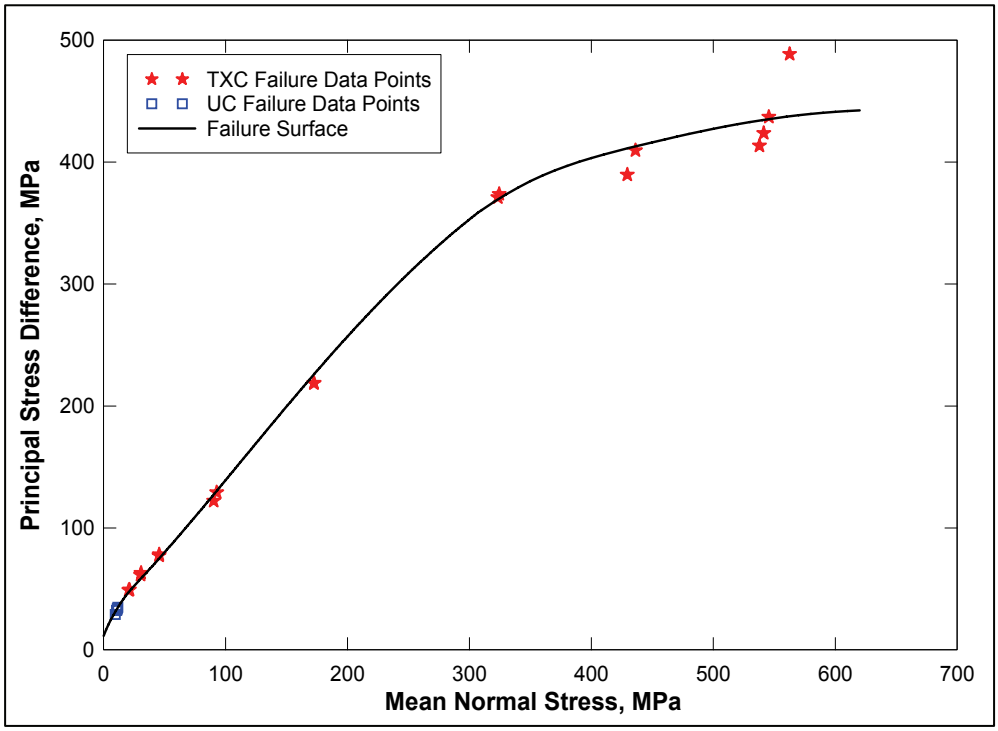

Figure 34. Failure points from UC and TXC tests and recommended compression failure surface

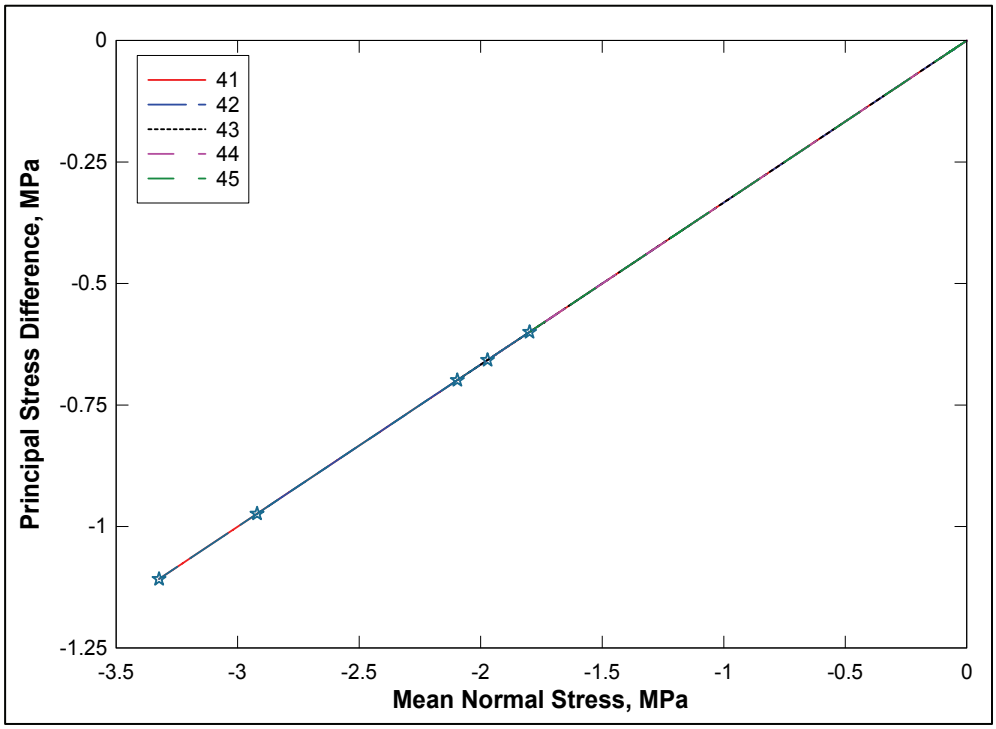

Figure 35. Stress paths from DP tests

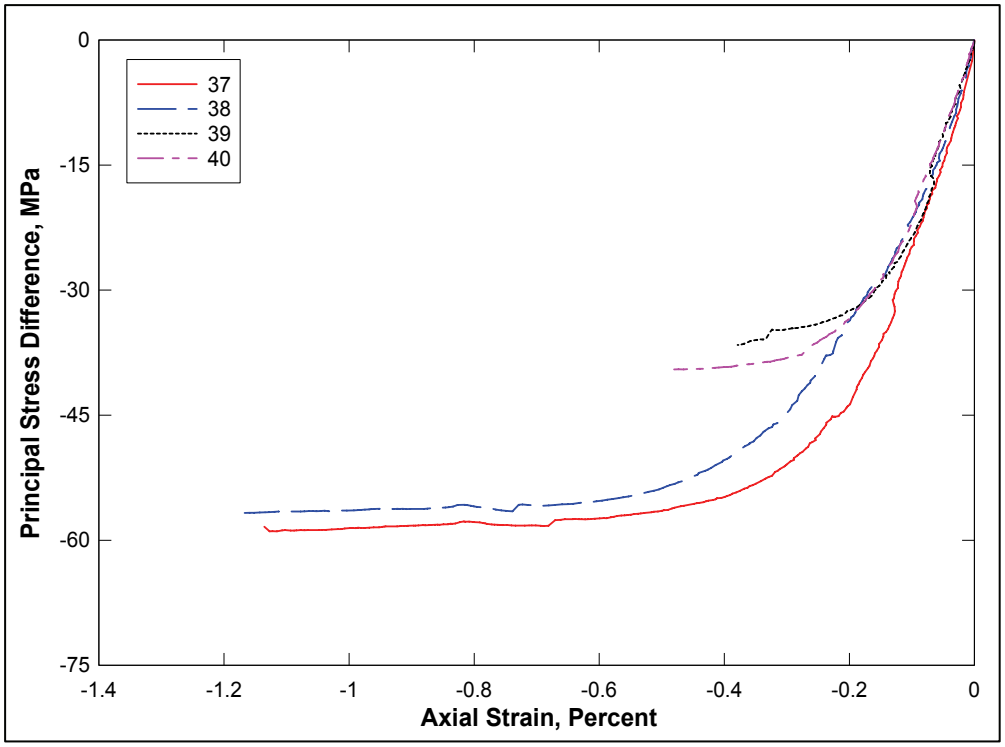

Figure 36. Stress-strain curves from RTE tests

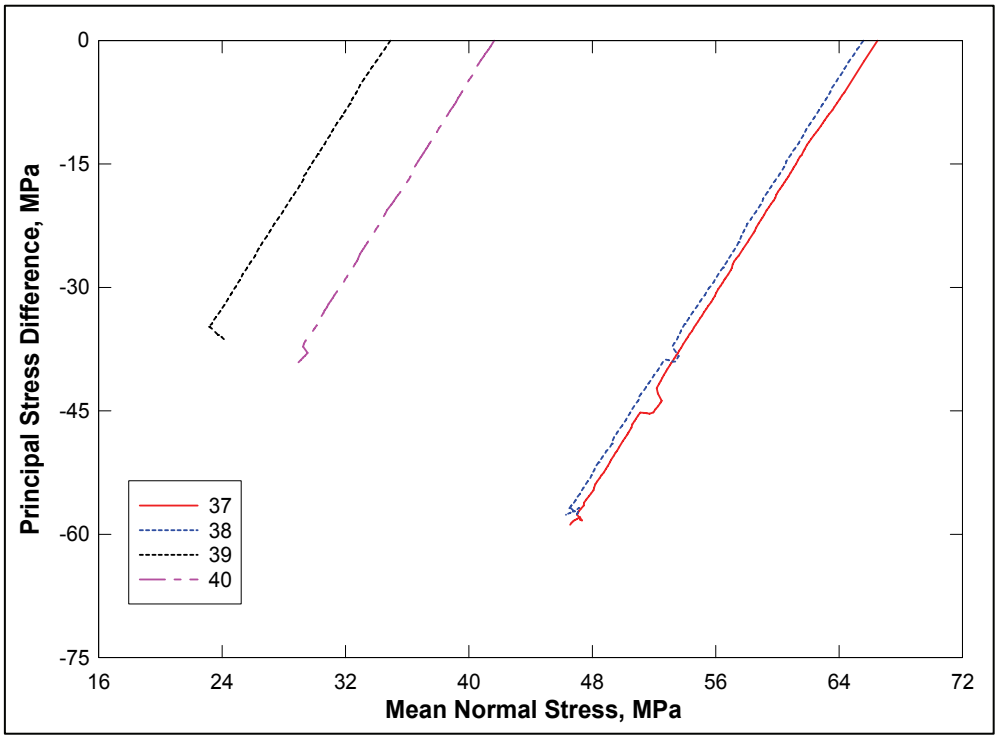

Figure 37. Stress paths from RTE tests

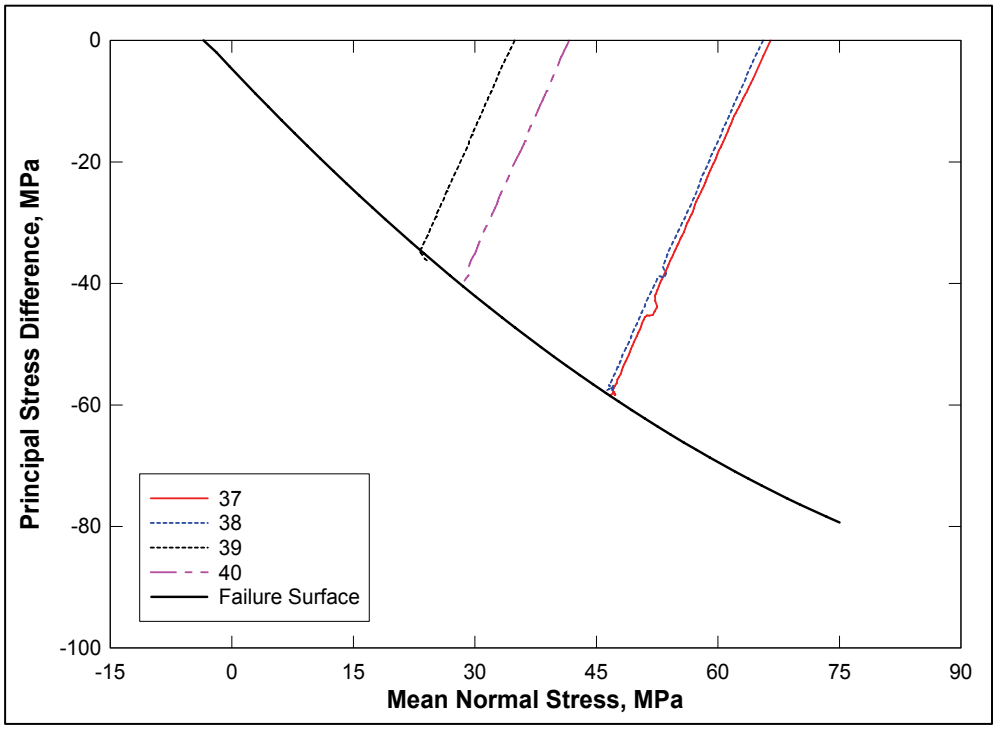

Figure 38. Stress paths from RTE tests at confining pressures between 35 and 65 MPa and the recommended extension failure surface

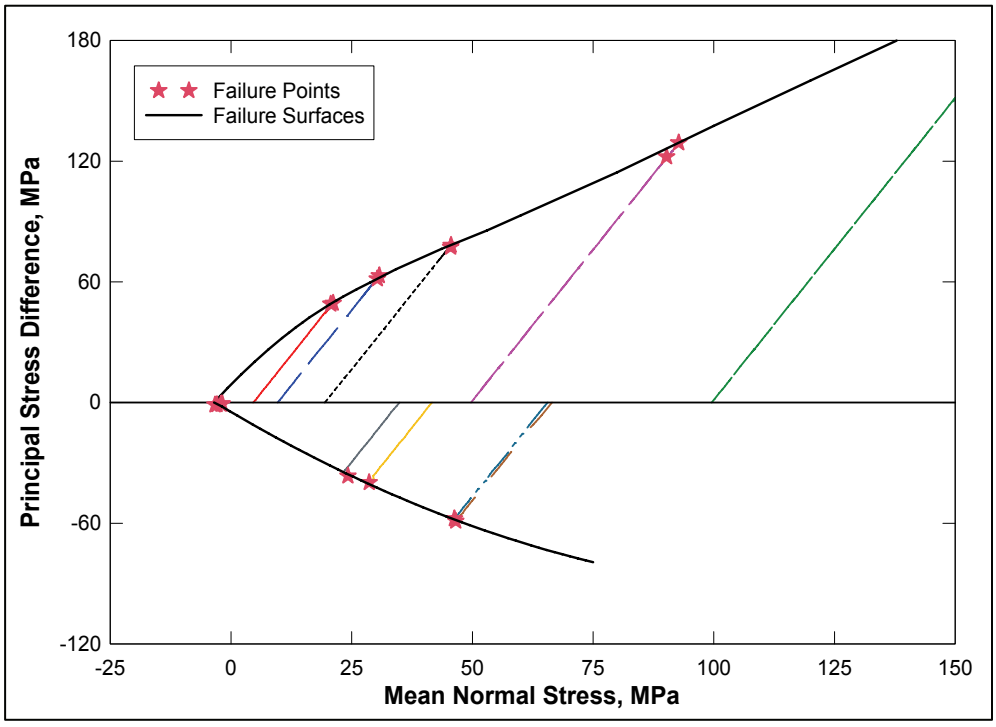

Figure 39. Failure surfaces and stress paths from RTE tests and the TXC tests between 5 MPa to 100 MPa

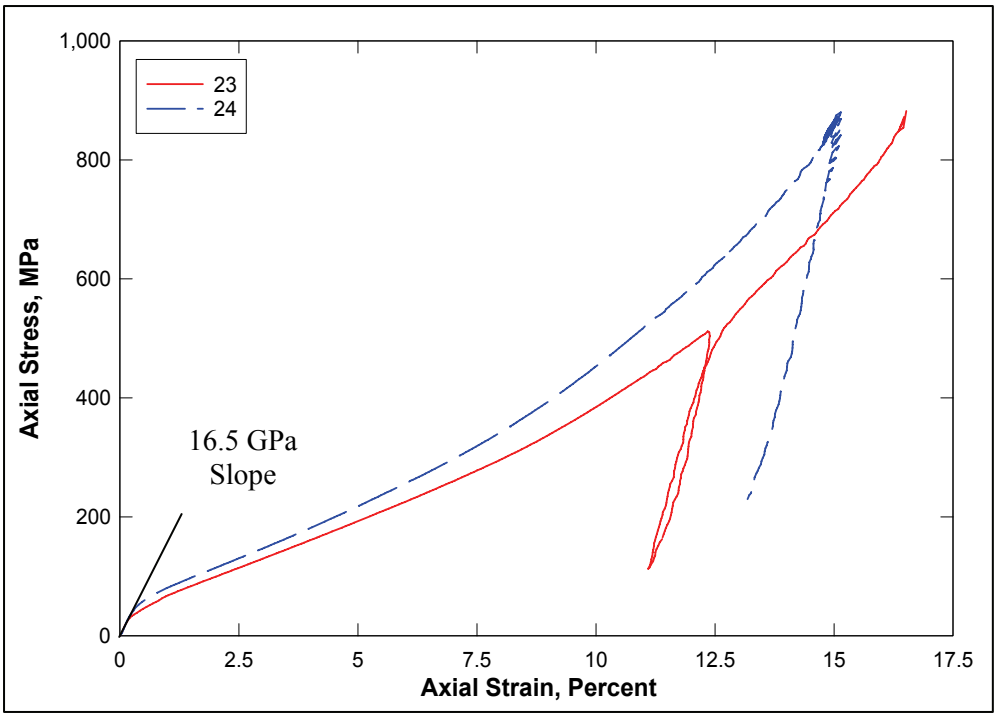

Figure 40. Stress-strain curves from UX tests

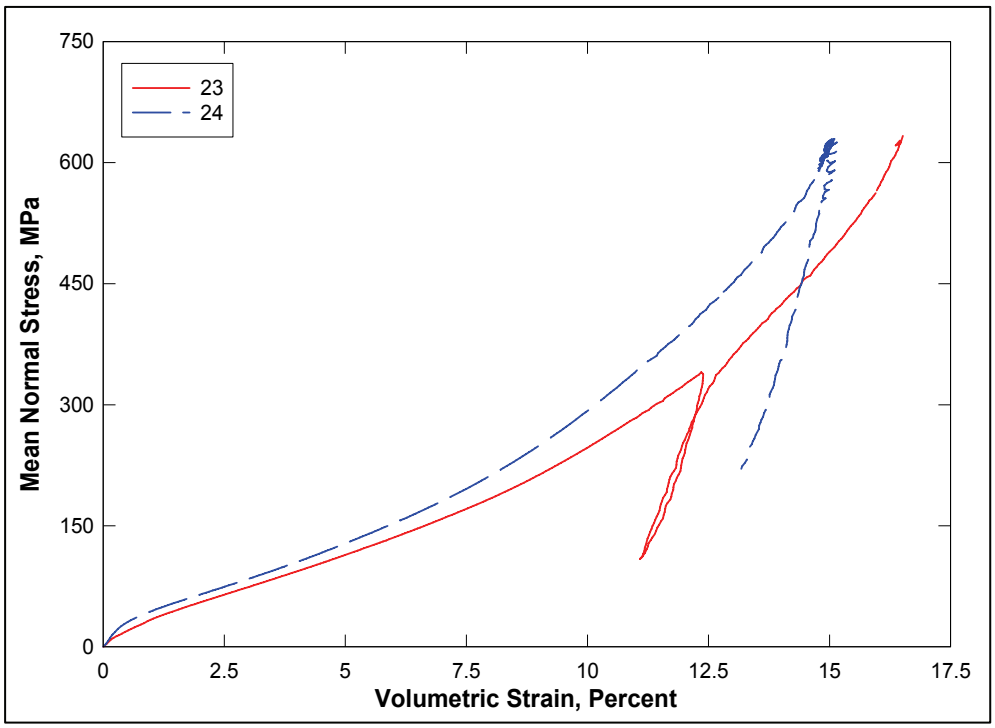

Figure 41. Pressure-volume data from UX tests

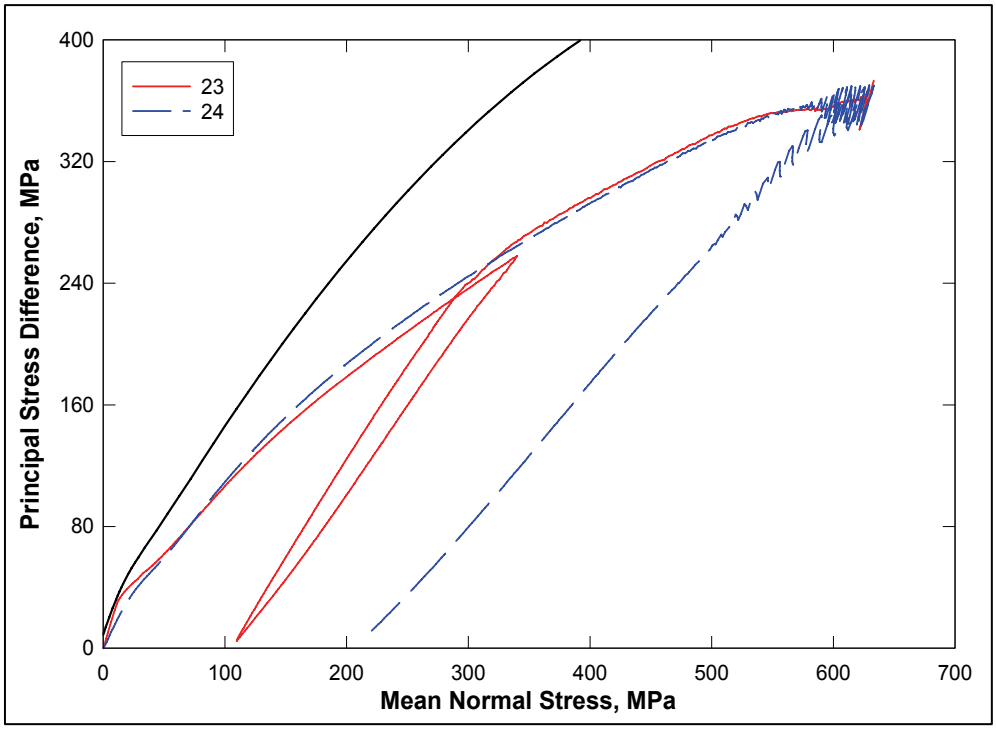

Figure 42. Stress paths from UX tests and failure surface from TXC tests

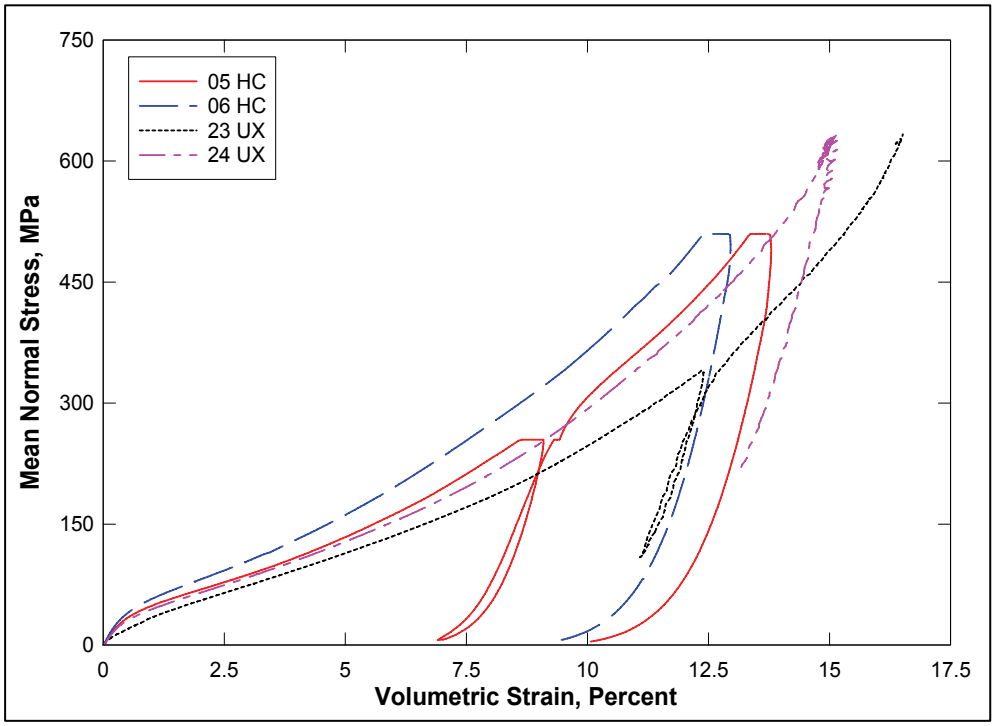

Figure 43. Comparison of pressure-volume data from HC and UX tests

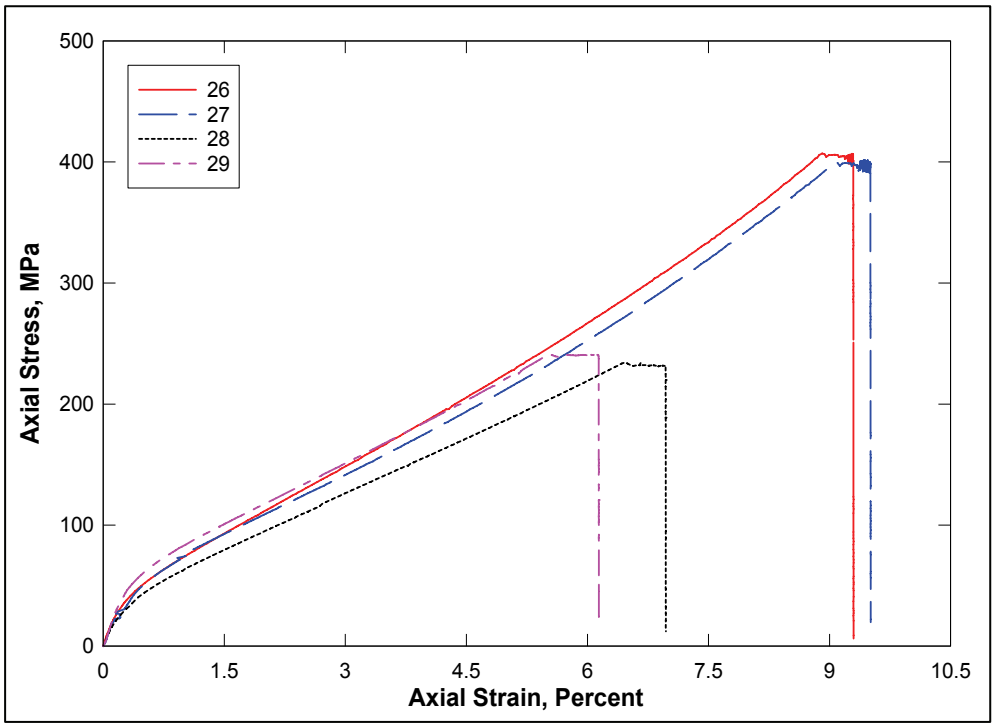

Figure 44. Stress-strain curves from UX/BX tests

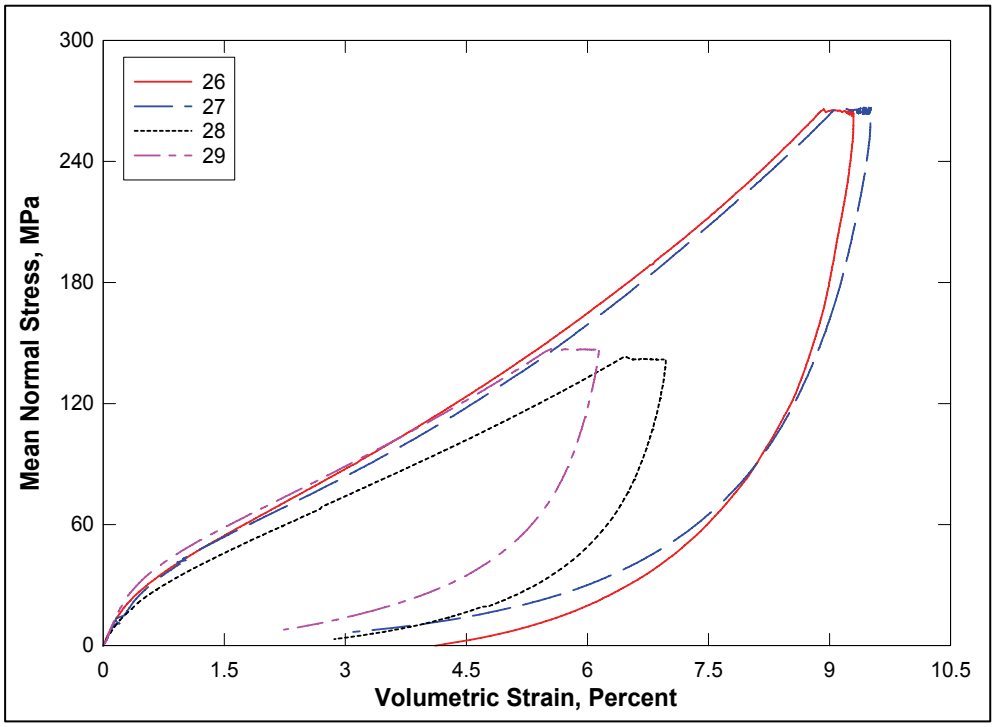

Figure 45. Pressure-volume data from UX/BX tests

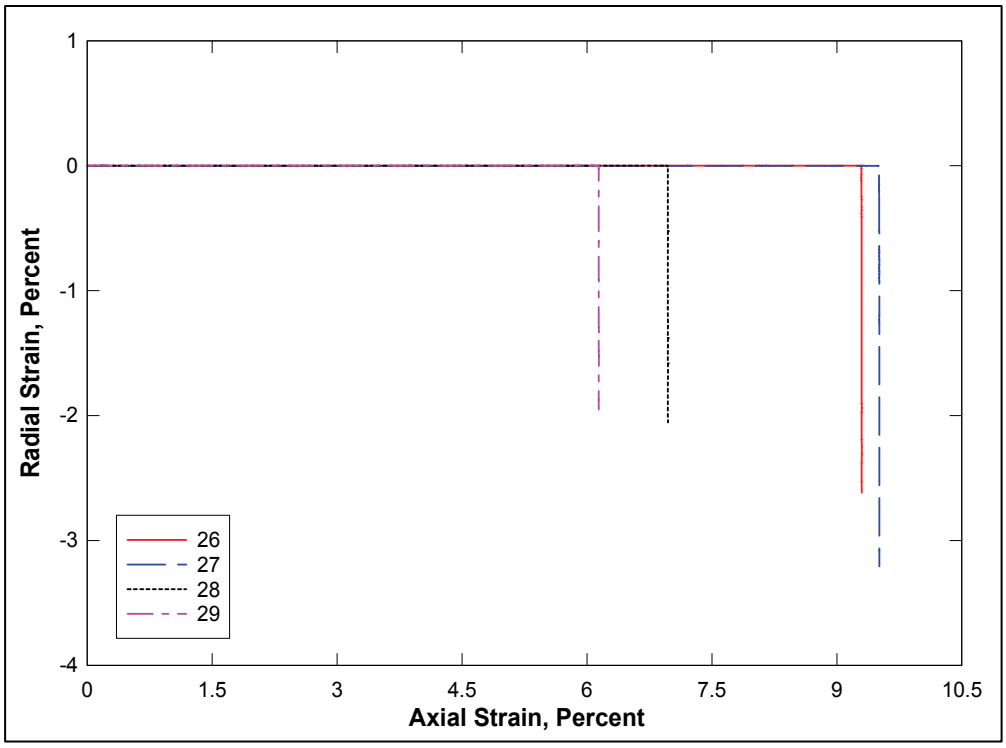

Figure 46. Strain paths from UX/BX tests

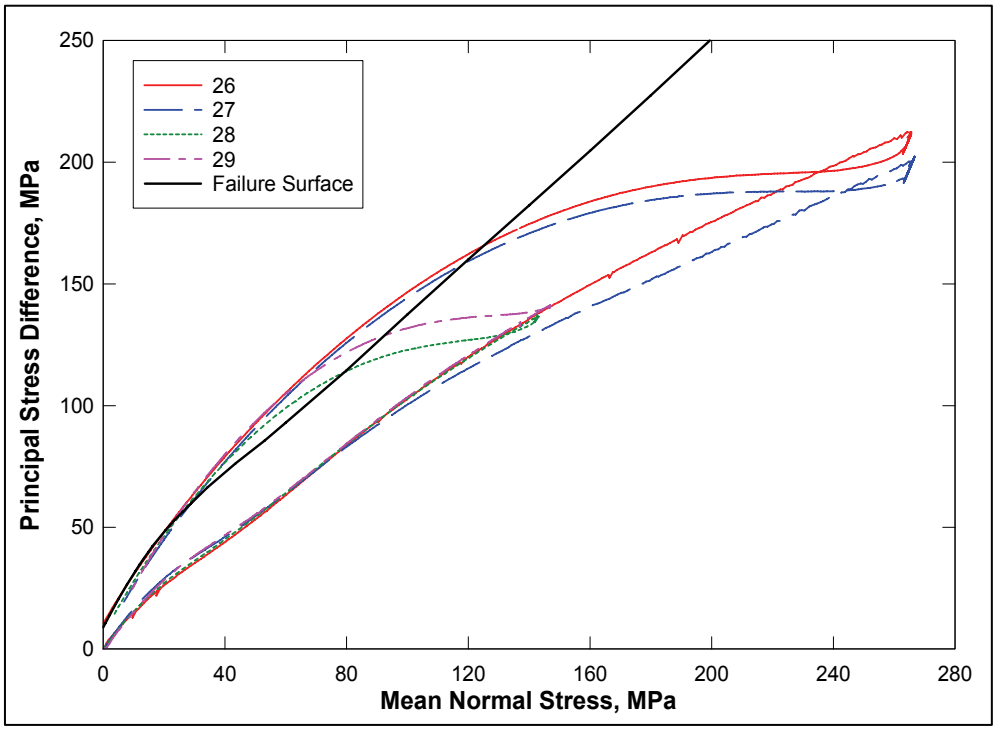

Figure 47. Stress paths from UX/BX tests and failure surface from TXC tests

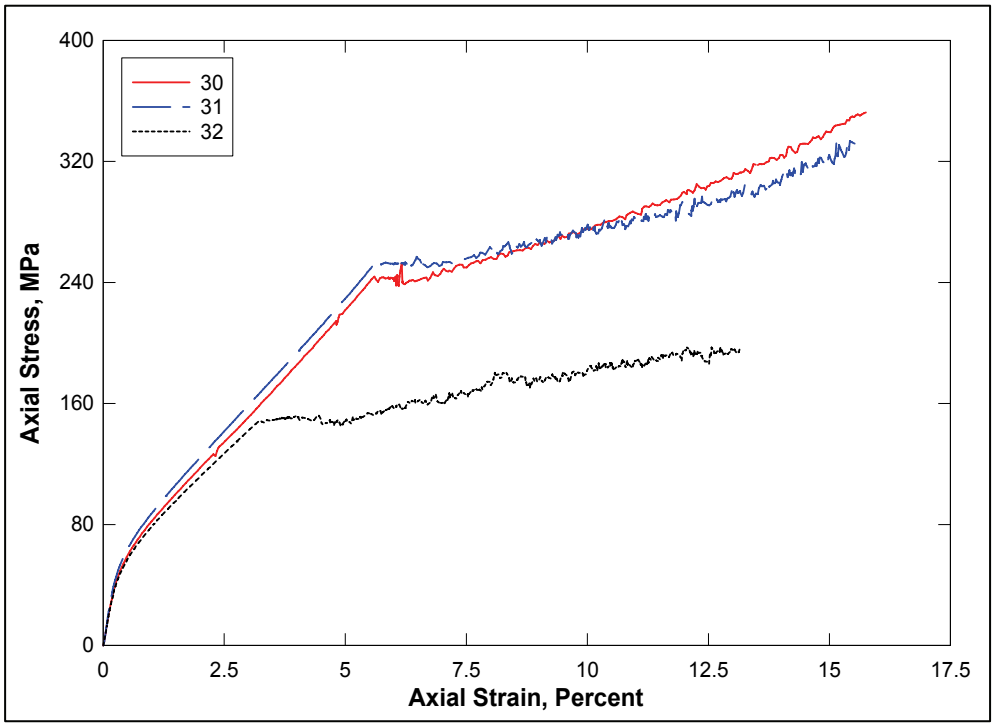

Figure 48. Stress-strain curves from UX/CV tests

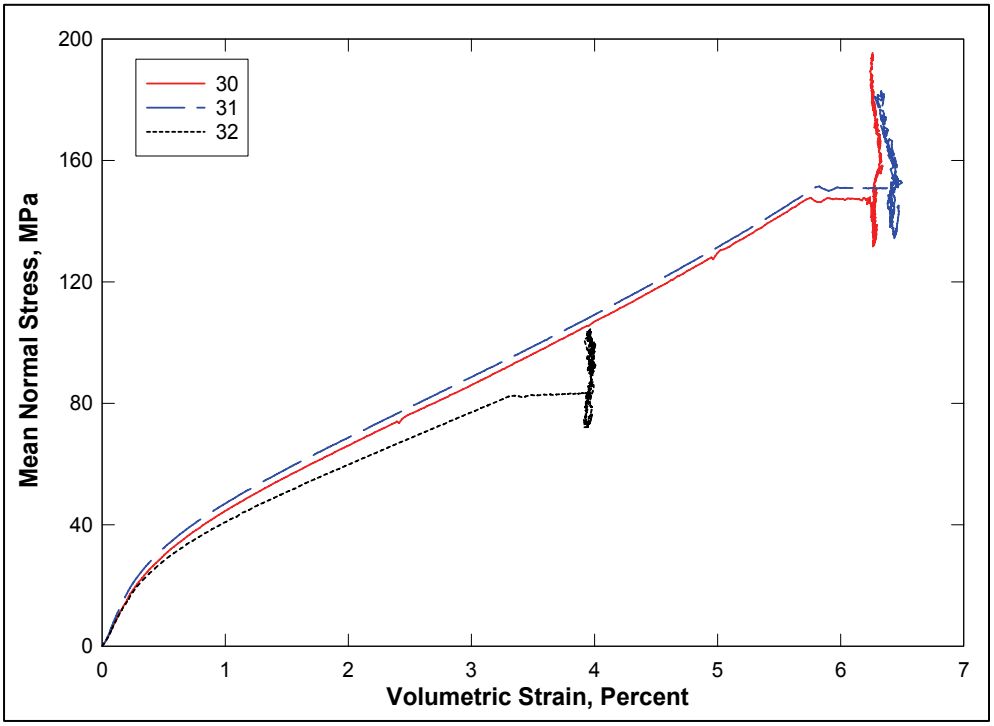

Figure 49. Pressure-volume data from UX/CV tests

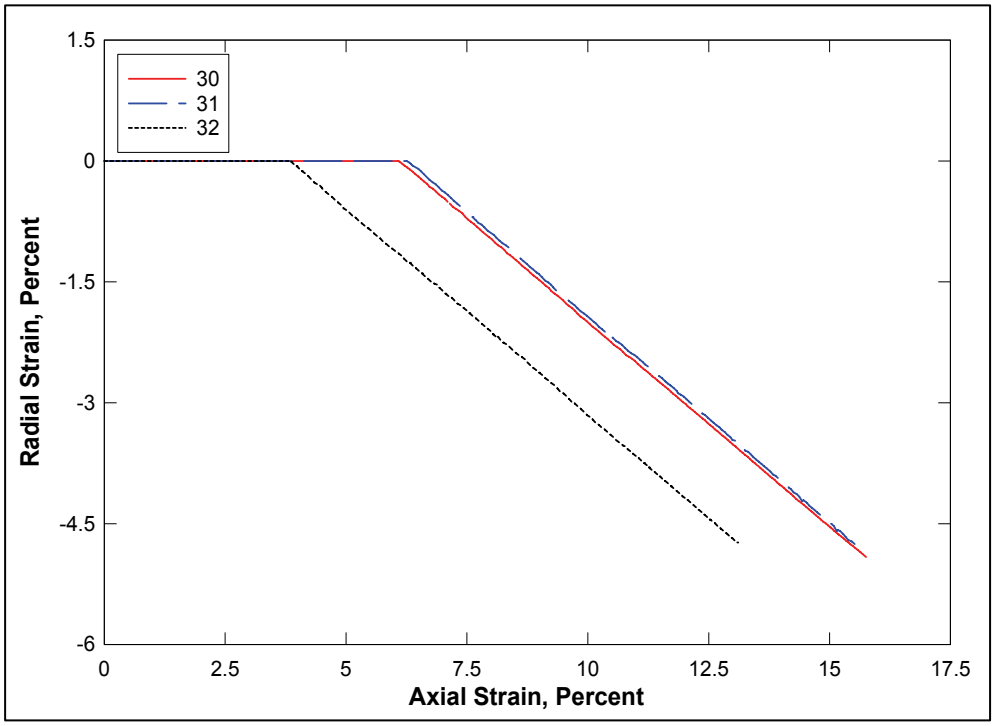

Figure 50. Strain paths from UX/CV tests

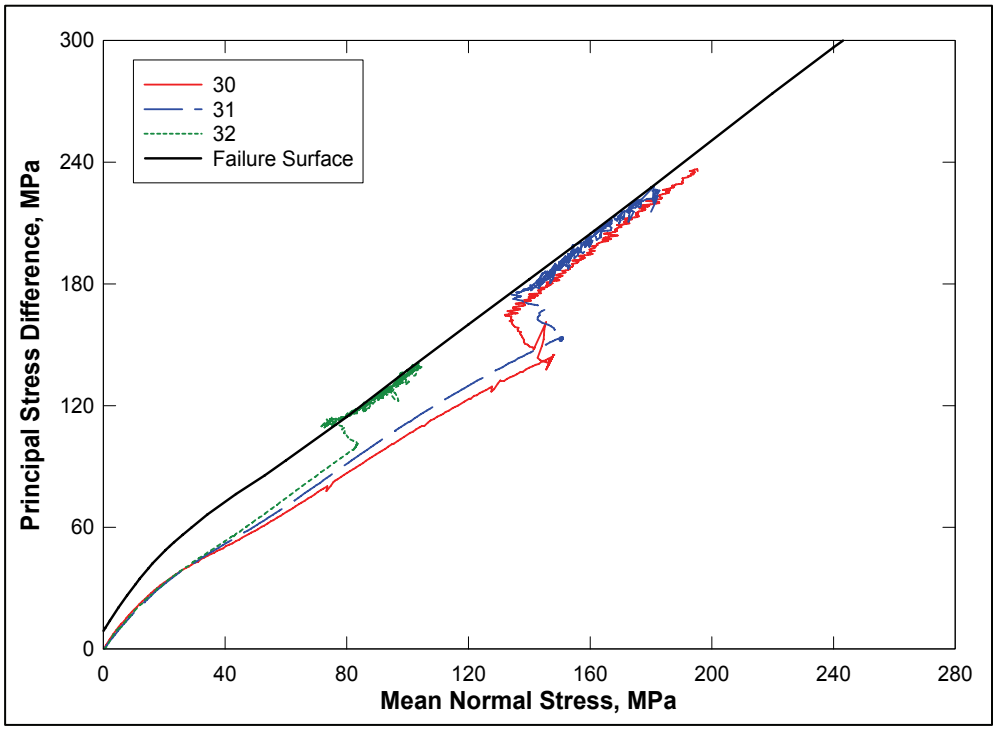

Figure 51. Stress paths from UX/CV tests and failure surface from TXC tests

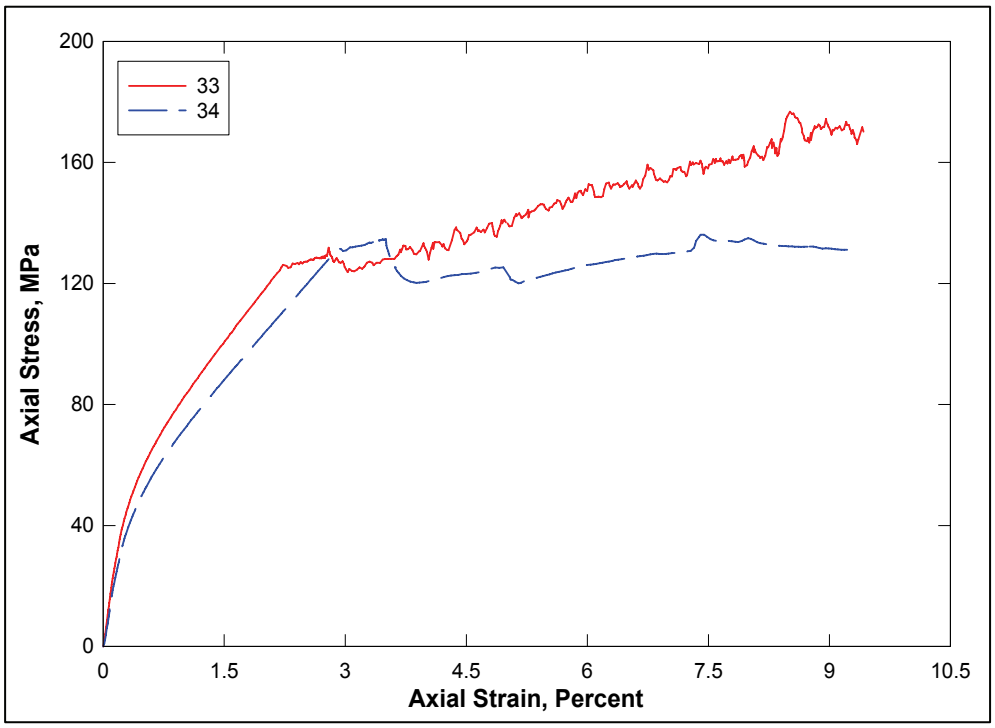

Figure 52. Stress-strain curves from UX/SR tests

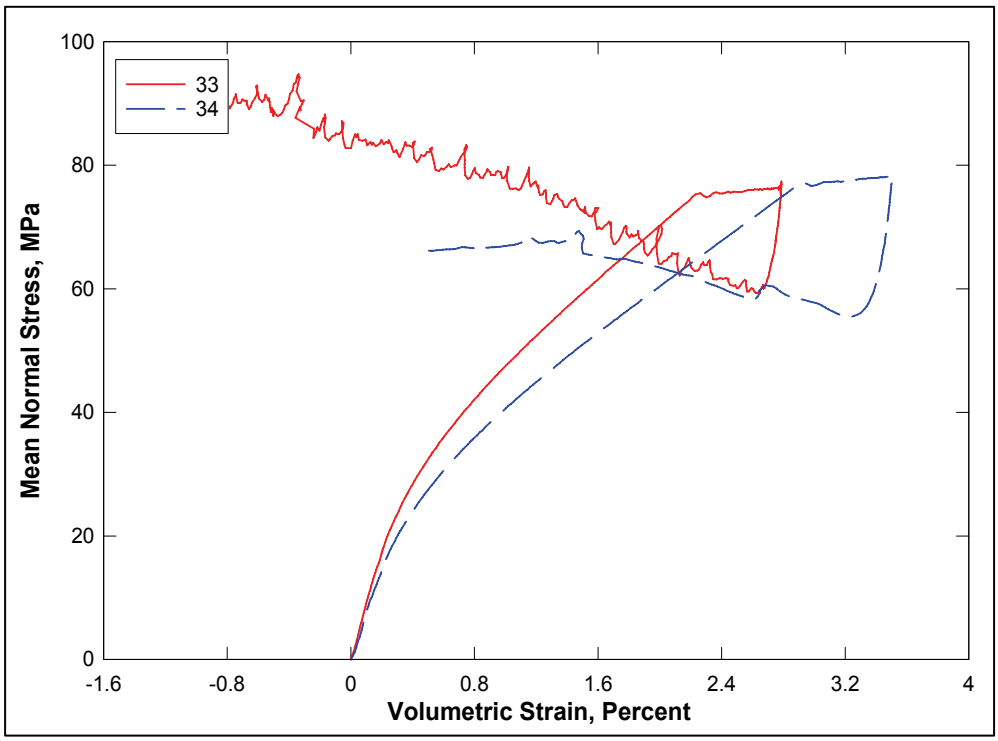

Figure 53. Pressure-volume data from UX/SR tests

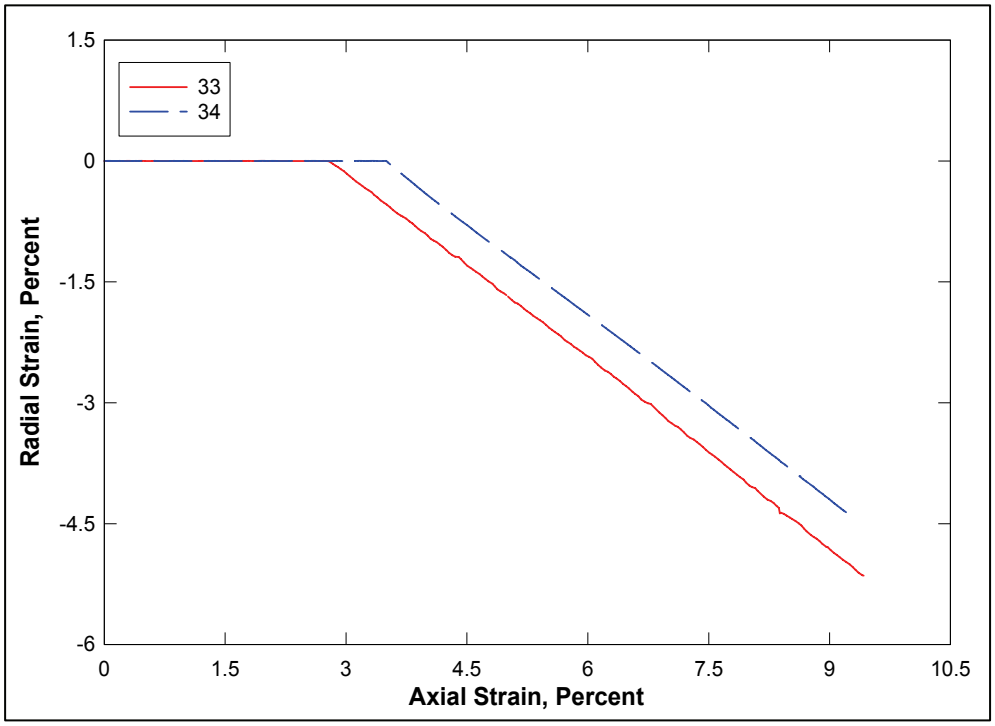

Figure 54. Strain paths from UX/SR tests

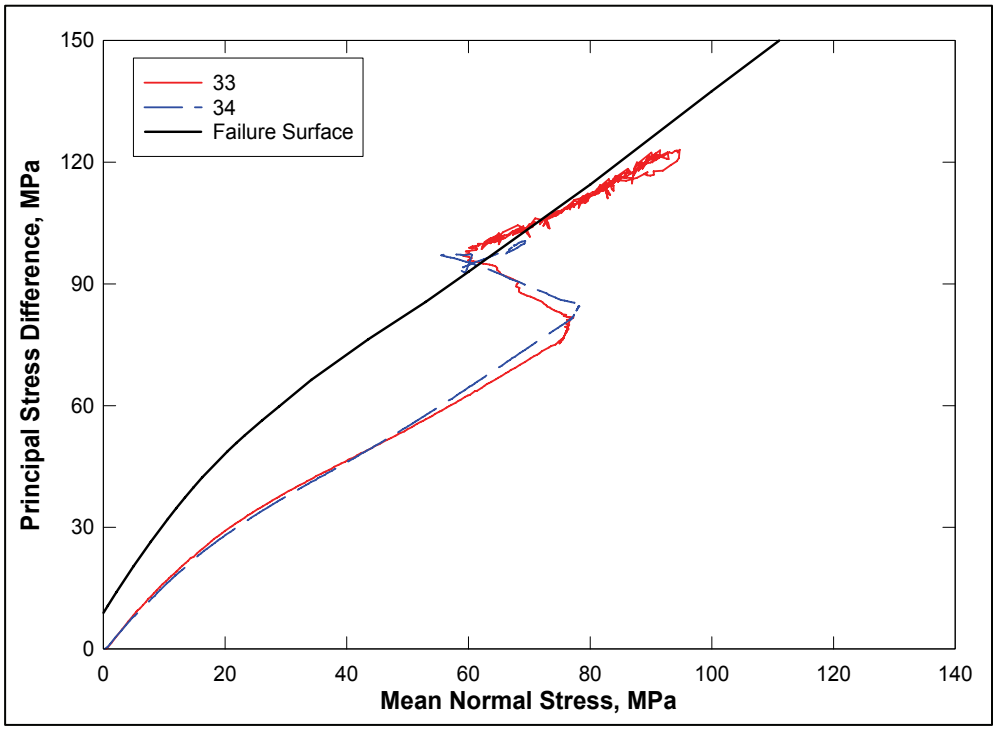

Figure 55. Stress paths from UX/SR tests and failure surface from TXC tests

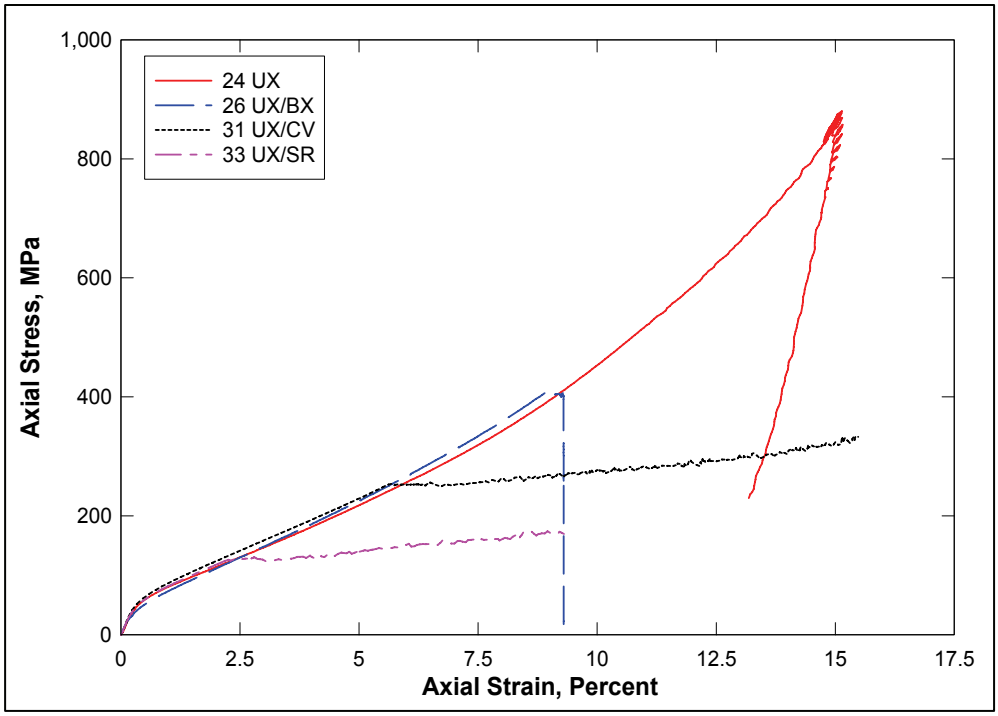

Figure 56. Stress-strain curves from selected UX, UX/BX, UX/SR, and UX/CV tests

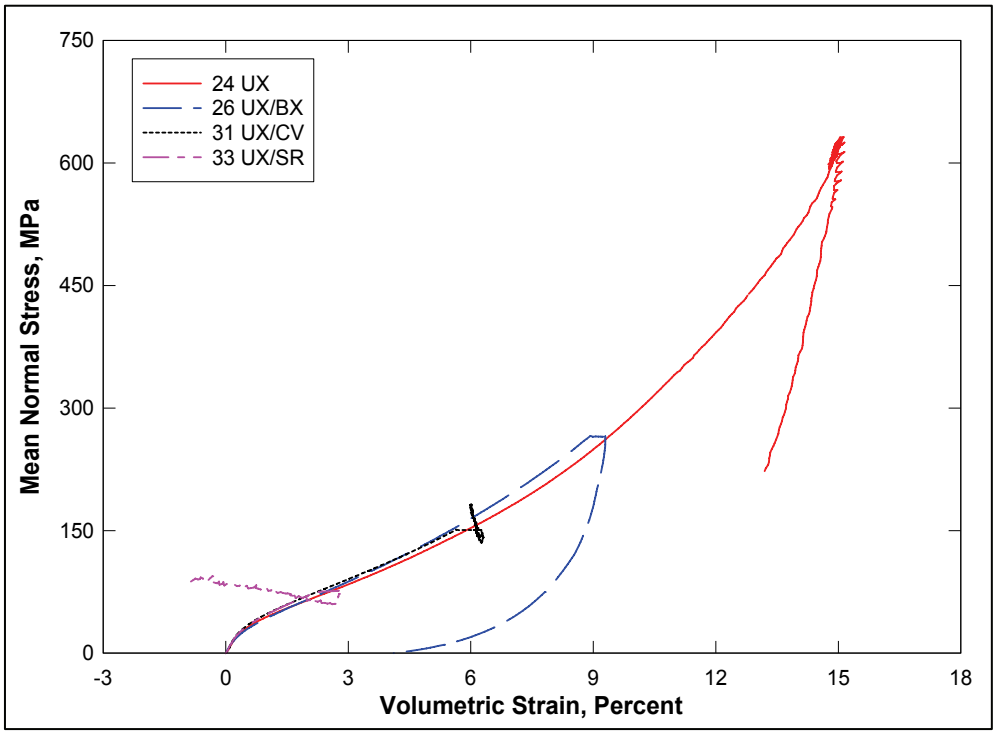

Figure 57. Pressure-volume data from selected UX, UX/BX, UX/SR, and UX/CV tests

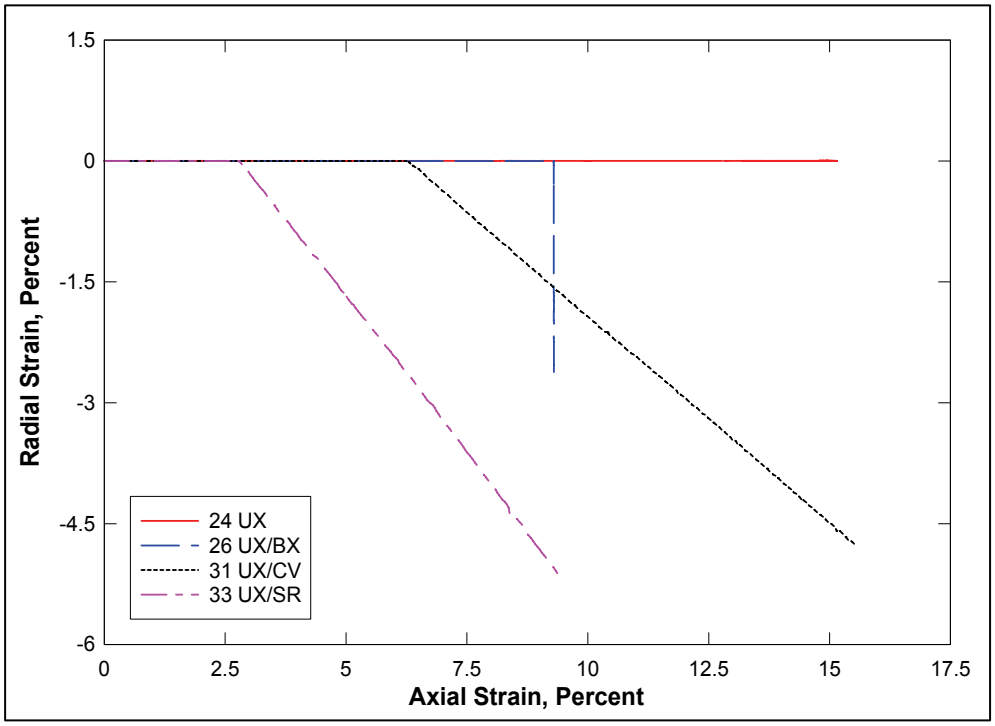

Figure 58. Strain paths from selected UX, UX/BX, UX/SR, and UX/CV tests

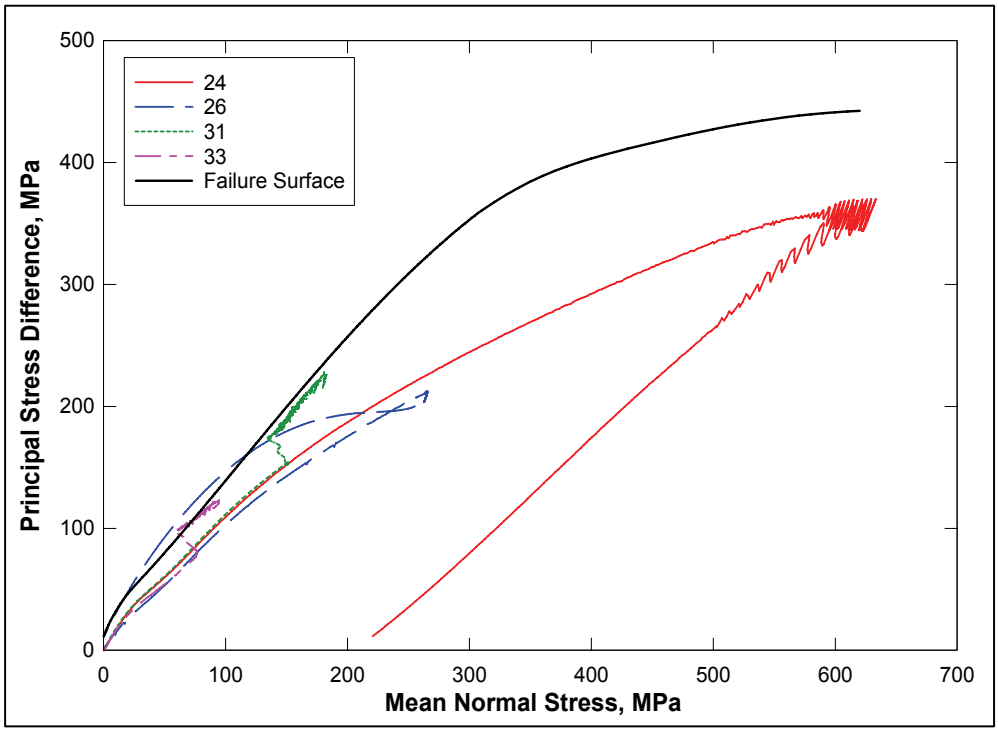

Figure 59. Stress paths from selected UX, UX/BX, UX/SR, and UX/CV tests and failure surface from TXC tests

4 Summary

Personnel in the Geotechnical and Structures Laboratory conducted a laboratory investigation to characterize the strength and constitutive property behavior of SAM-35 concrete. Forty-four successful mechanical property tests were conducted. These tests included two hydrostatic compression tests, four unconfined compression tests, 18 triaxial compression tests, two uniaxial strain tests, four uniaxial strain/biaxial unloading tests, three uniaxial strain/constant volume tests, two uniaxial strain/constant strain ratio tests, five direct-pull tests, and four reduced triaxial extension tests. Composition properties were obtained for each test specimen along with nondestructive pulse-velocity data.

The overall quality of the test data was very good; limited scatter was observed in the data over repeated loading paths. Creep was observed at high mean normal stress levels during the HC and UX tests. The TXC tests exhibited a continuous increase in principal stress difference, with increasing confining stress until full saturation was approached at a confining pressure of 400 MPa. A compression failure surface was developed from the TXC test results at eight levels of confining stress and from the results of the unconfined compression tests. The results from the RTE tests along with the DP tests were used to develop a recommended extension failure surface for SAM-35. The resulting compression and extension failure surfaces were well defined and nonsymmetric about the mean normal stress axis. During UX/BX tests, stress relaxation was evident during the change from uniaxial strain loading to biaxial strain unloading. Good correlations were observed between the stress paths obtained from the UX/CV and UX/SR strain path tests and the failure surface from the TXC tests.

References

Akers, S. A., Reed, P. A., and Ehrgott, J. Q. (1986). *WES high-pressure uniaxial strain and triaxial shear test equipment*. Vicksburg, MS.

American Society for Testing and Materials. (2002). *2002 Annual book of ASTM standards*. Philadelphia, PA.

a. Designation C 39-01. "Standard test method for compressive strength of concrete specimens."
b. Designation C 42-99. "Standard test method for obtaining and testing drilled cores and sawed beams of concrete."
c. Designation C 597-97. "Standard test method for pulse velocity through concrete."
d. Designation C 801-98. "Standard test method for determining the mechanical properties of hardened concrete under triaxial loads."
e. Designation D 2216-98. "Standard test method for laboratory determination of water (moisture) content of soil and rock by mass."
f. Designation D 4543-01. "Standard test method for preparing rock core specimens and determining dimensional and shape tolerances."

Bishop, A. W., and Henkel, D. J. (1962). *The measurement of soil properties in the triaxial test*. Edward Arnold, Ltd., London, pp 72-74.

SAM-35 Concrete
Test No. 05

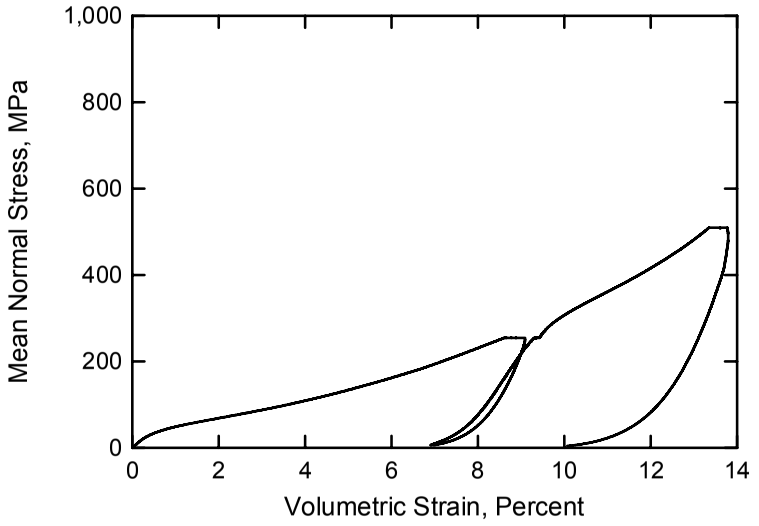

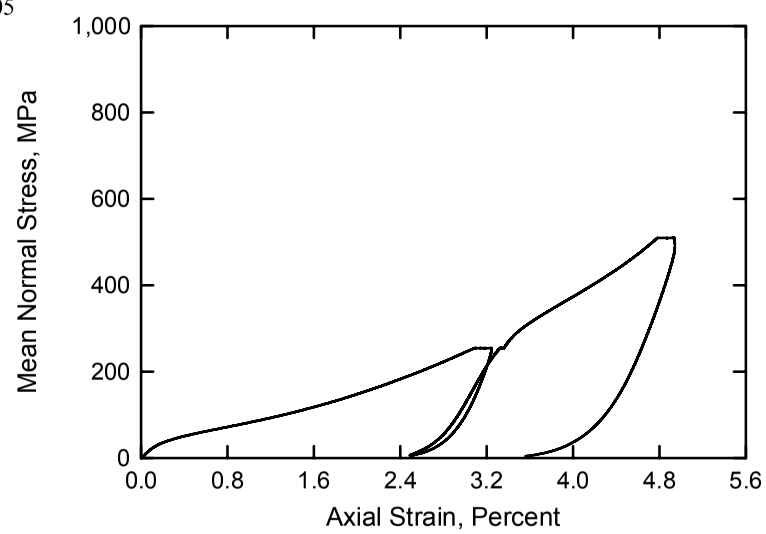

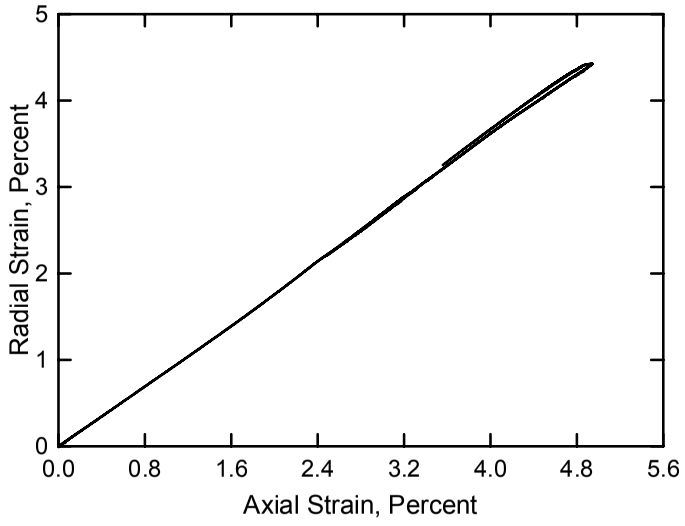

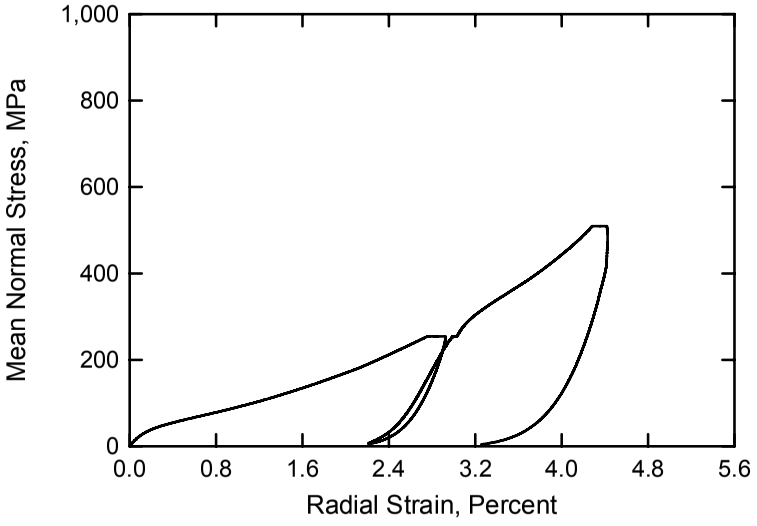

Plate 1

SAM-35 Concrete
Test No. 06

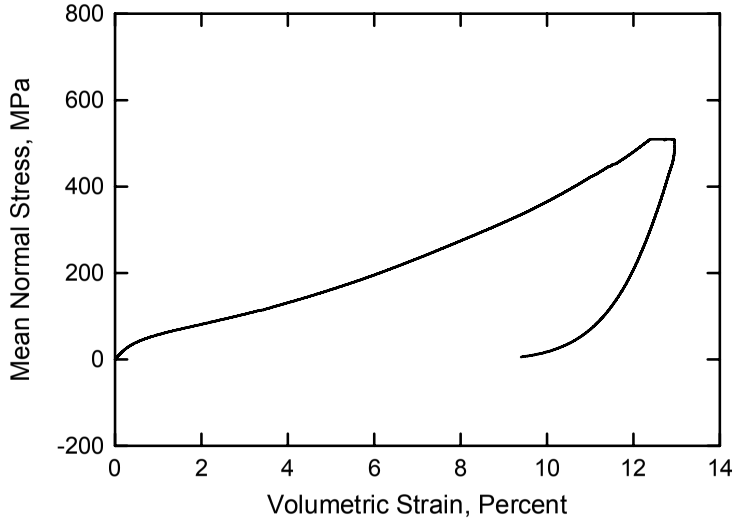

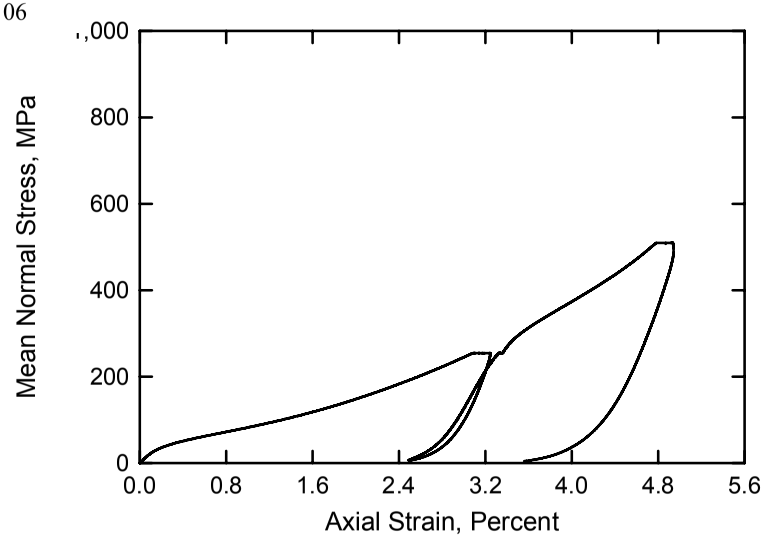

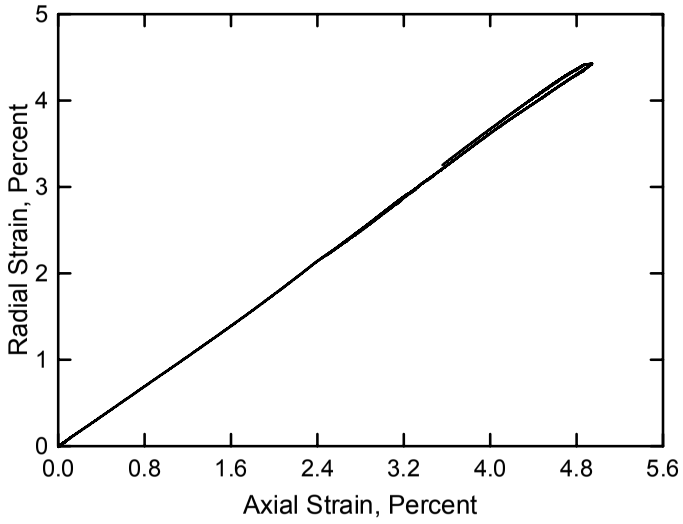

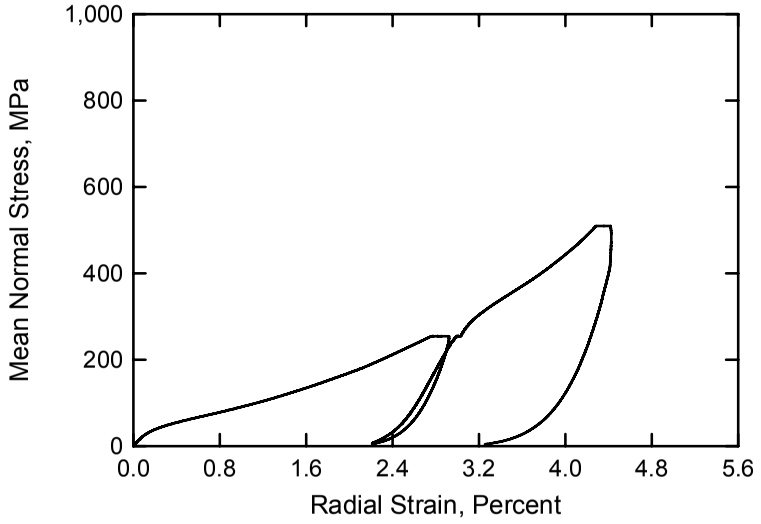

Plate 2

SAM-35 Concrete
Test No. 01

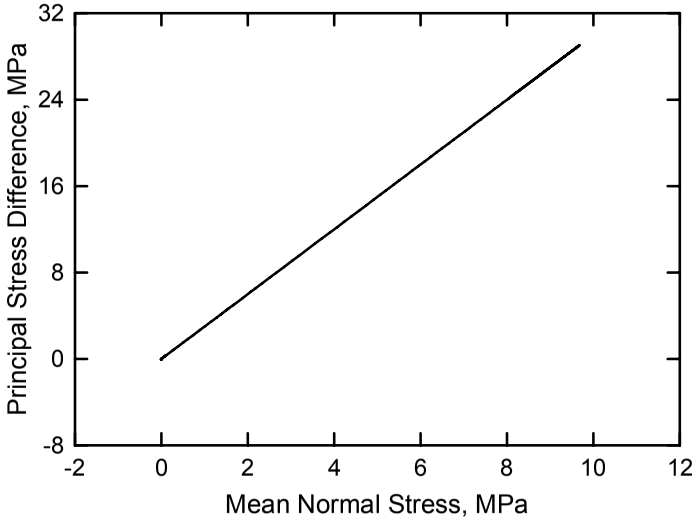

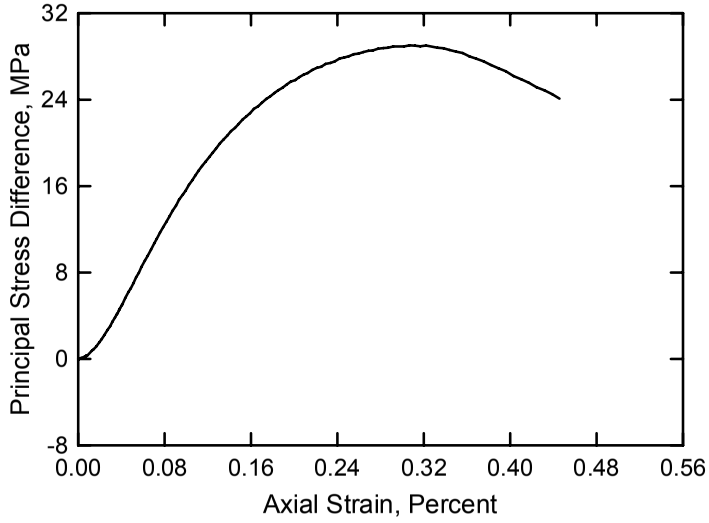

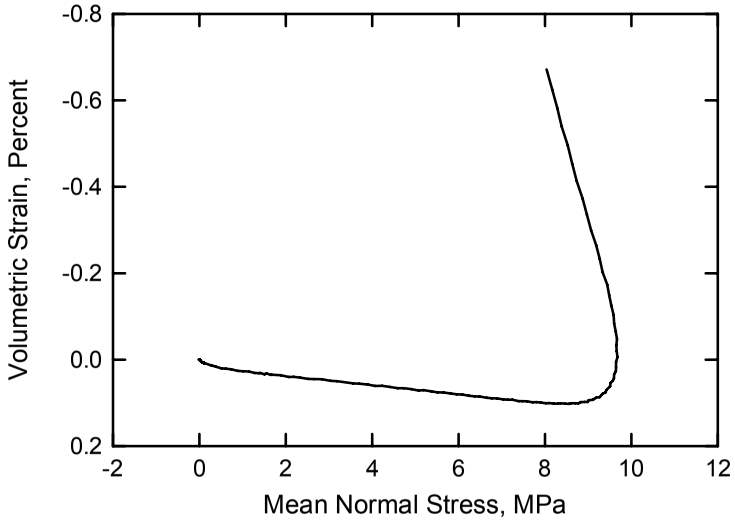

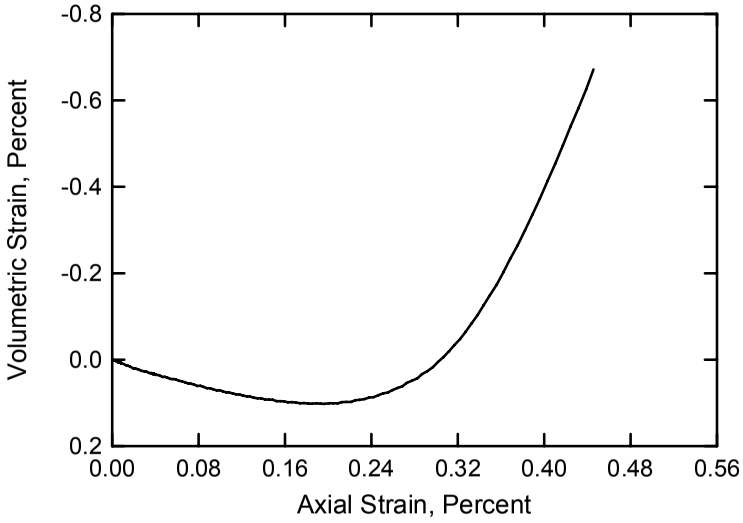

Plate 3

SAM-35 Concrete
Test No. 02

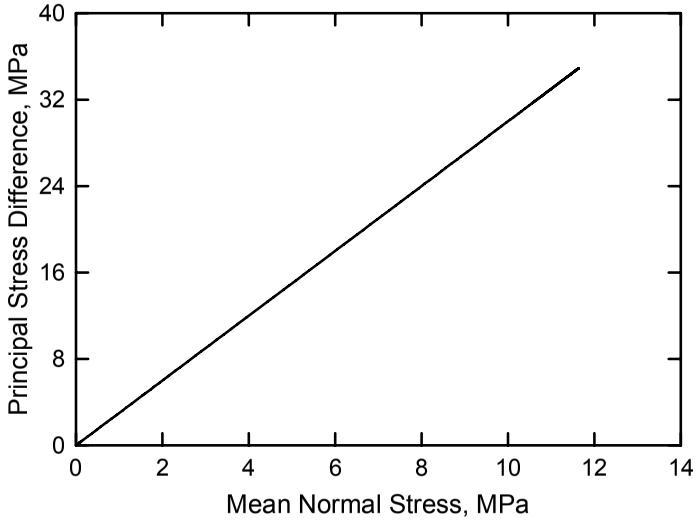

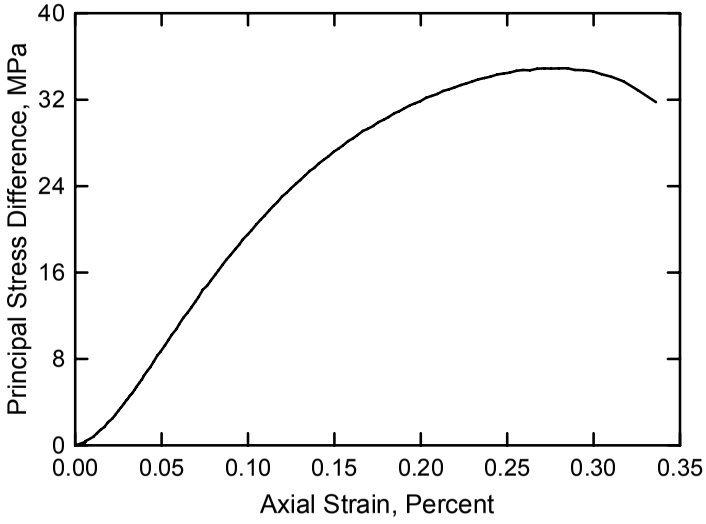

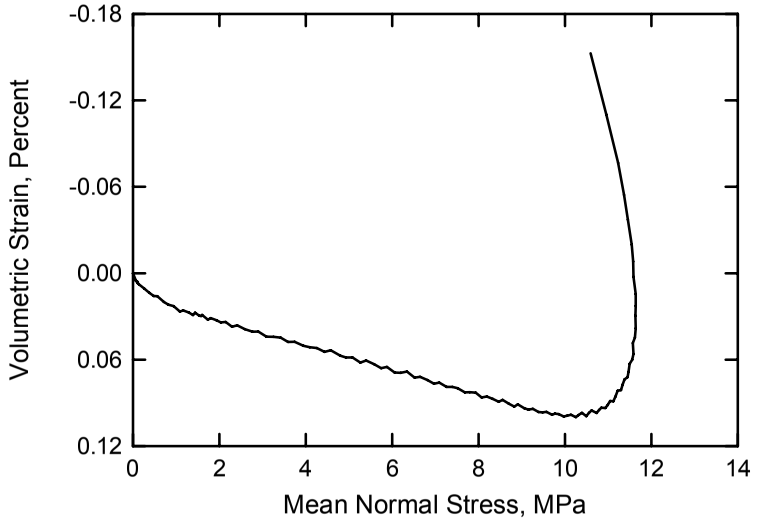

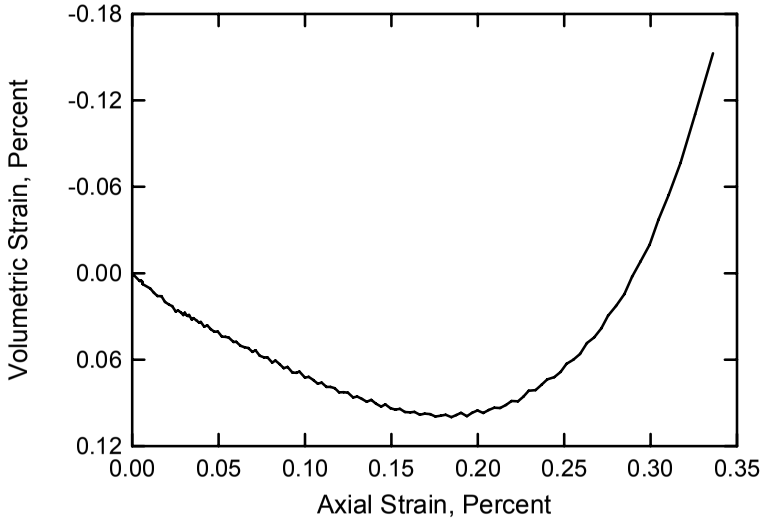

Plate 4

SAM-35 Concrete
Test No. 03

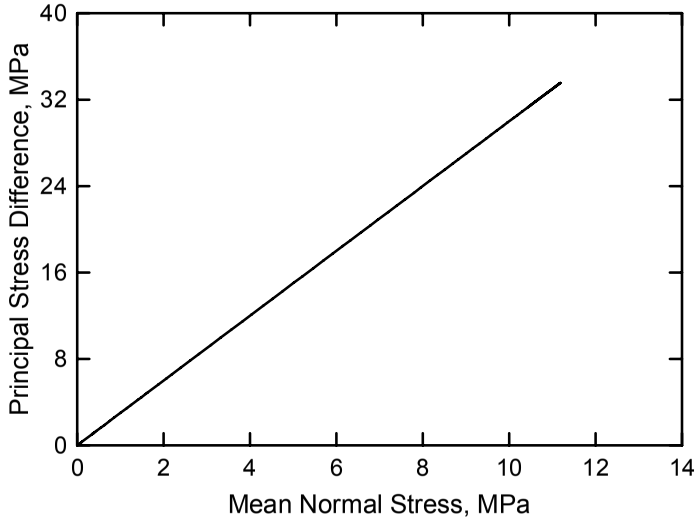

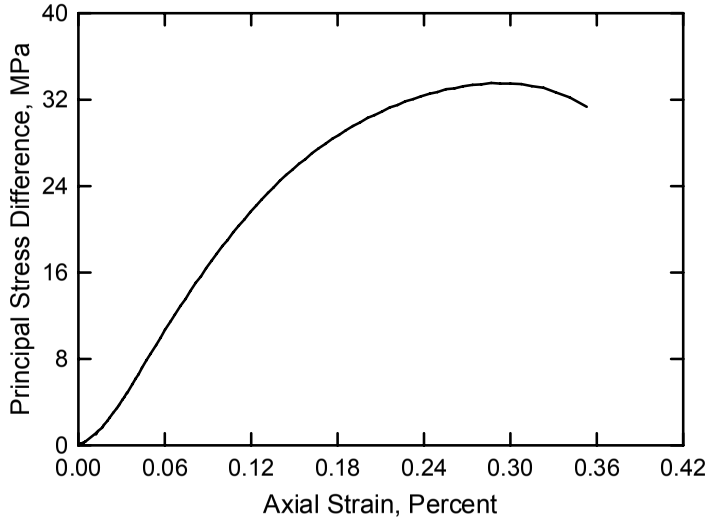

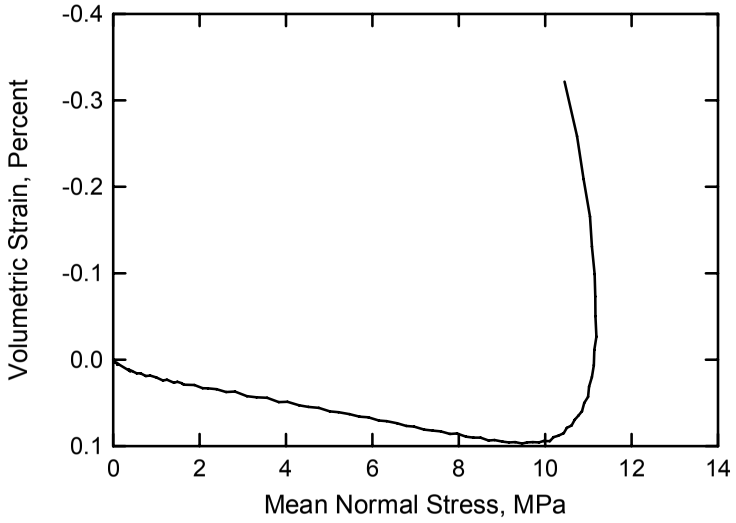

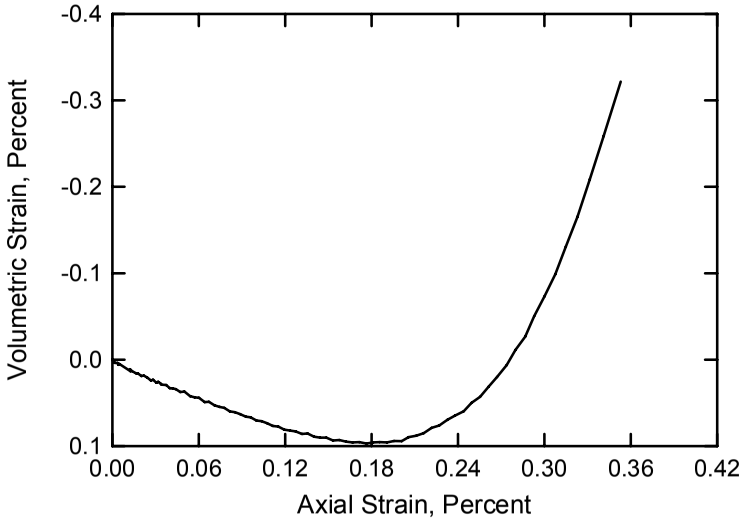

Plate 5

SAM-35 Concrete
Test No. 04

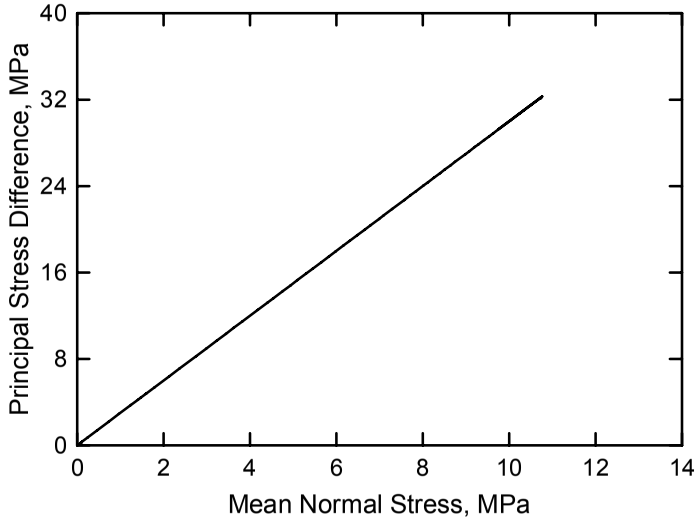

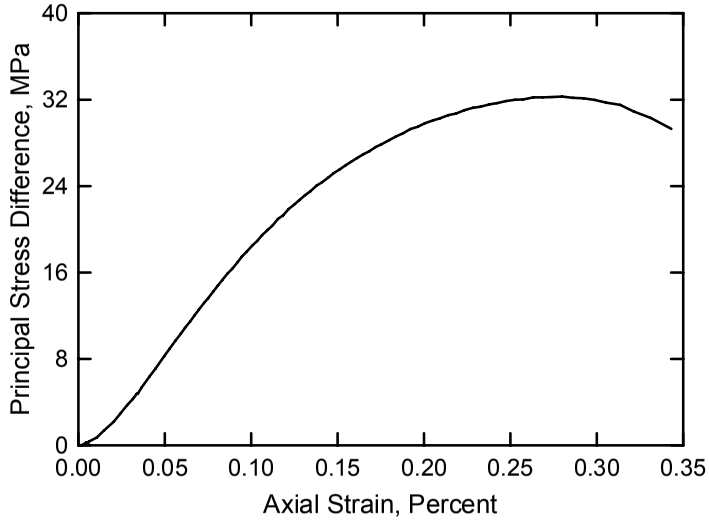

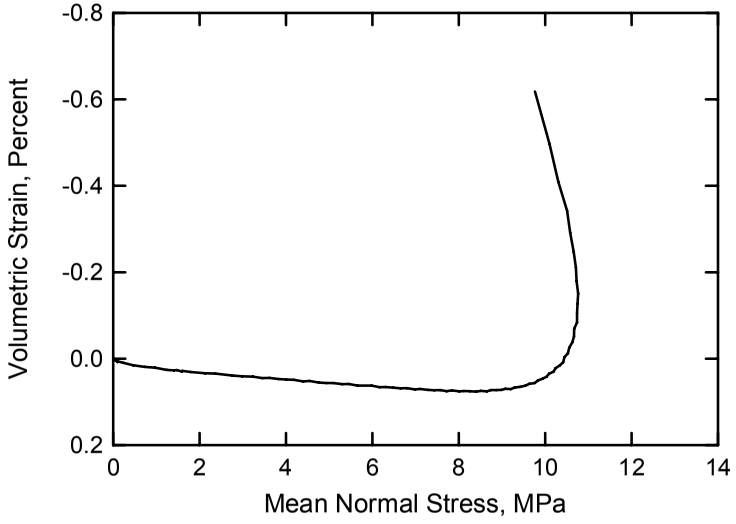

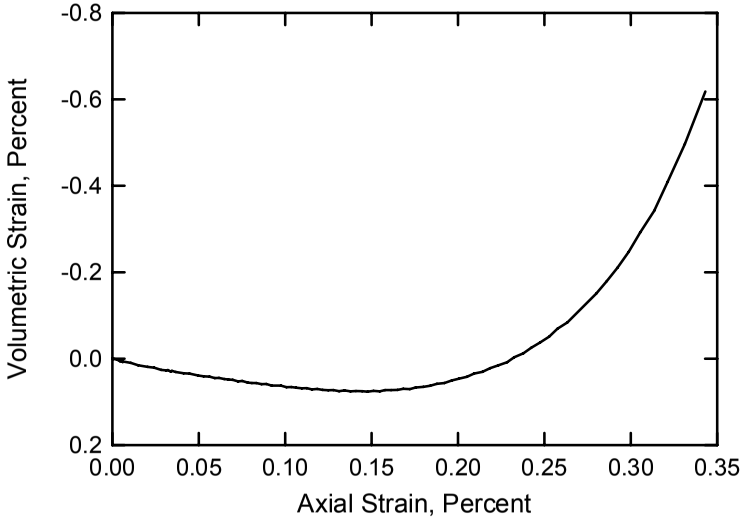

Plate 6

SAM-35 Concrete
Test No. 07

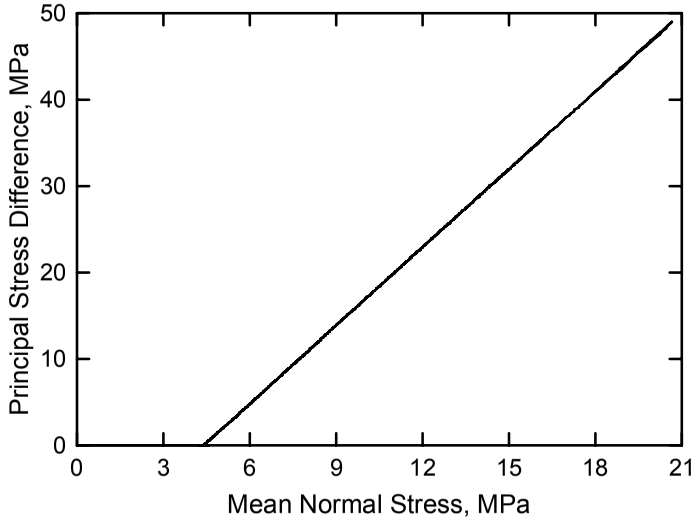

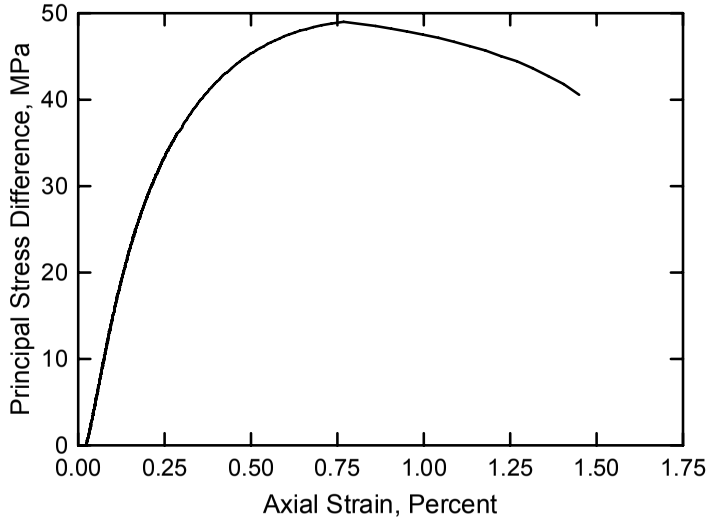

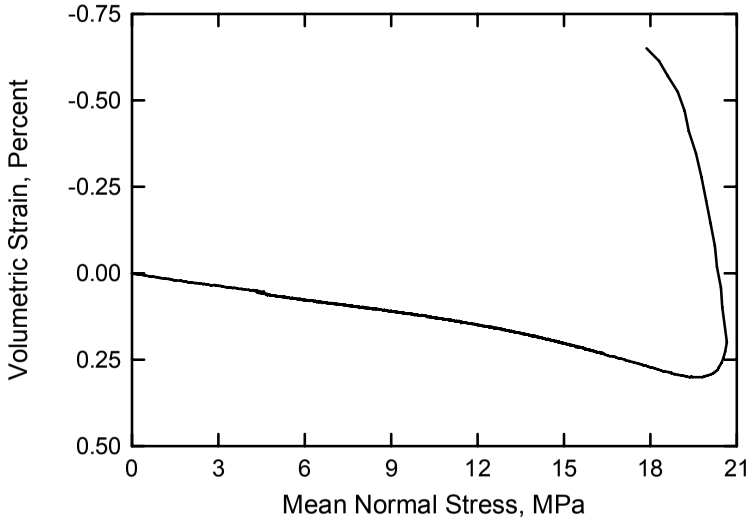

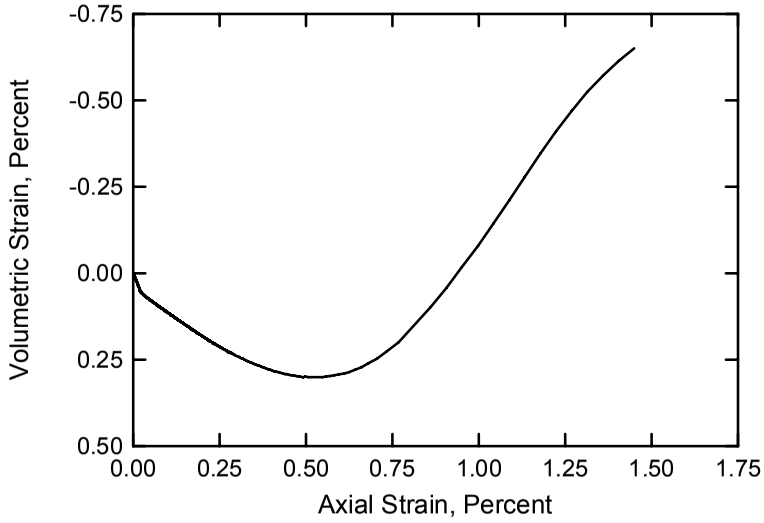

Plate 7

SAM-35 Concrete
Test No. 08

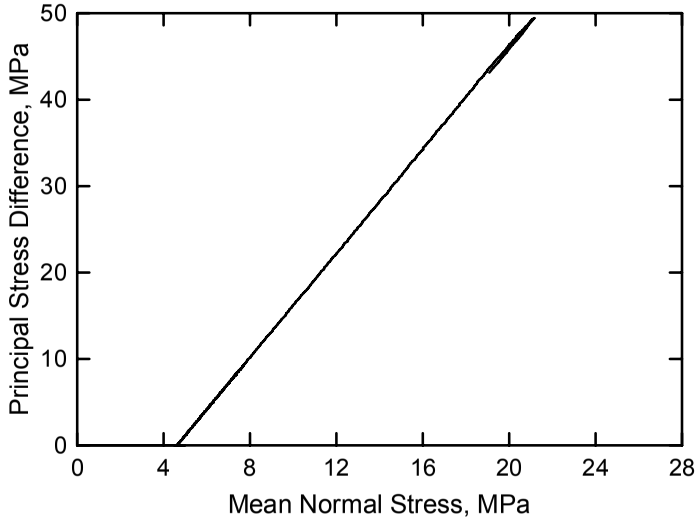

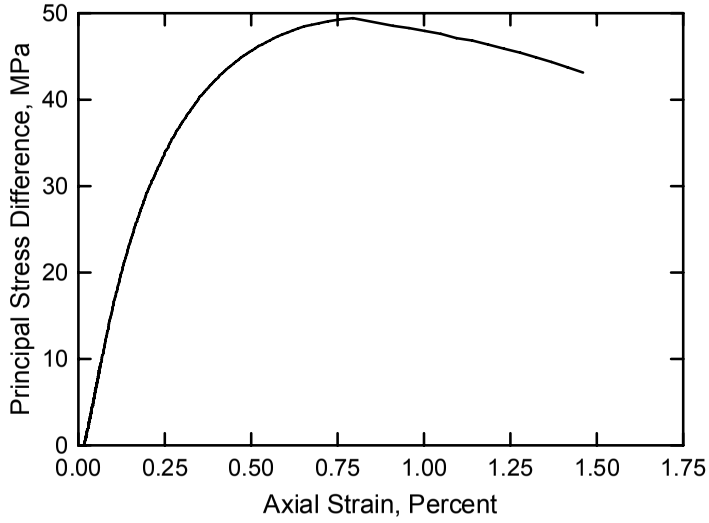

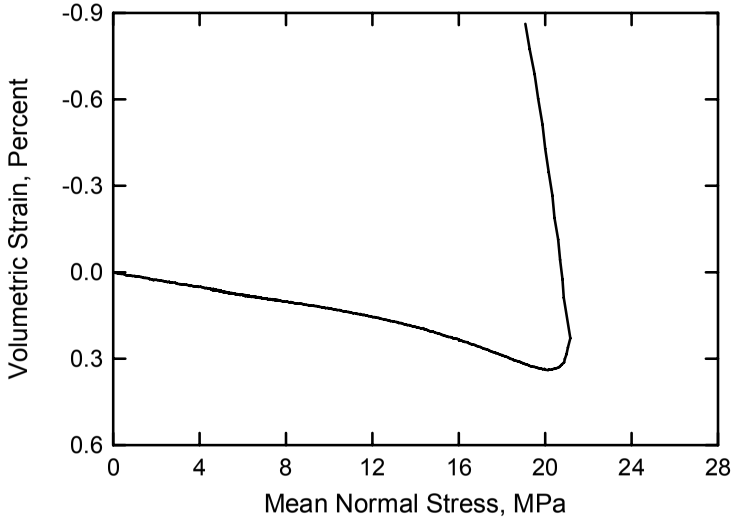

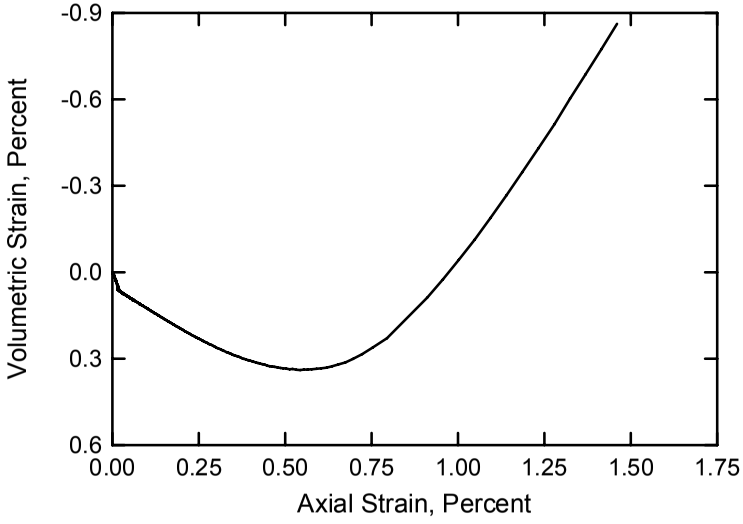

Plate 8

SAM-35 Concrete
Test No. 09

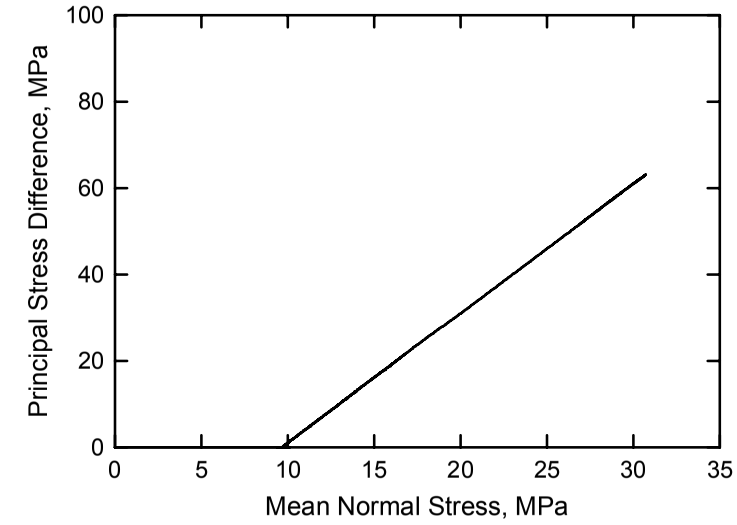

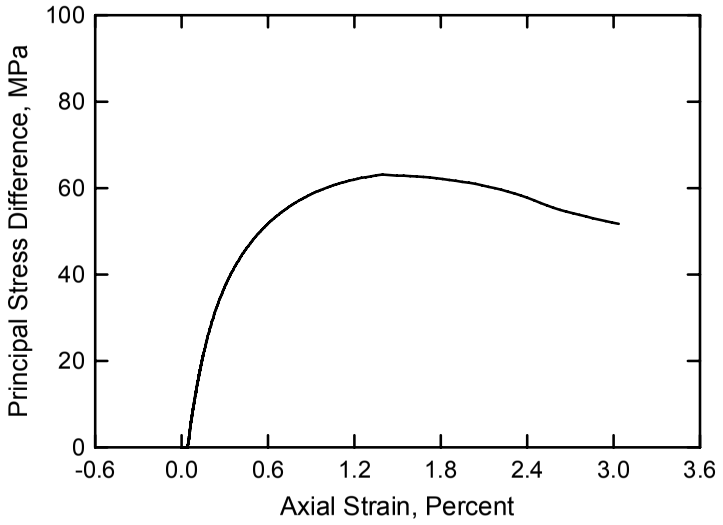

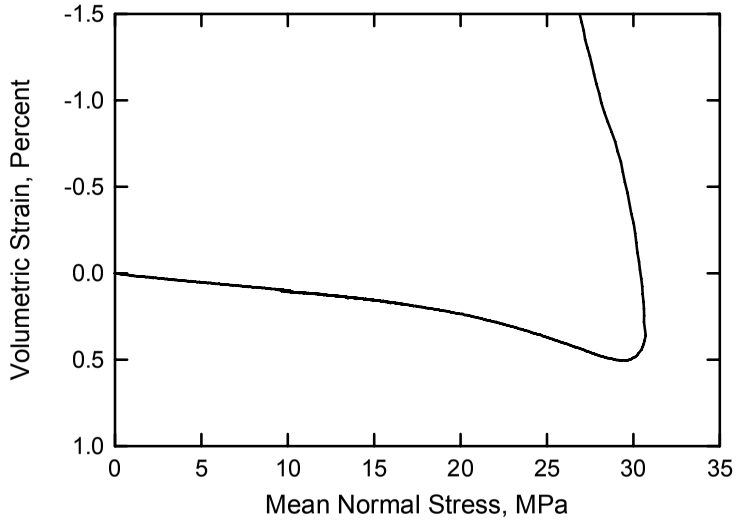

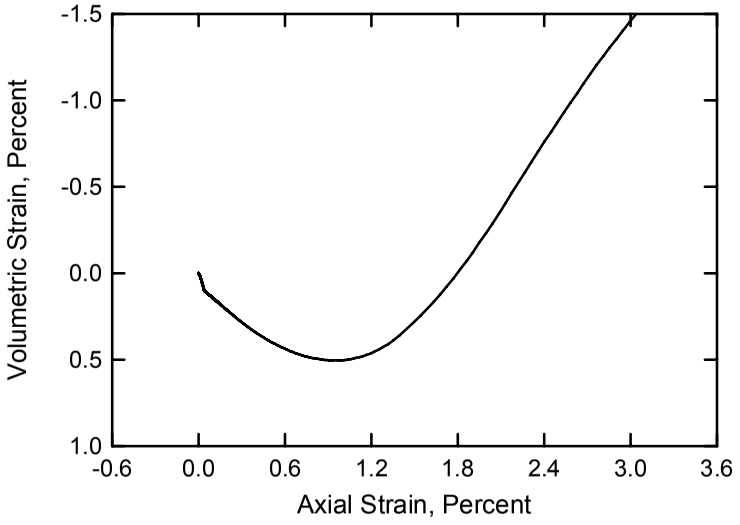

Plate 9

SAM-35 Concrete
Test No. 10

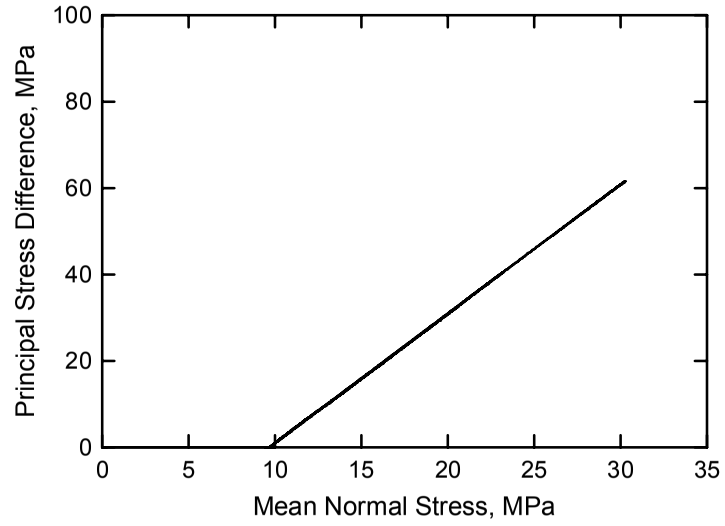

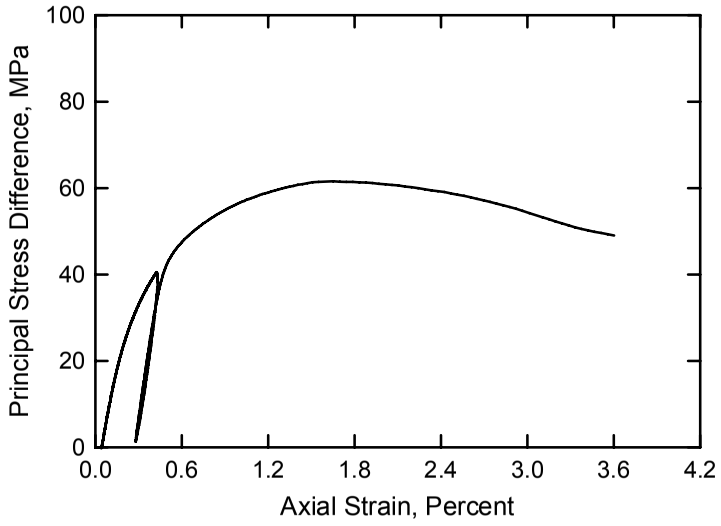

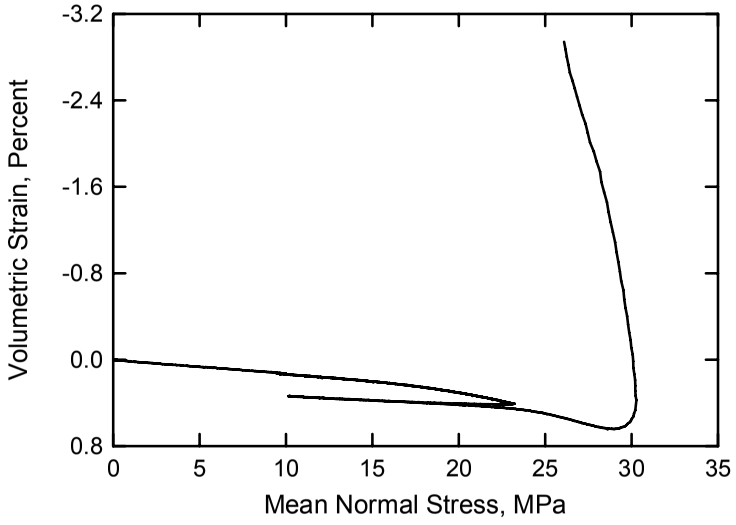

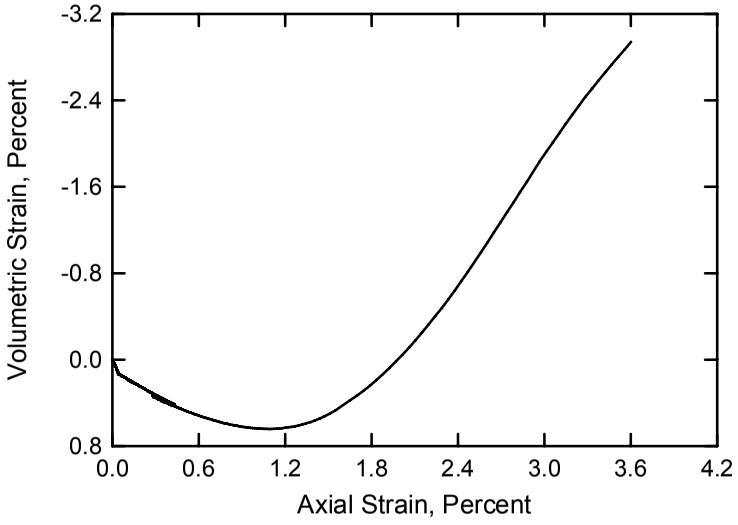

Plate 10

SAM-35 Concrete
Test No. 11

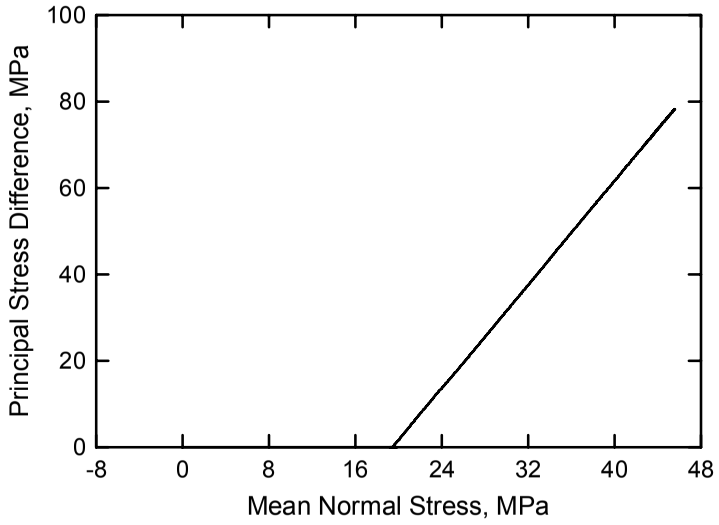

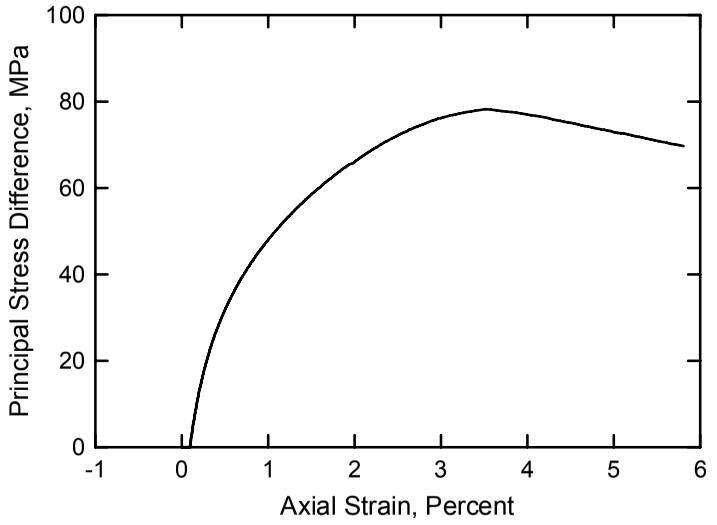

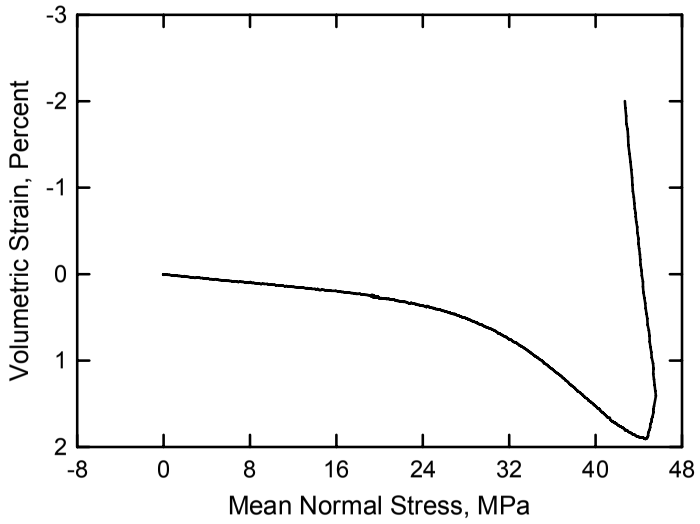

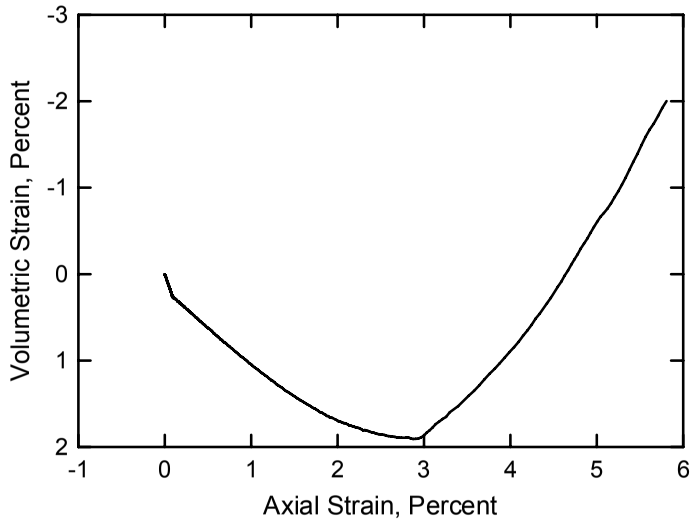

Plate 11

SAM-35 Concrete
Test No. 12

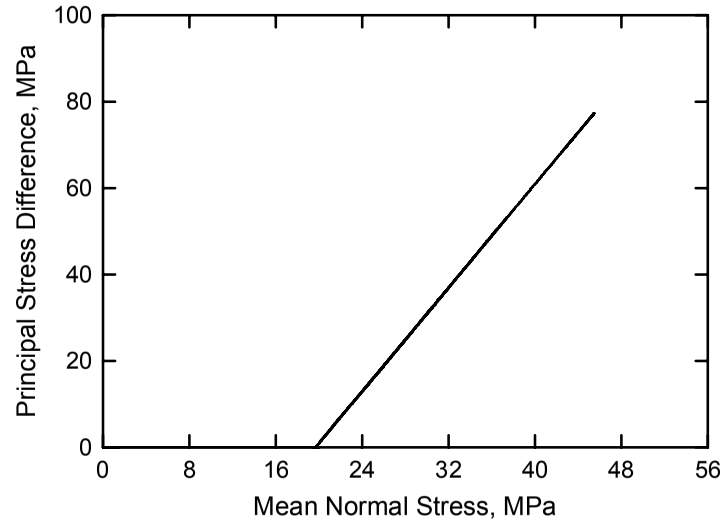

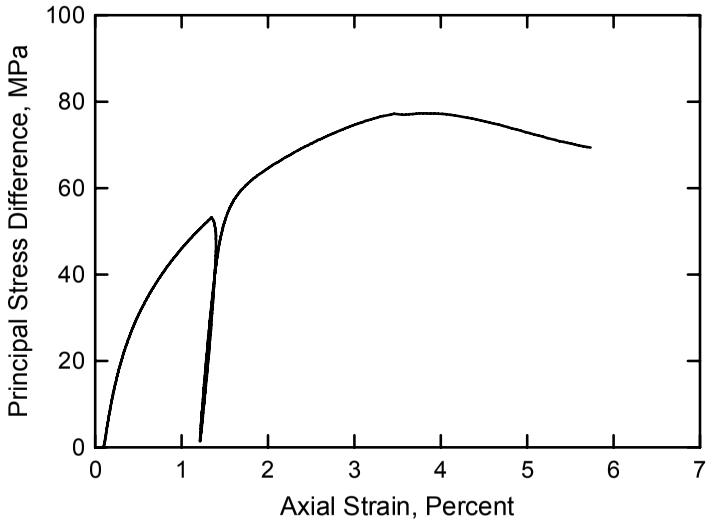

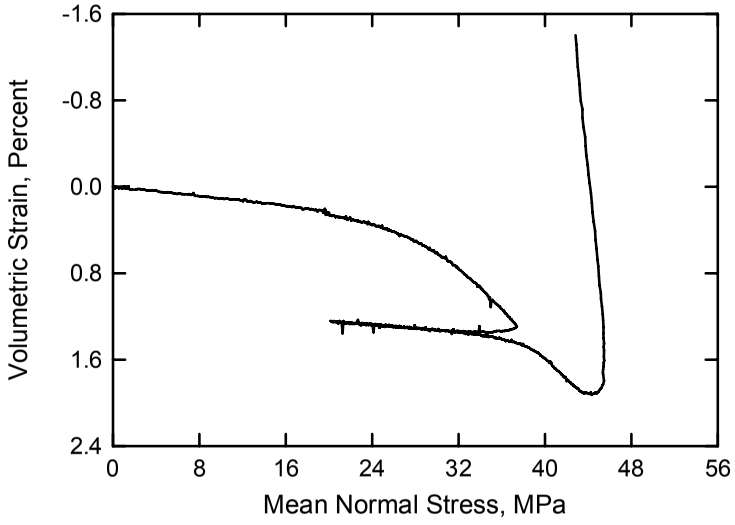

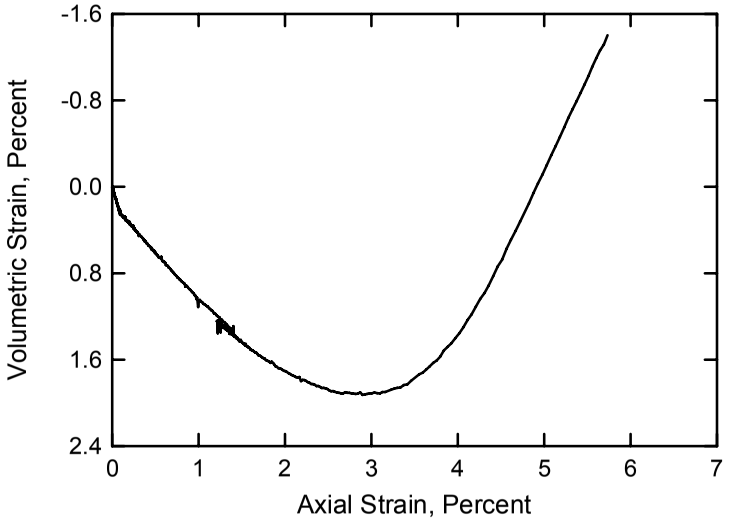

Plate 12

SAM-35 Concrete
Test No. 13

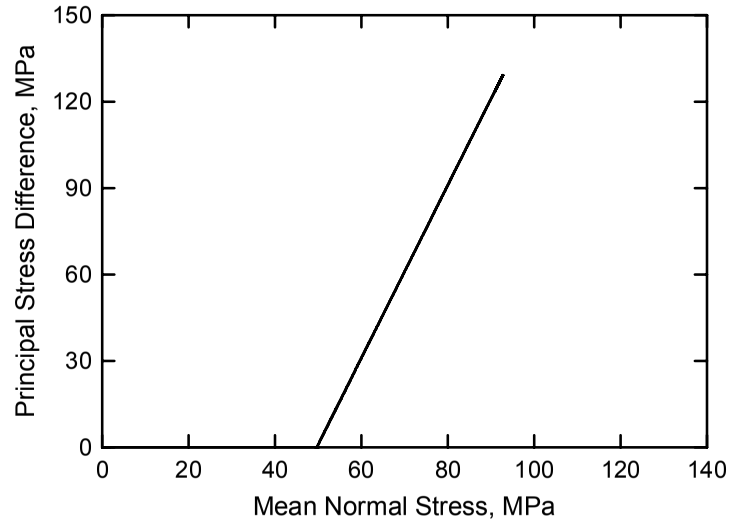

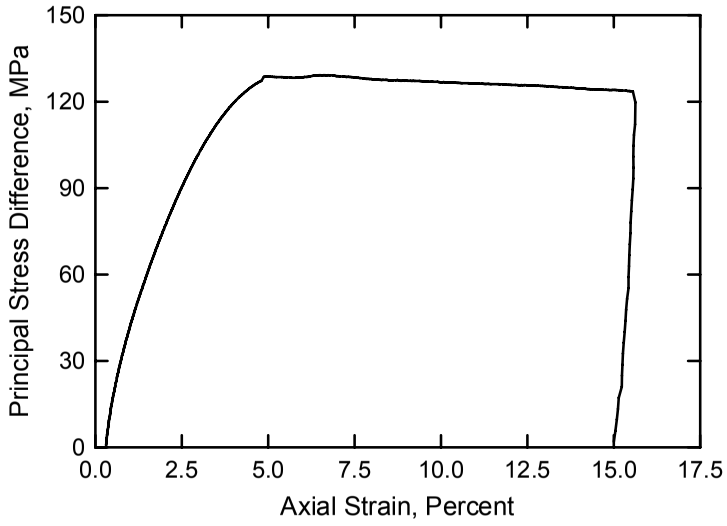

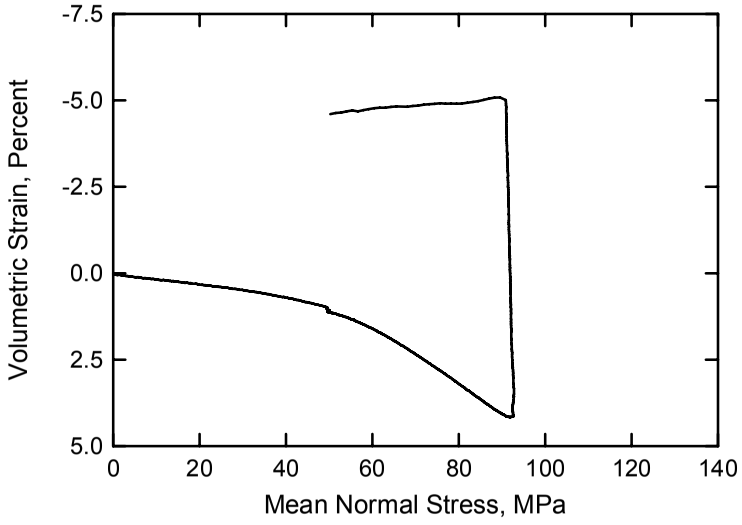

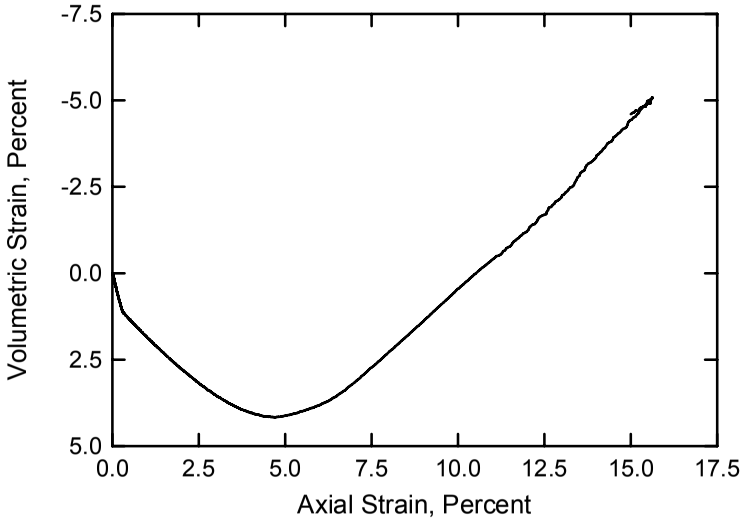

Plate 13

SAM-35 Concrete
Test No. 14

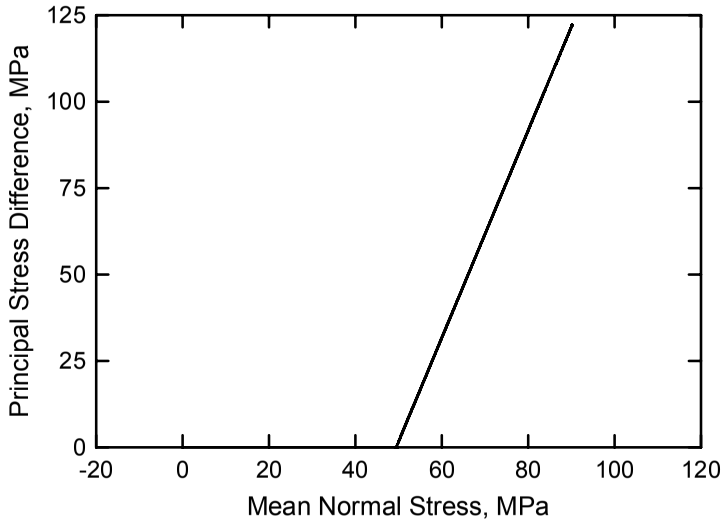

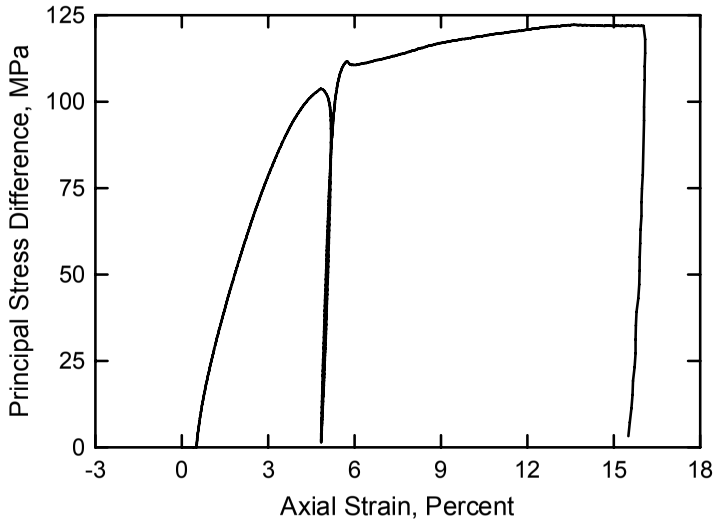

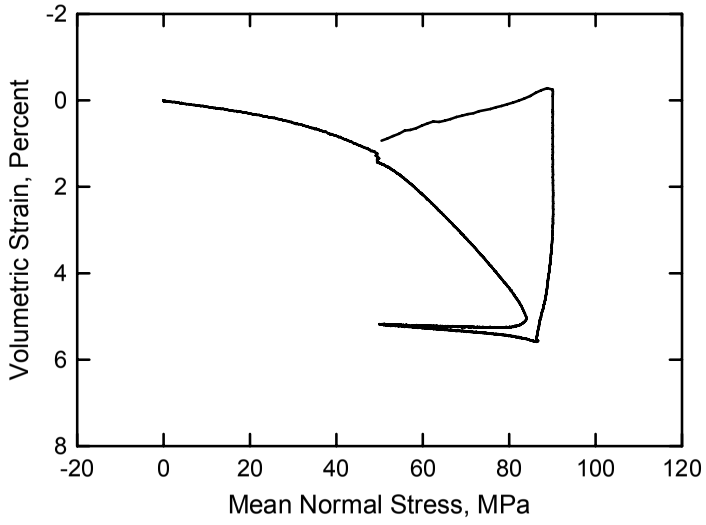

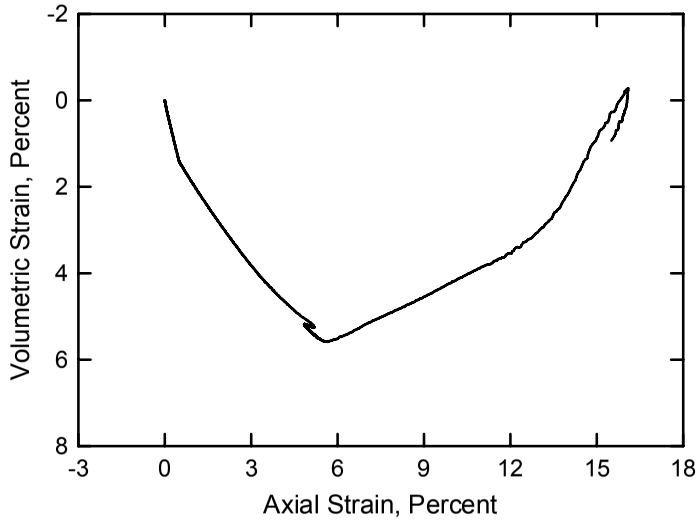

Plate 14

SAM-35 Concrete
Test No. 15

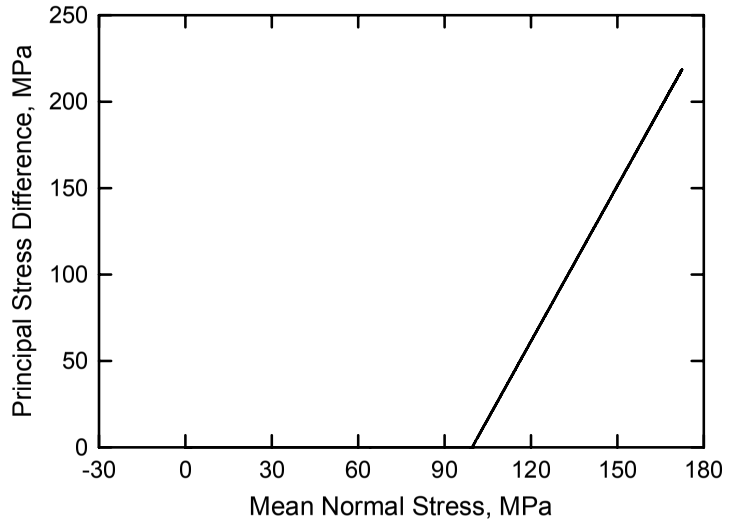

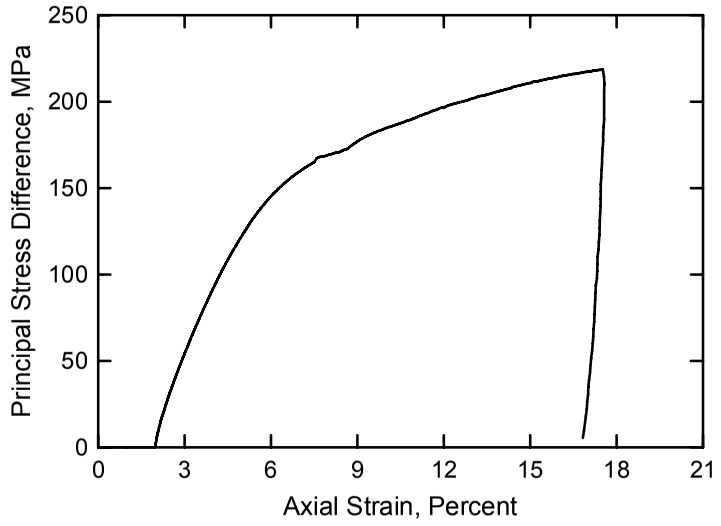

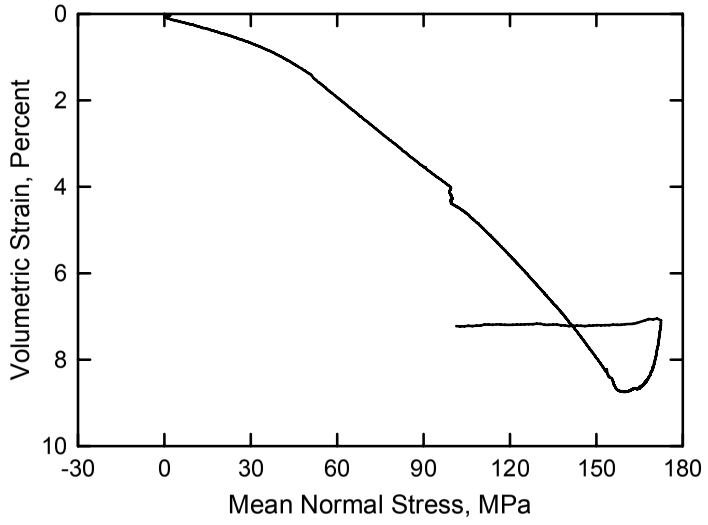

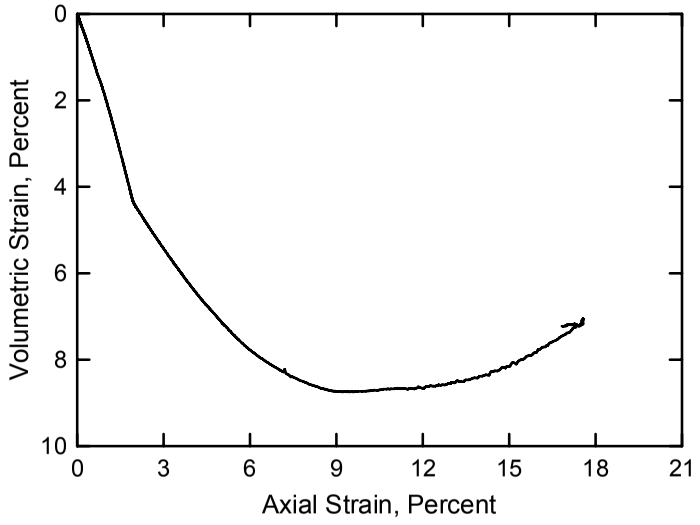

Plate 15

SAM-35 Concrete
Test No. 16

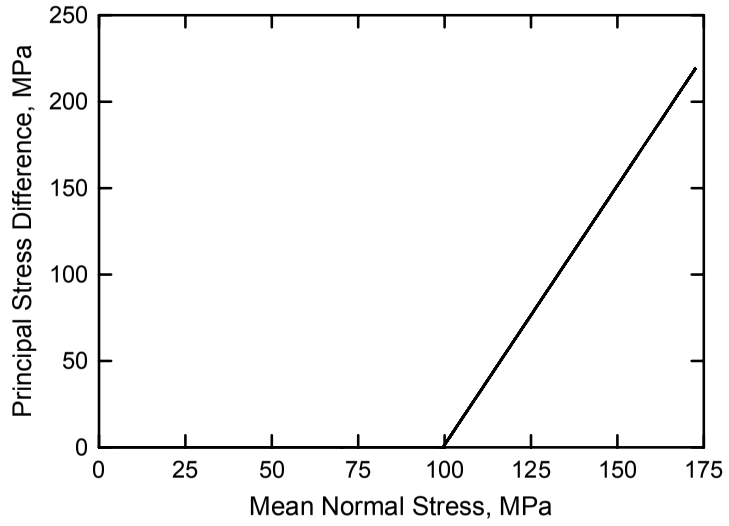

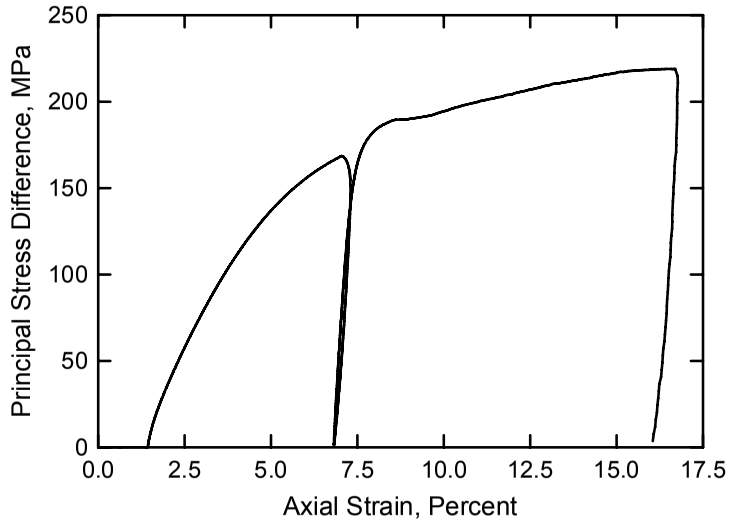

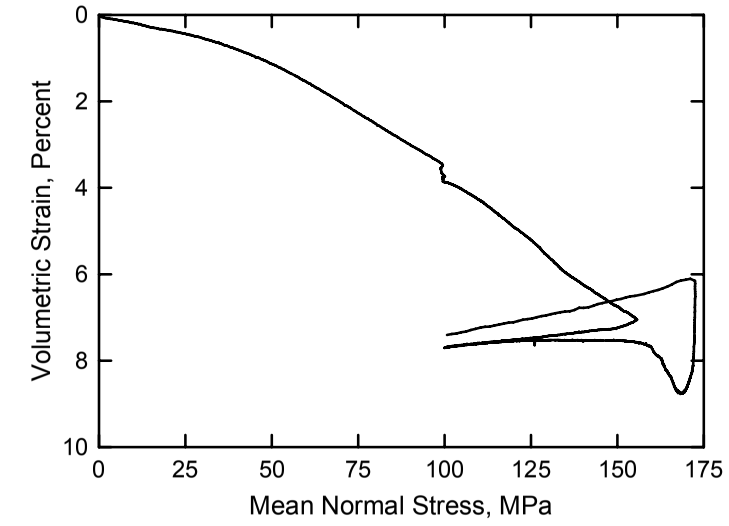

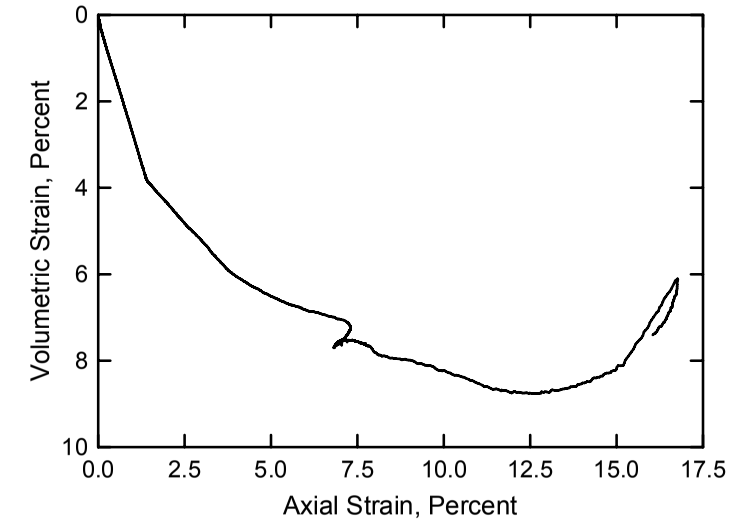

Plate 16

SAM-35 Concrete
Test No. 17

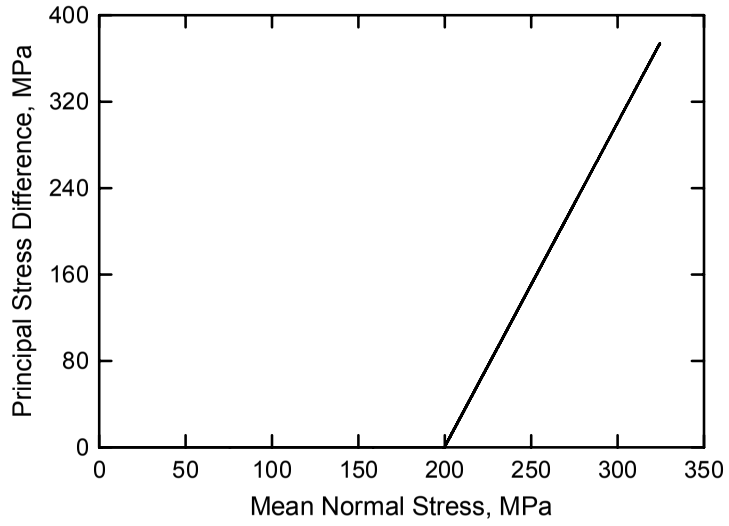

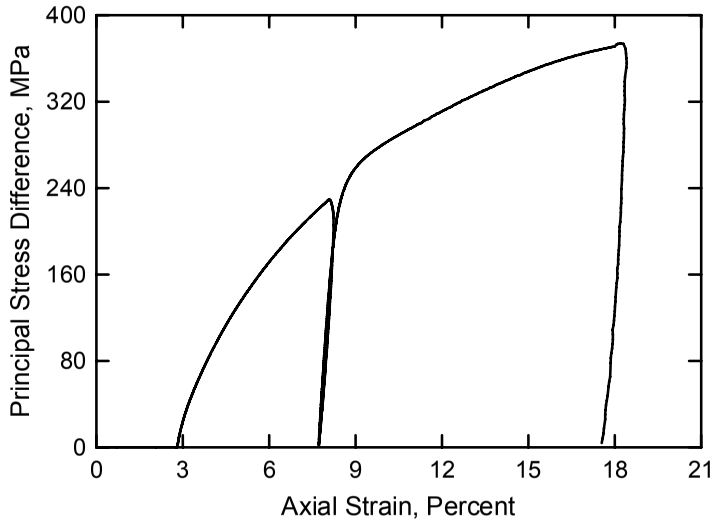

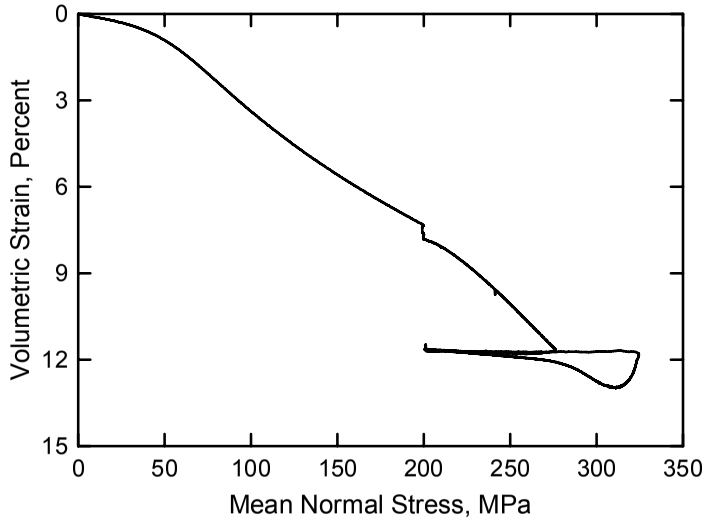

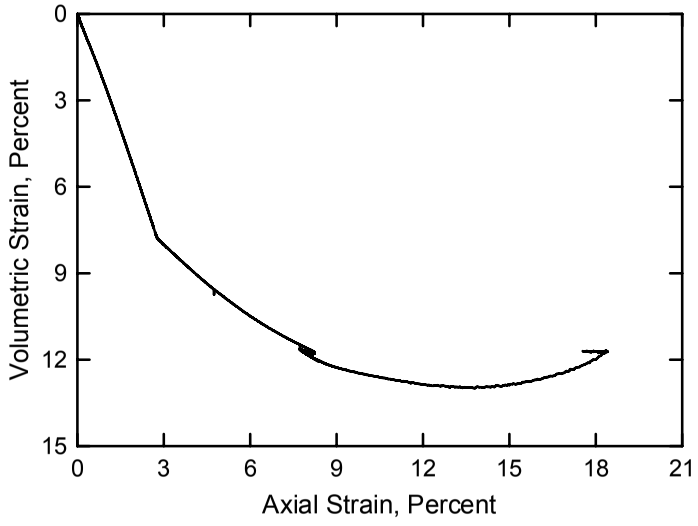

Plate 17

SAM-35 Concrete
Test No. 18

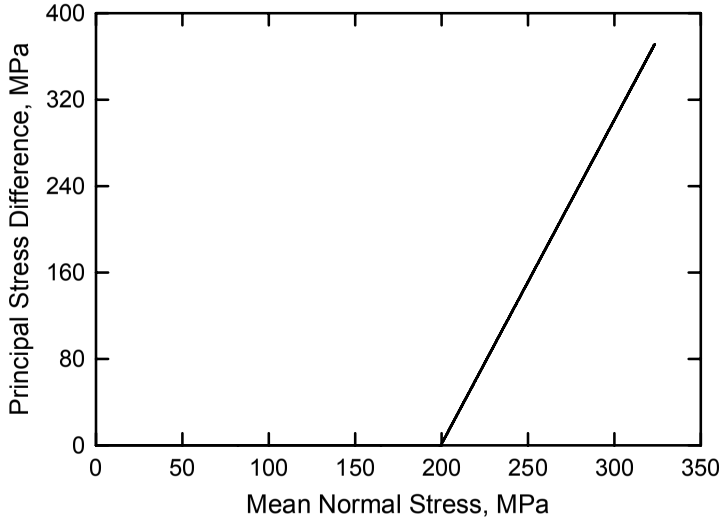

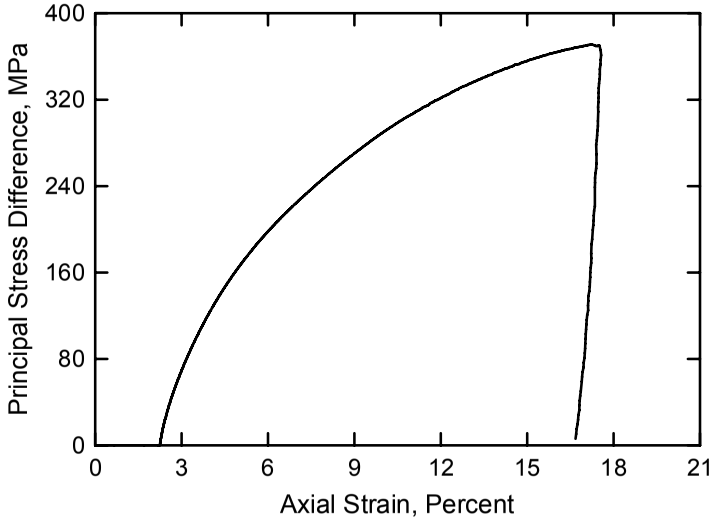

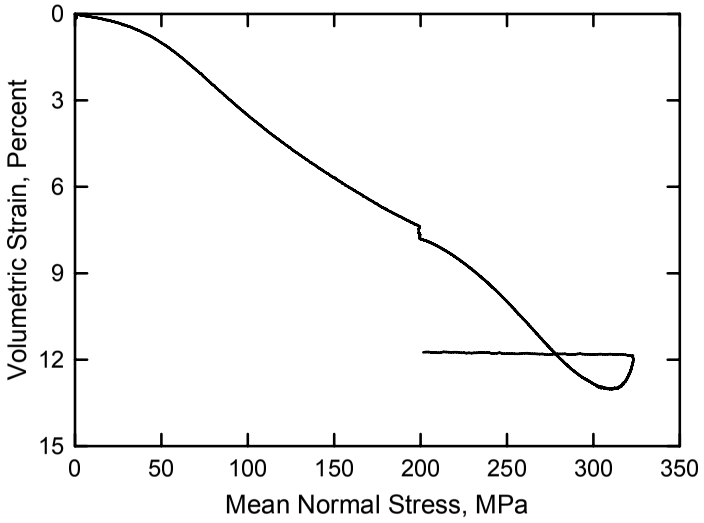

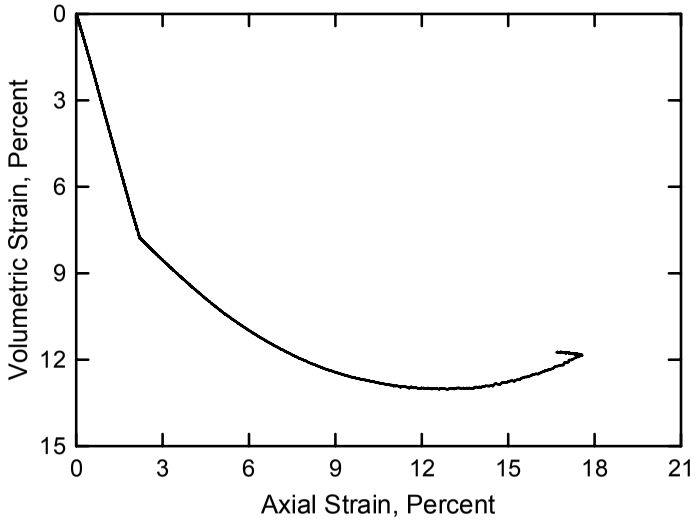

Plate 18

SAM-35 Concrete
Test No. 19

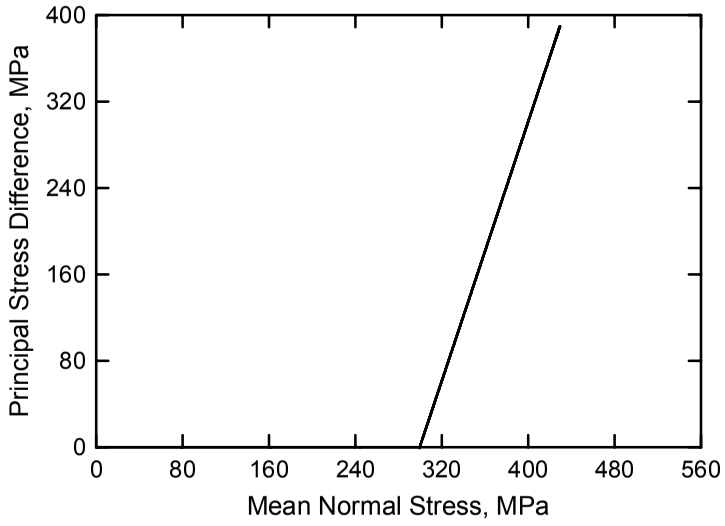

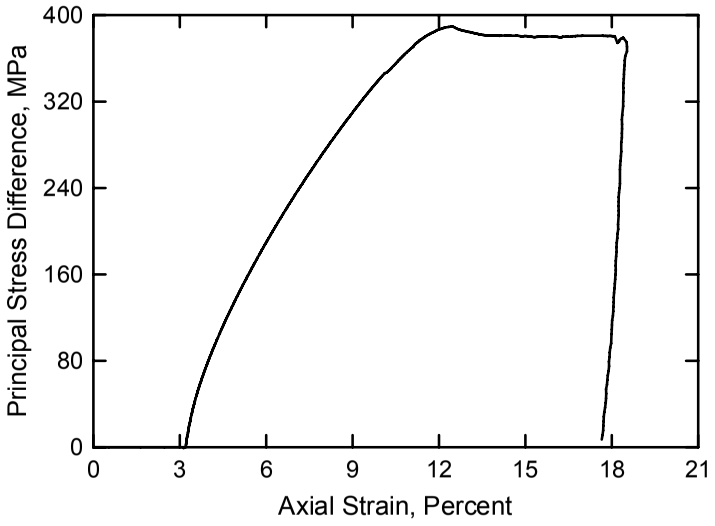

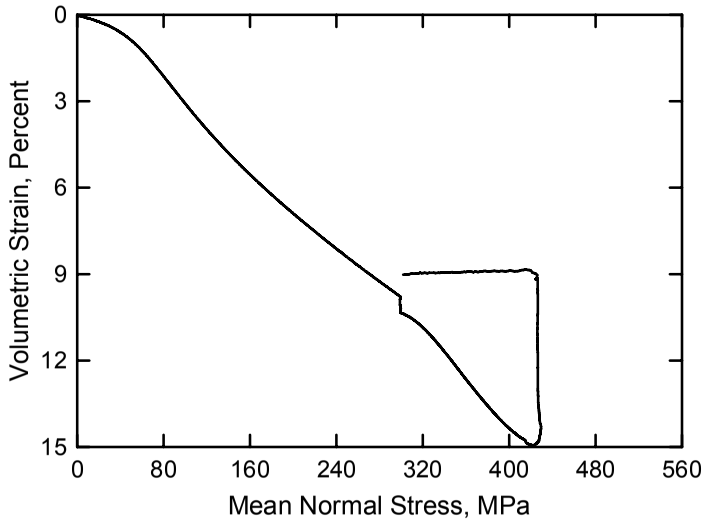

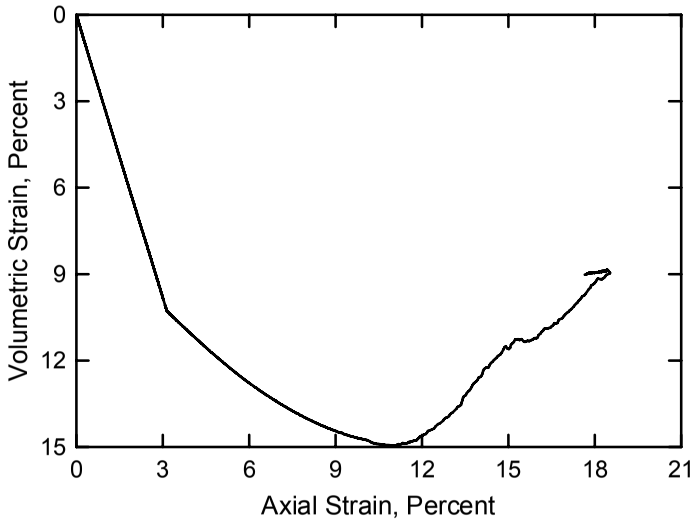

Plate 19

SAM-35 Concrete
Test No. 20

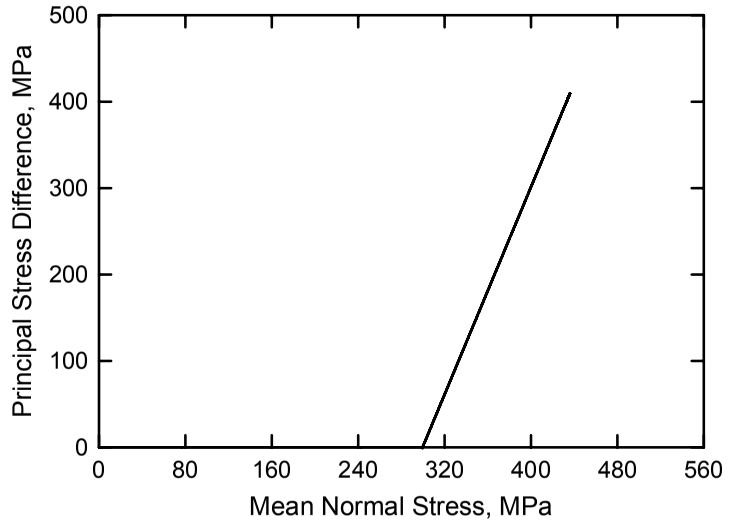

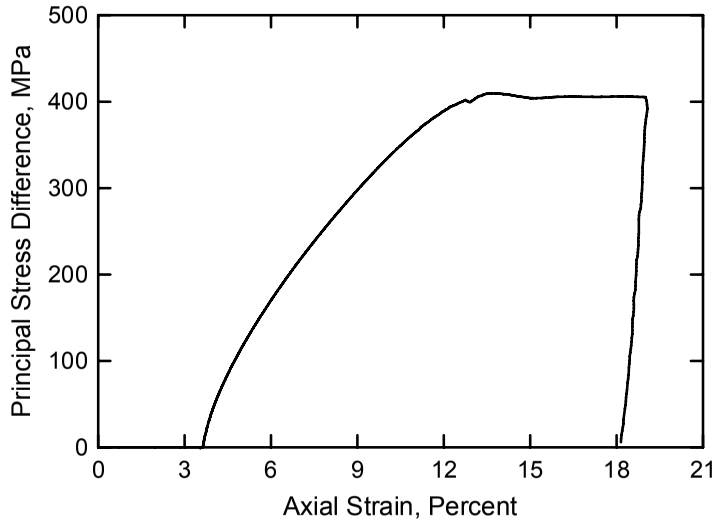

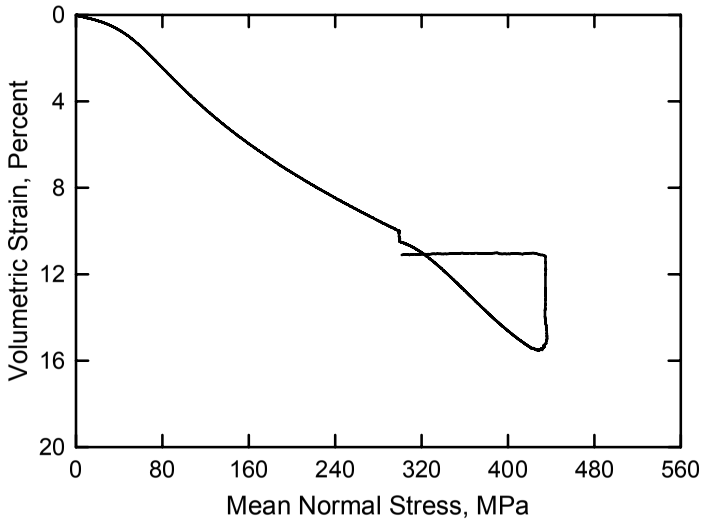

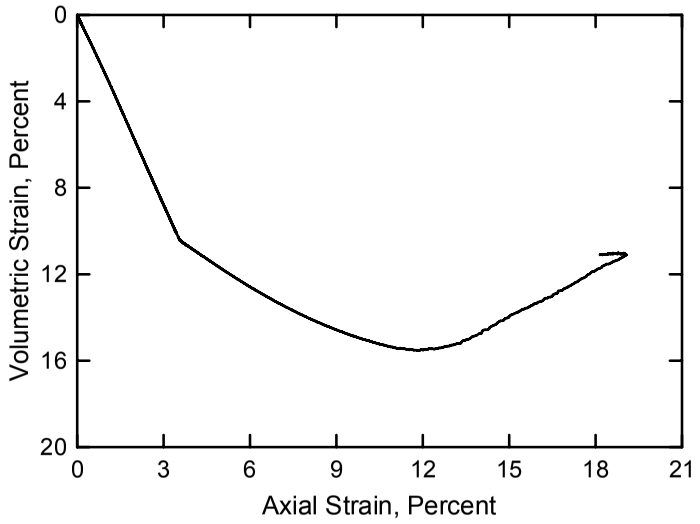

Plate 20

SAM-35 Concrete
Test No. 21

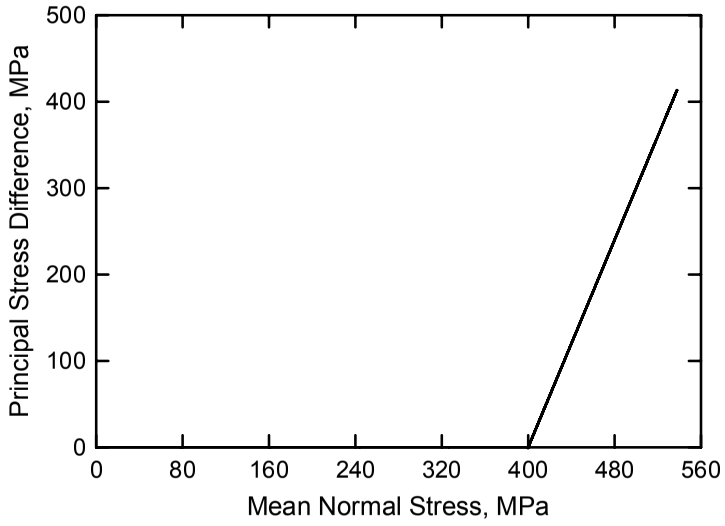

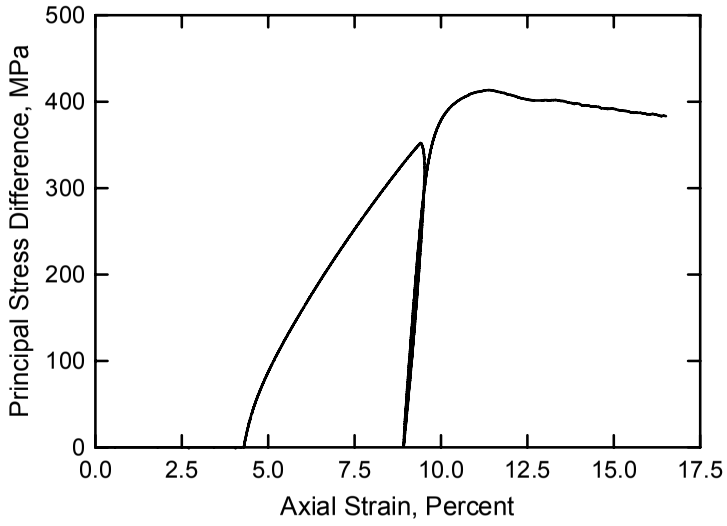

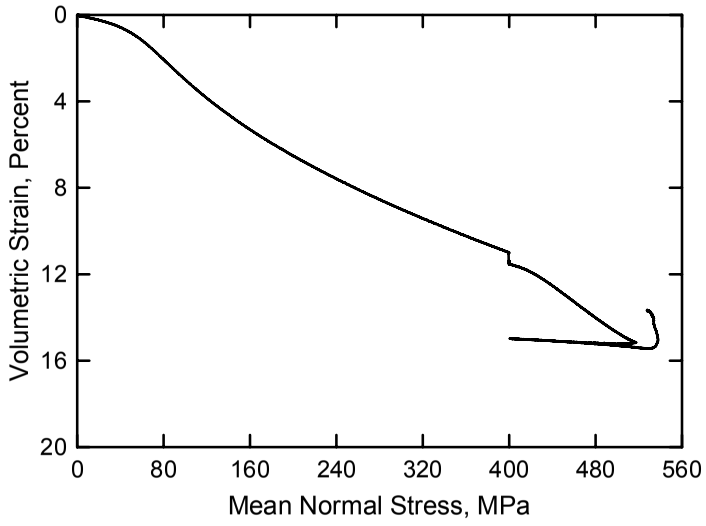

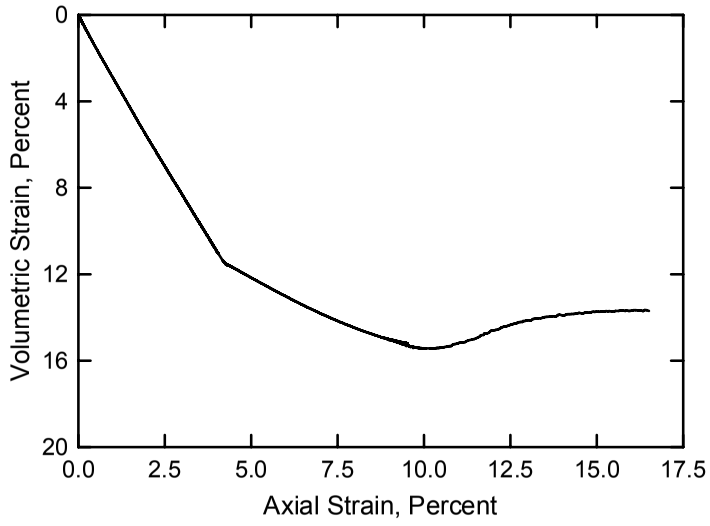

Plate 21

SAM-35 Concrete
Test No. 22

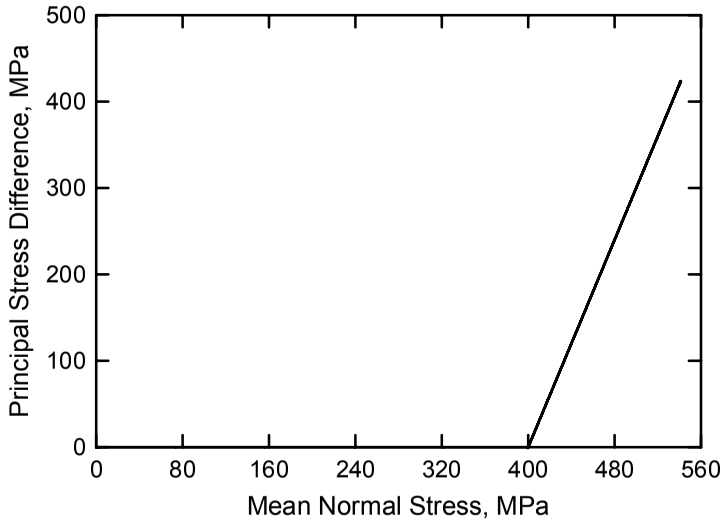

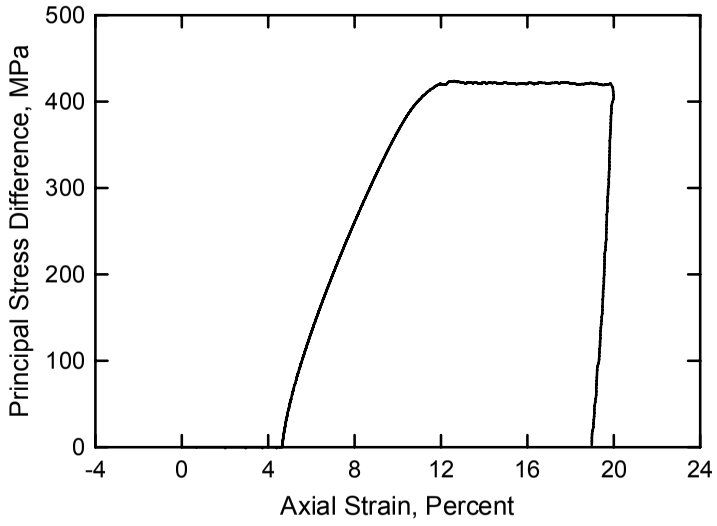

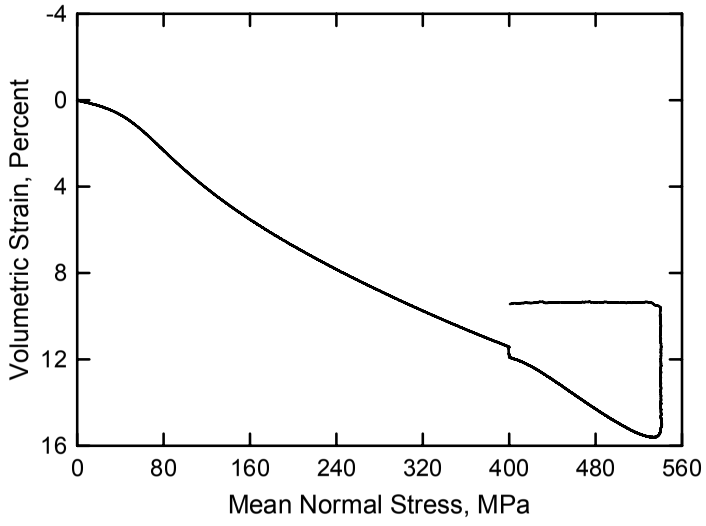

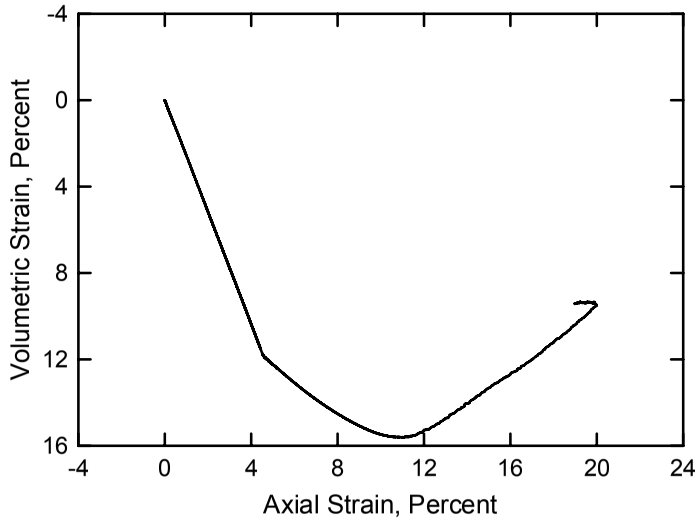

Plate 22

SAM-35 Concrete
Test No. 35

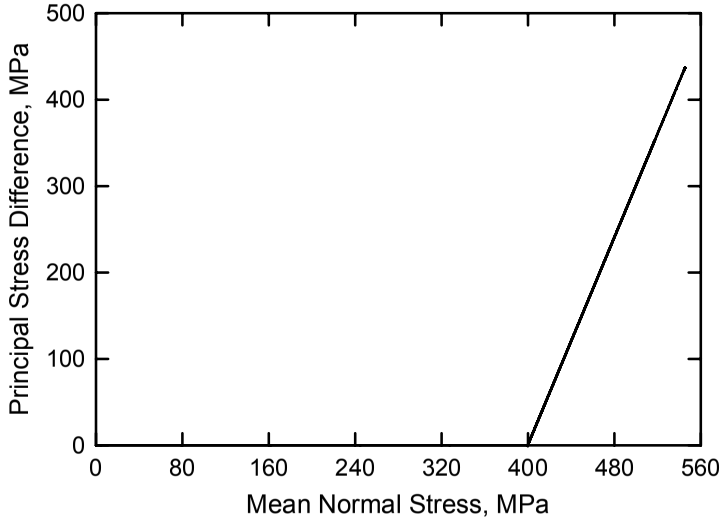

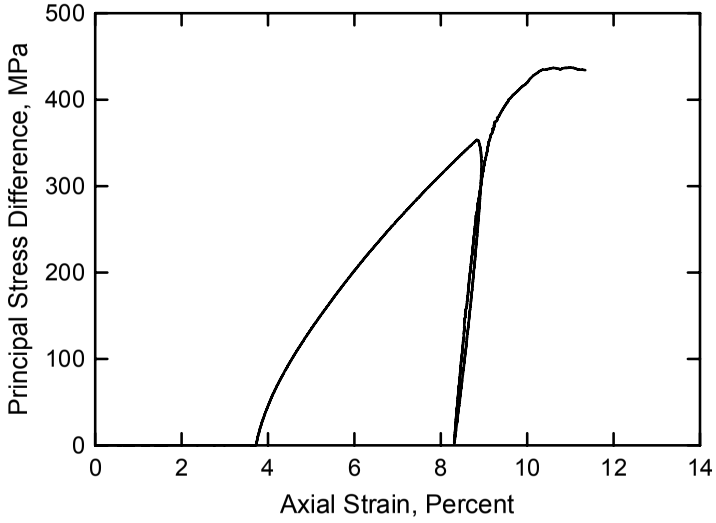

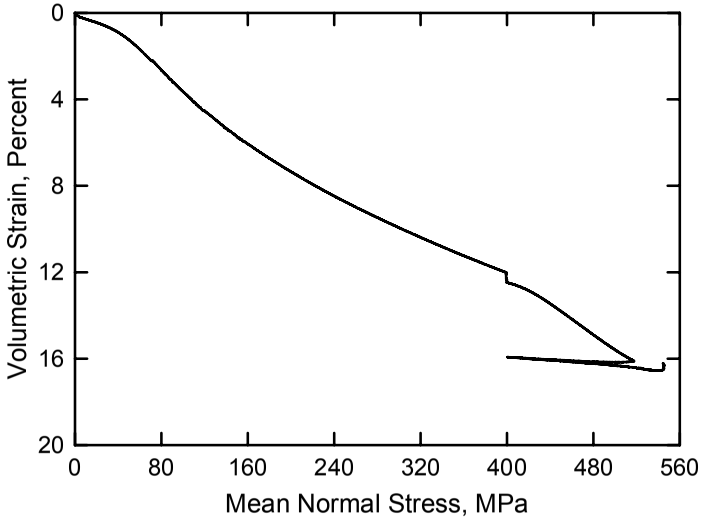

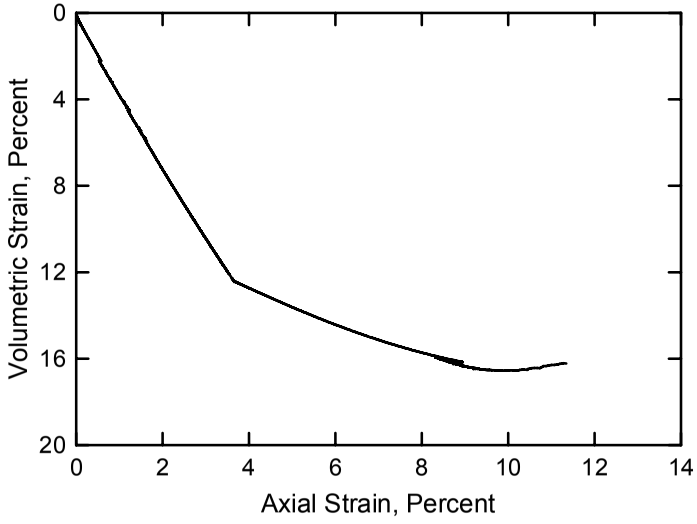

Plate 23

SAM-35 Concrete
Test No. 36

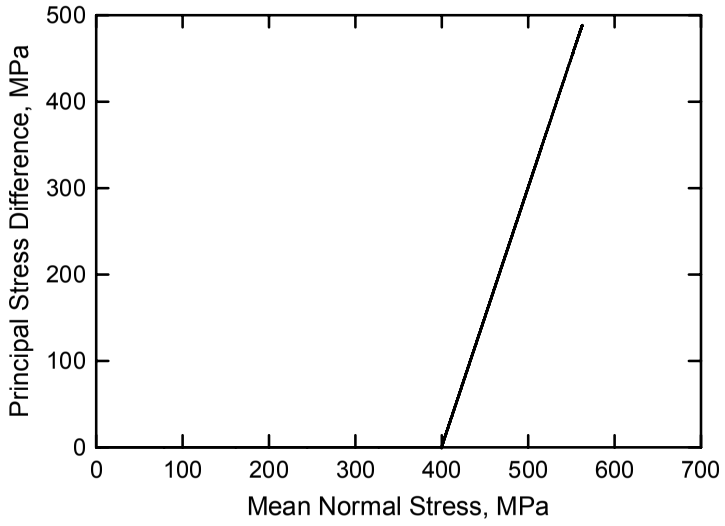

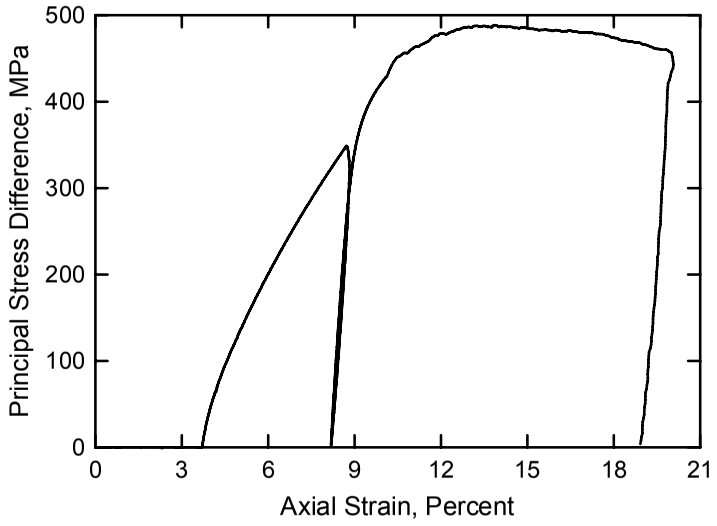

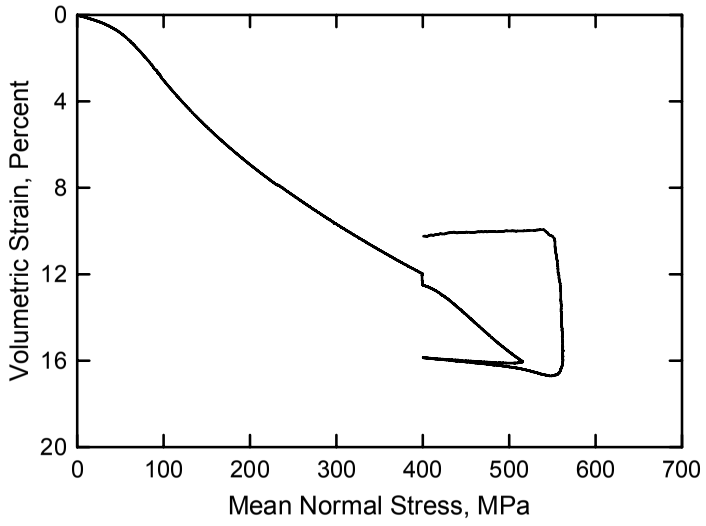

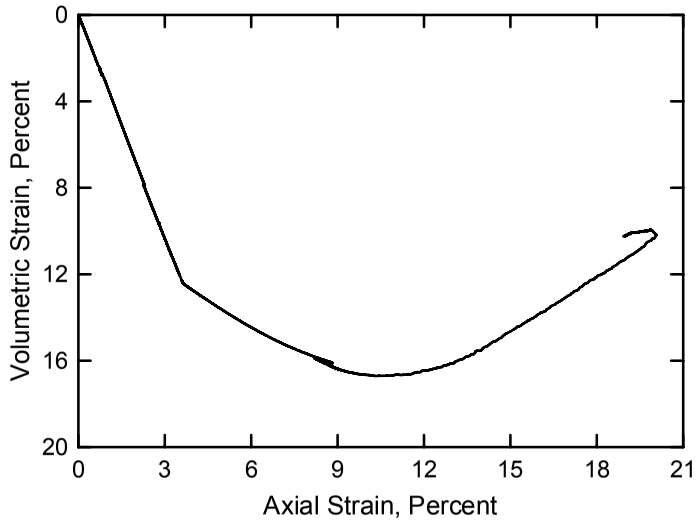

Plate 24

SAM-35 Concrete
Test No. 23

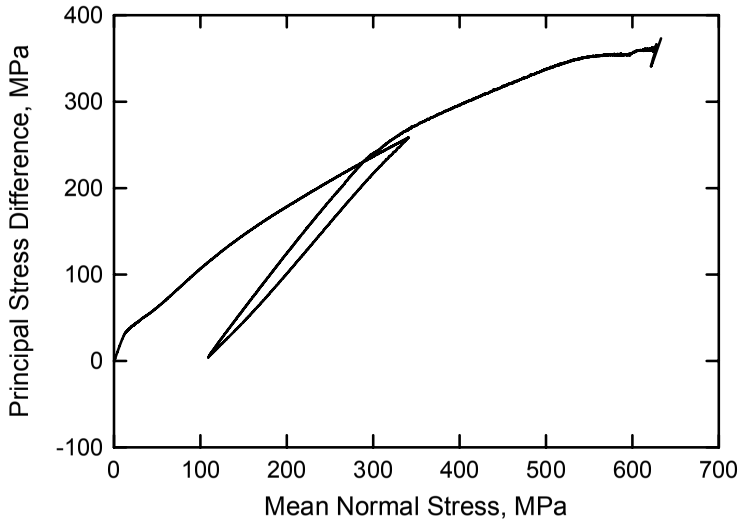

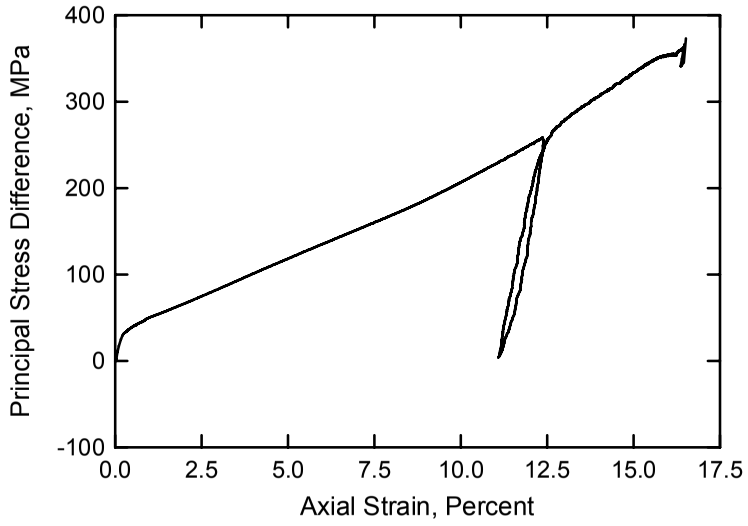

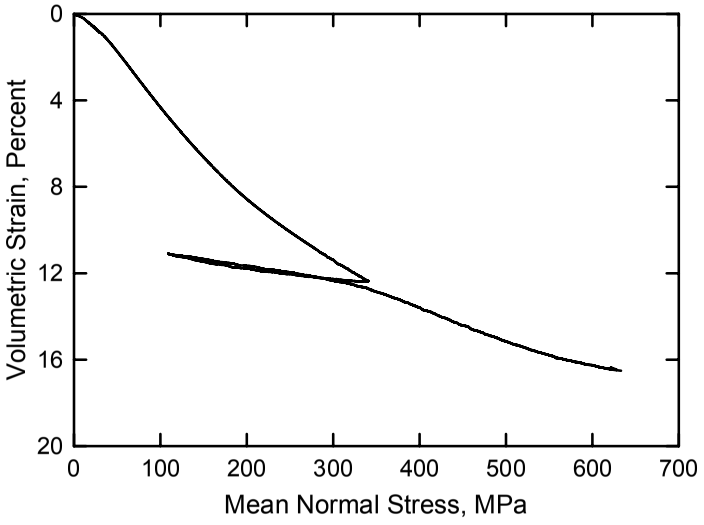

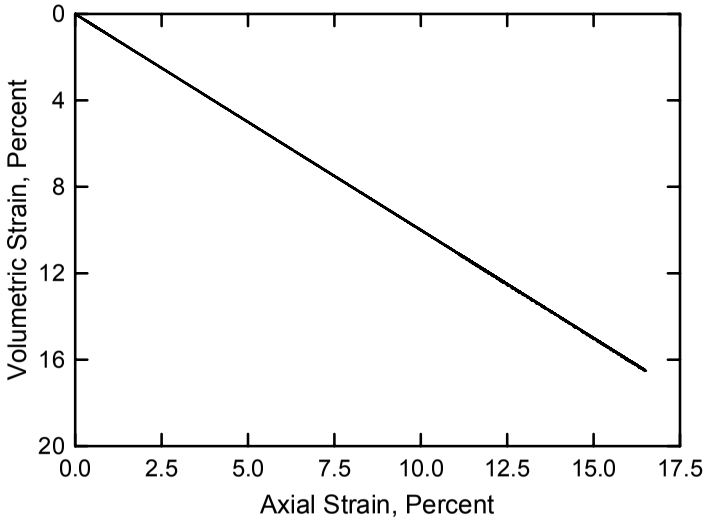

Plate 25

SAM-35 Concrete
Test No. 24

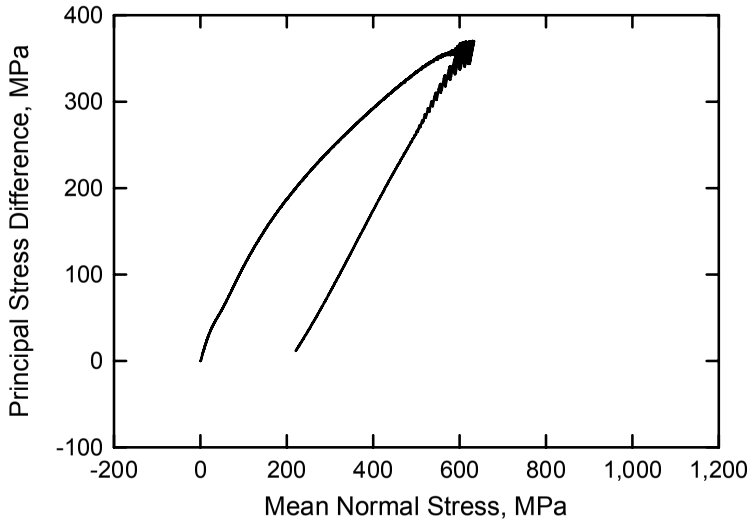

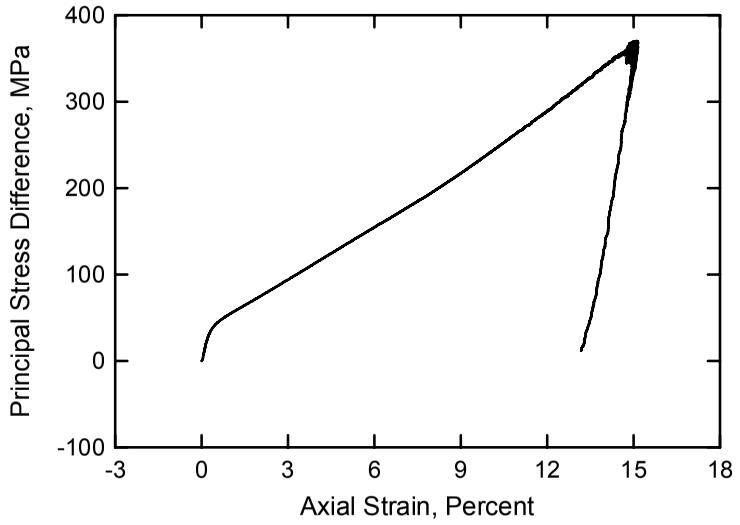

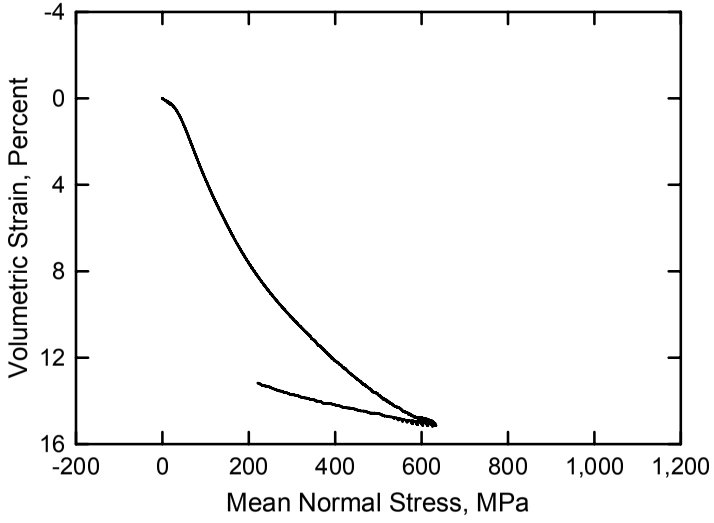

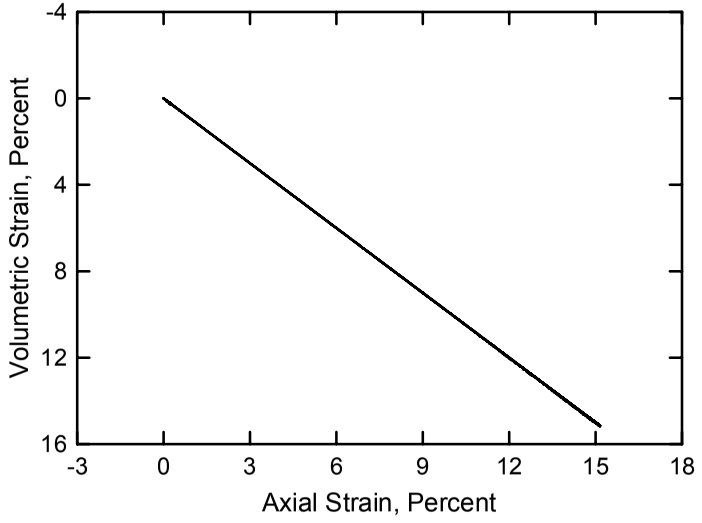

Plate 26

SAM-35 Concrete
Test No. 26

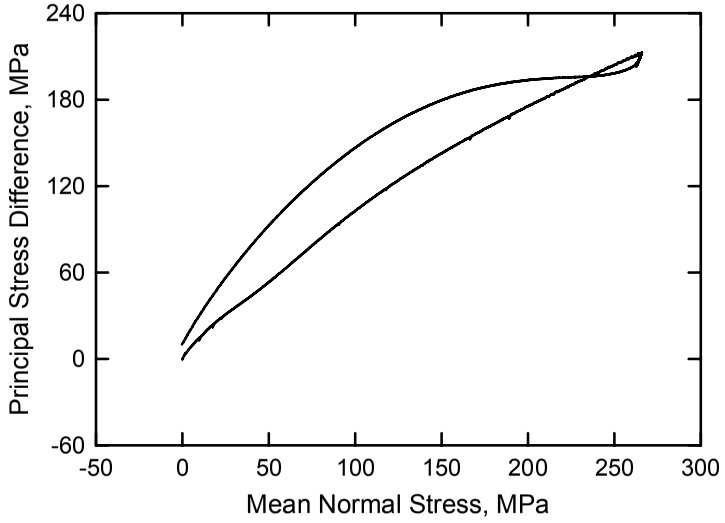

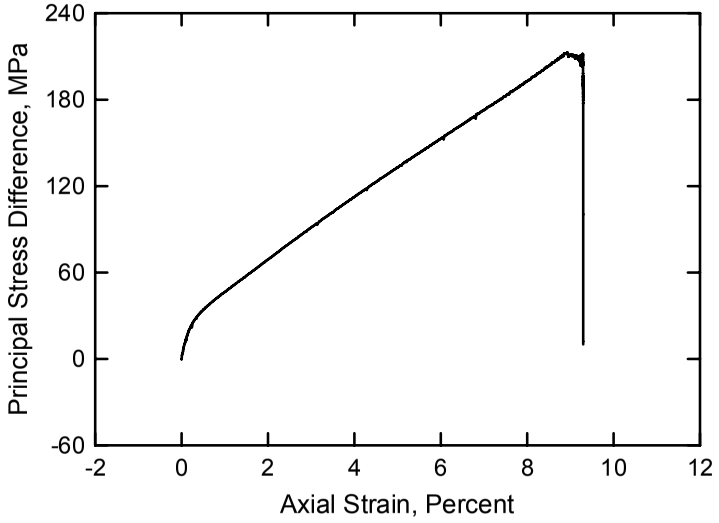

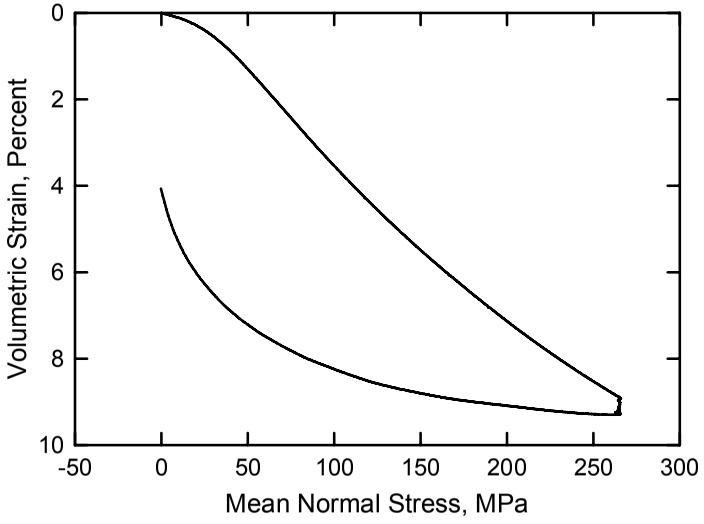

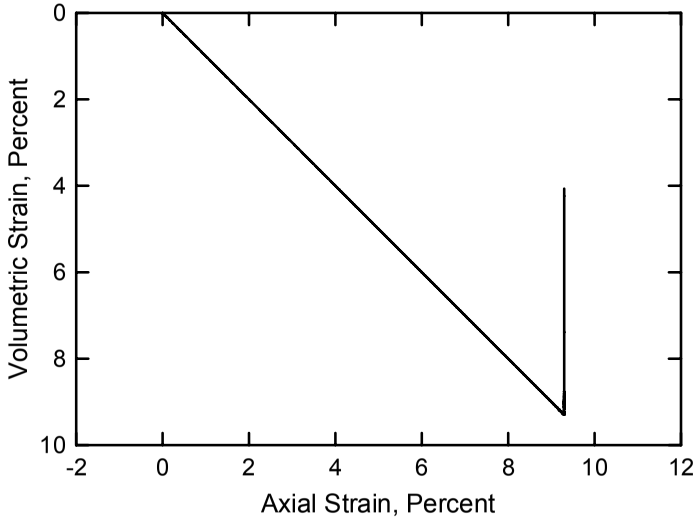

SAM-35 Concrete
Test No. 27

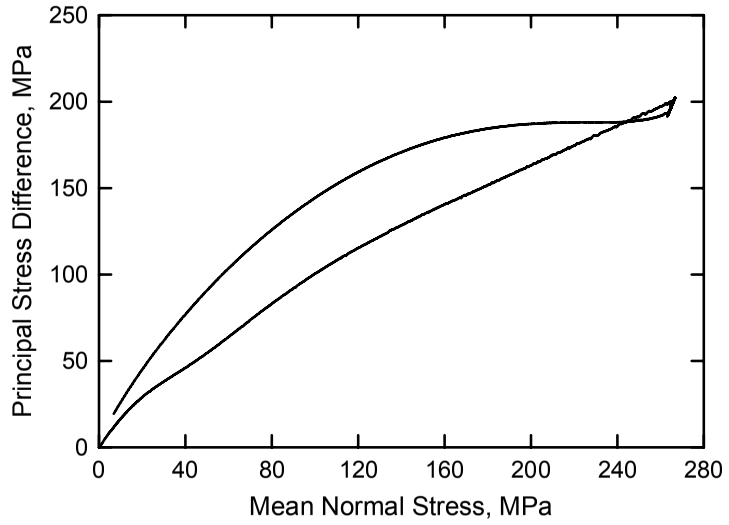

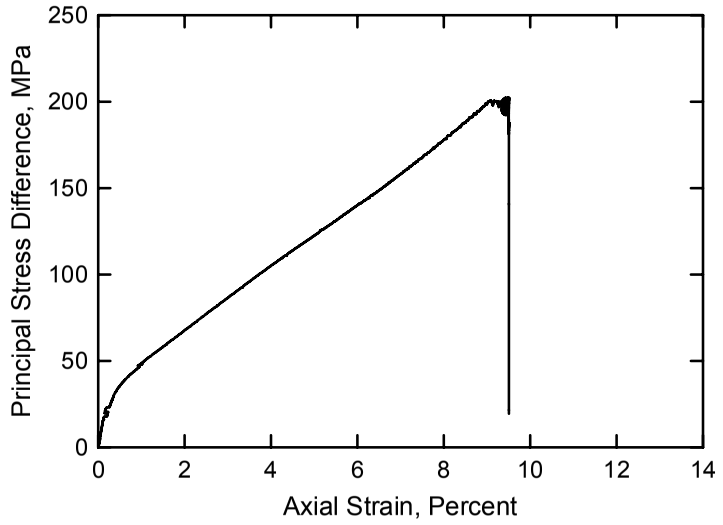

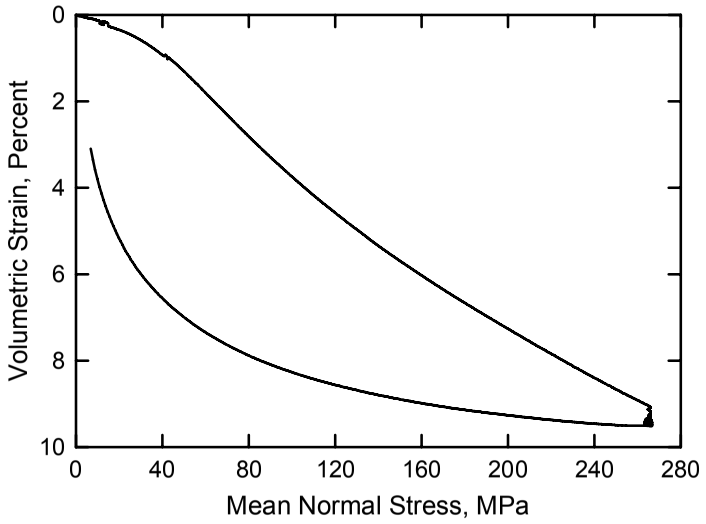

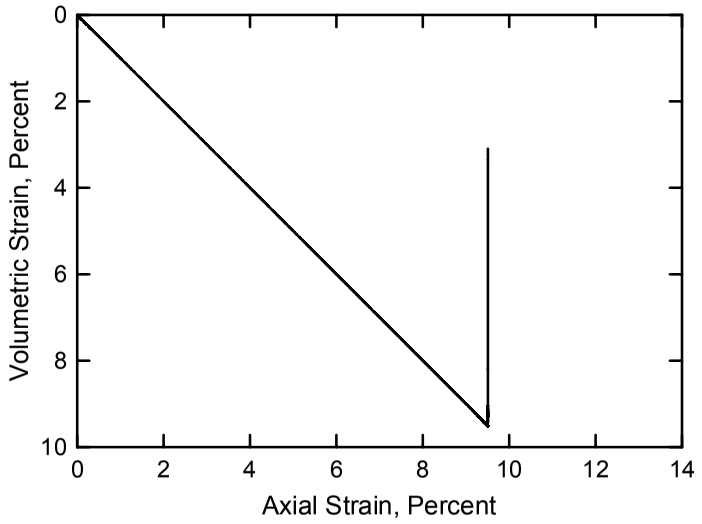

Plate 28

SAM-35 Concrete
Test No. 28

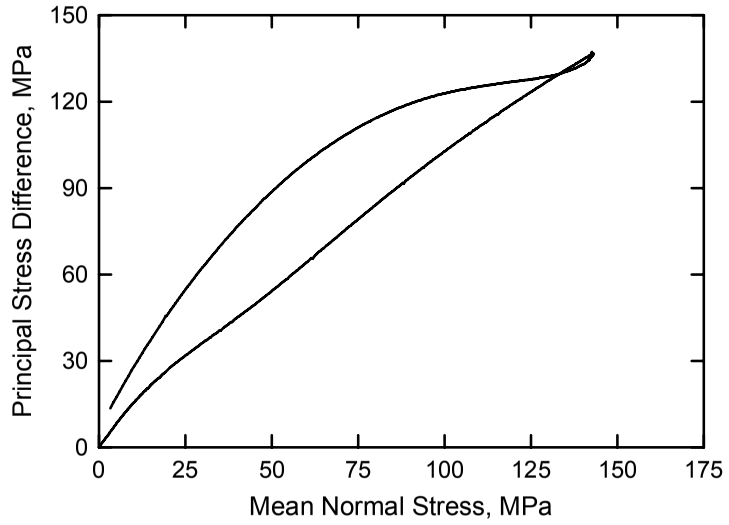

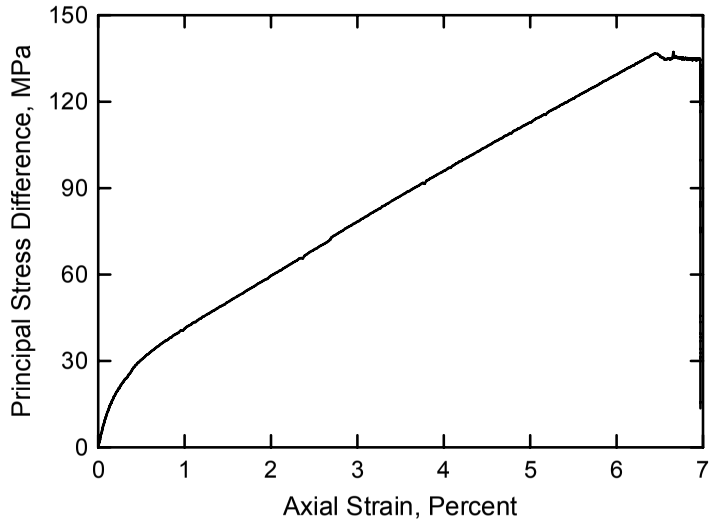

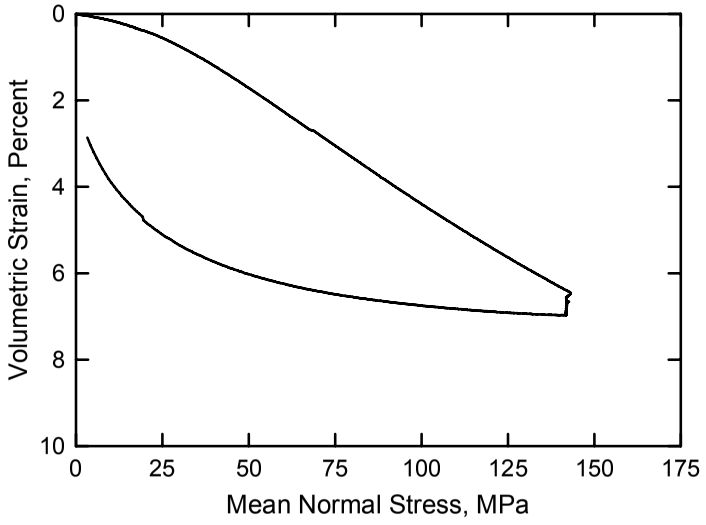

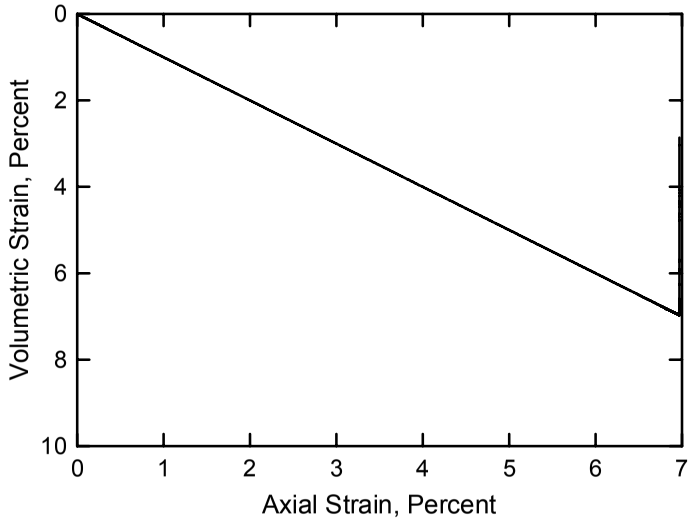

Plate 29

SAM-35 Concrete
Test No. 29

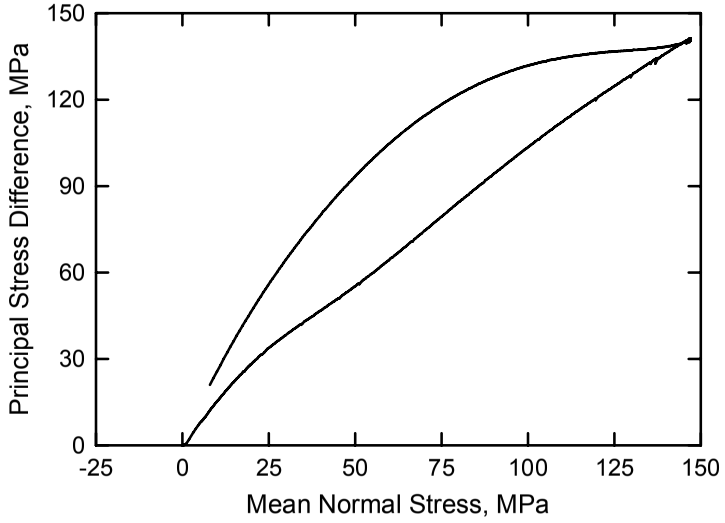

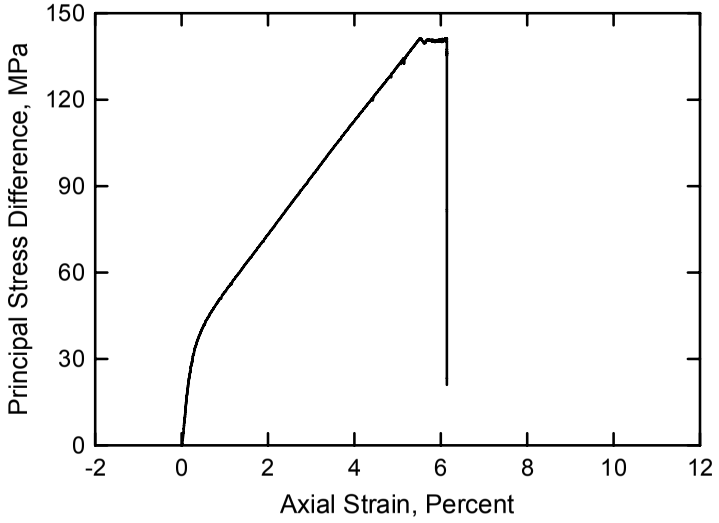

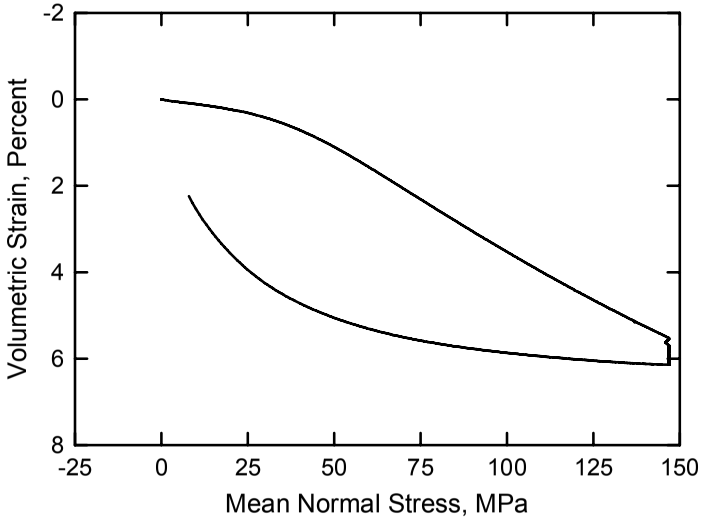

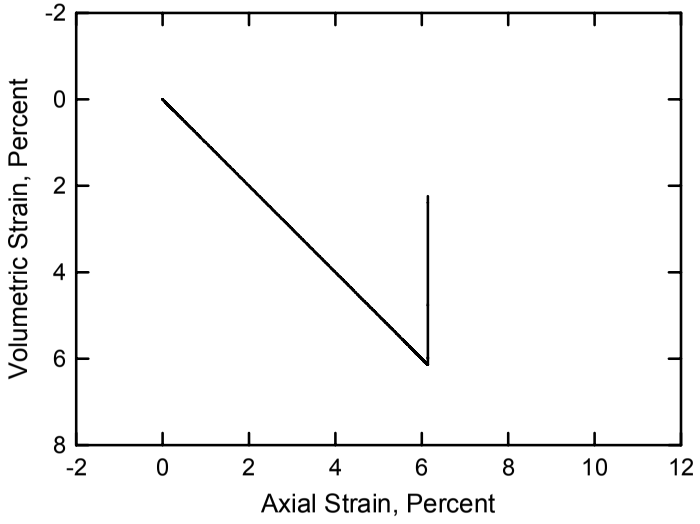

Plate 30

SAM-35 Concrete
Test No. 30

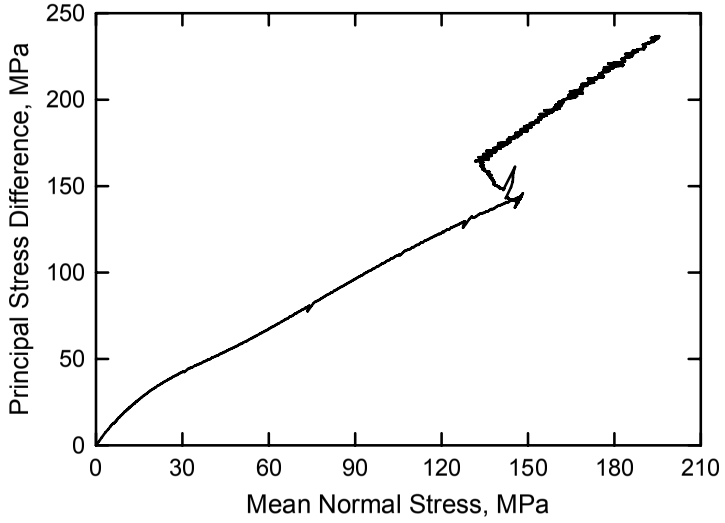

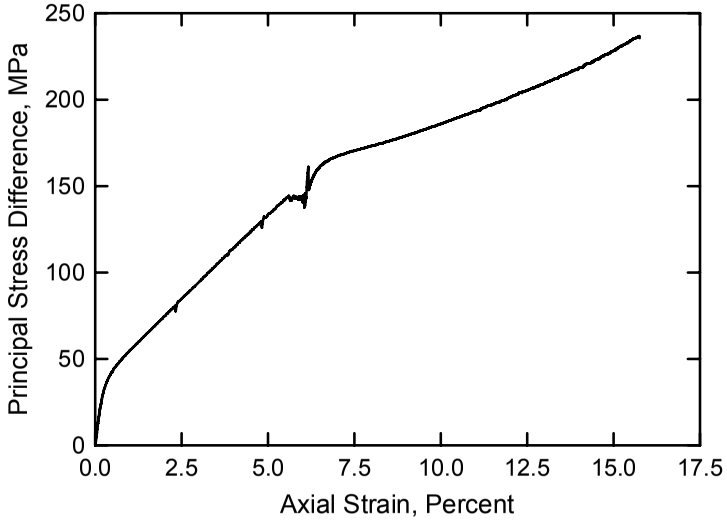

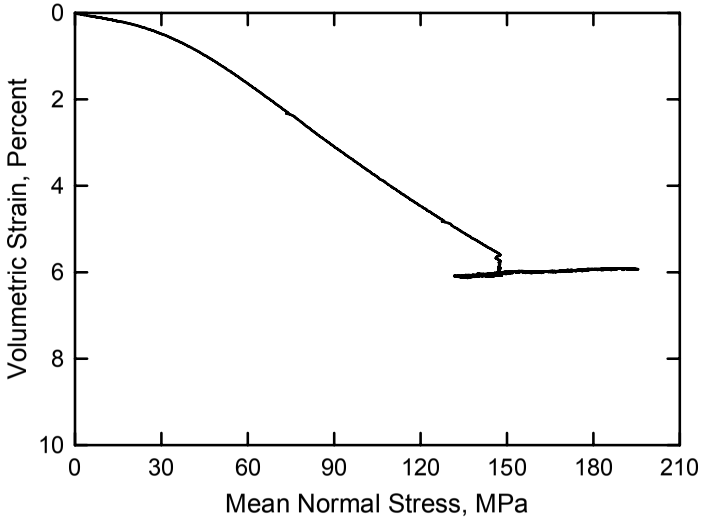

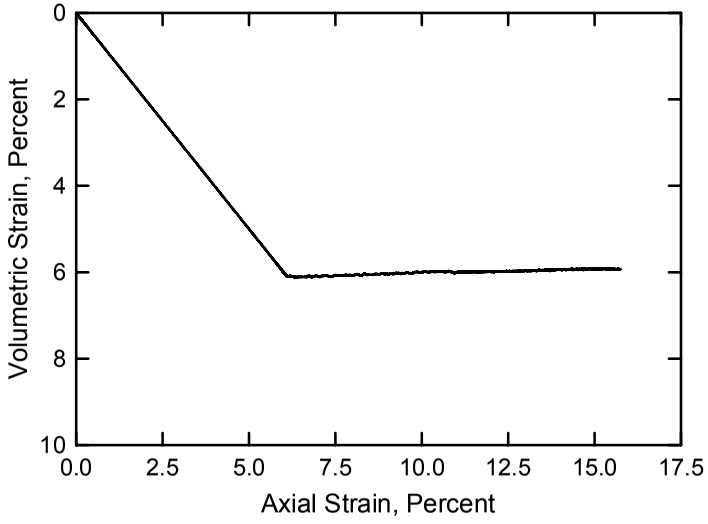

Plate 31

SAM-35 Concrete
Test No. 31

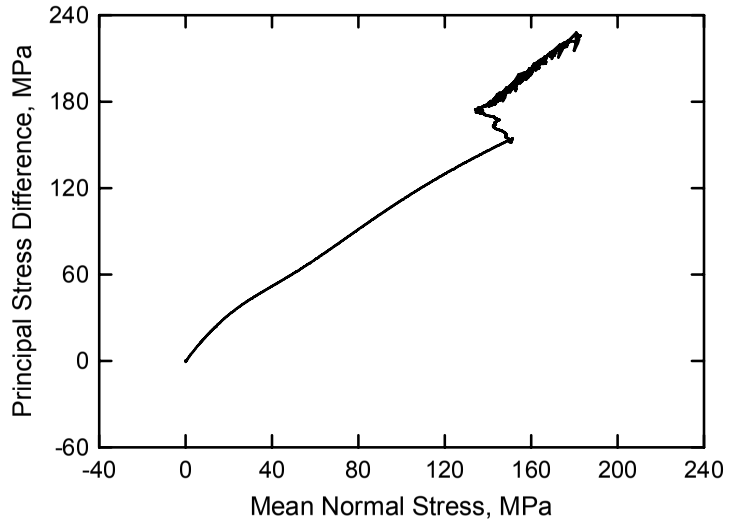

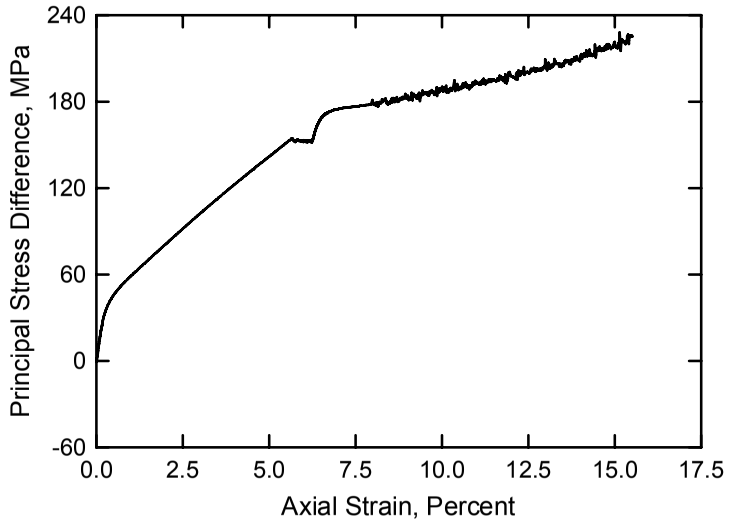

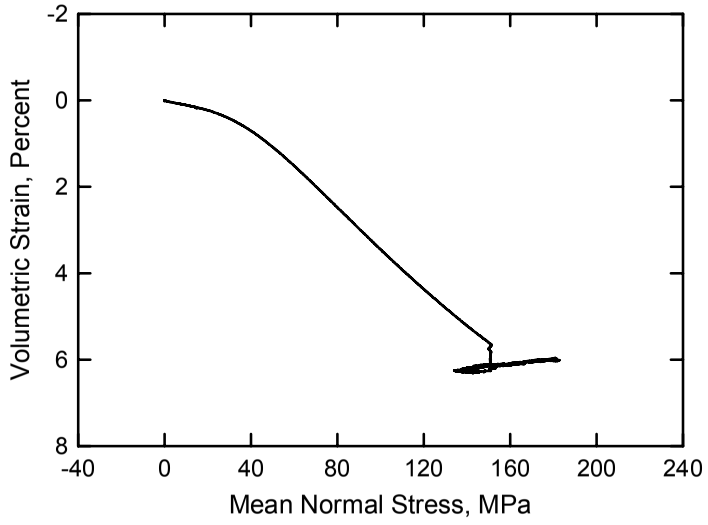

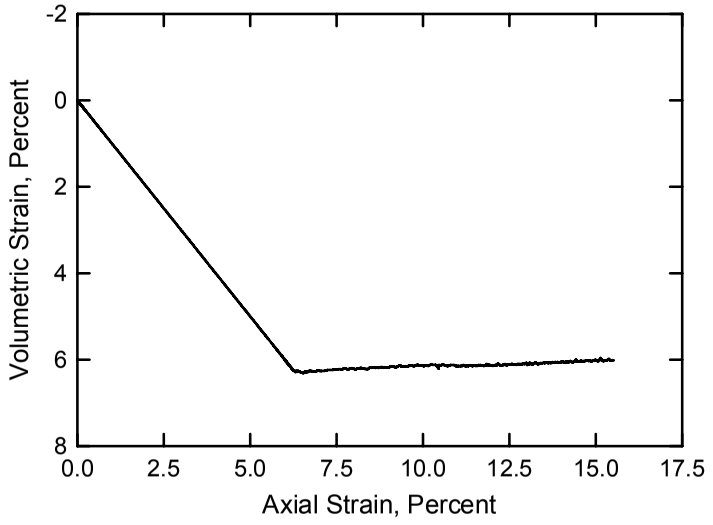

Plate 32

SAM-35 Concrete
Test No. 32

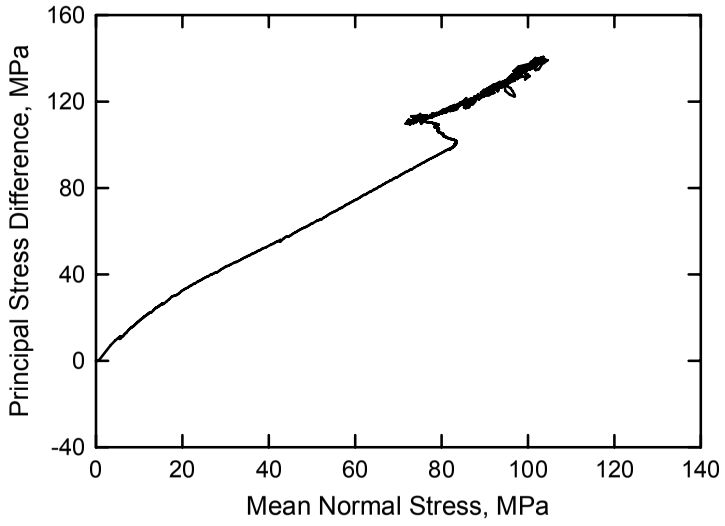

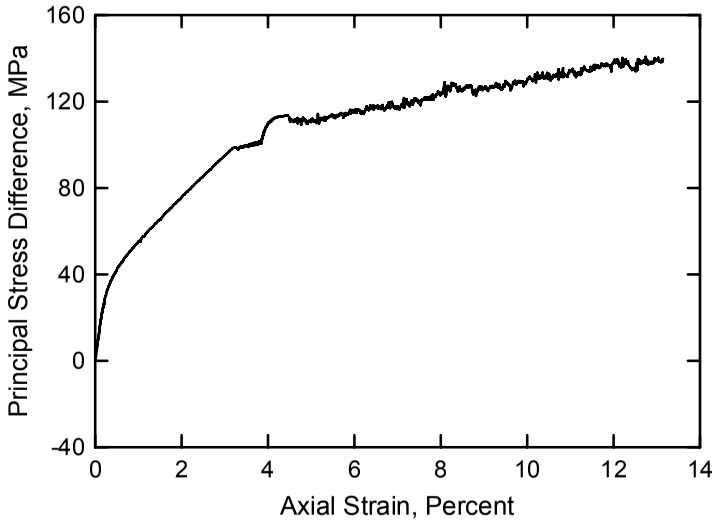

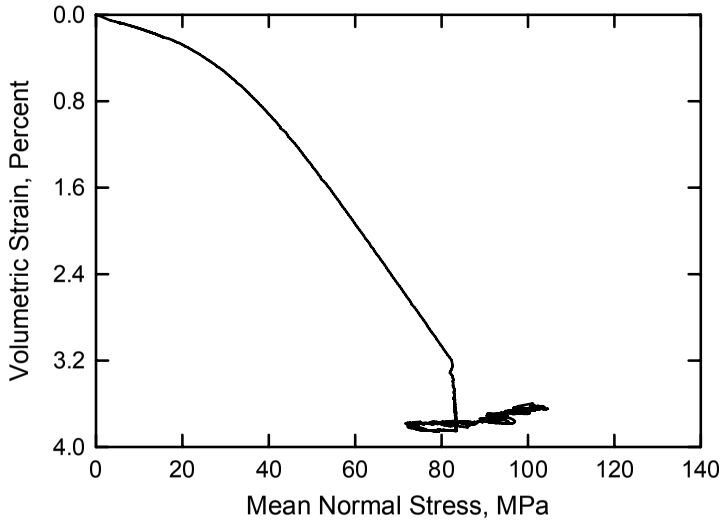

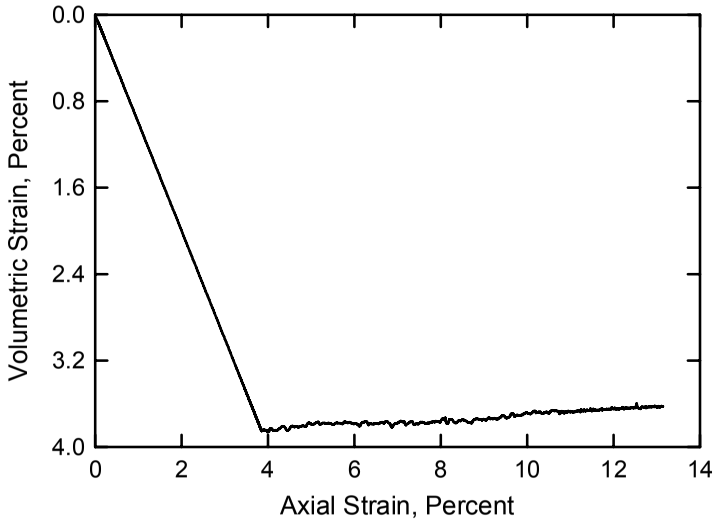

Plate 33

SAM-35 Concrete
Test No. 33

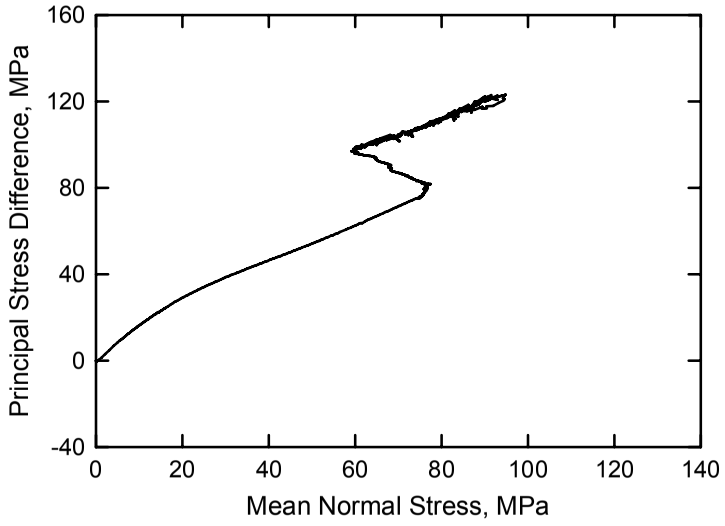

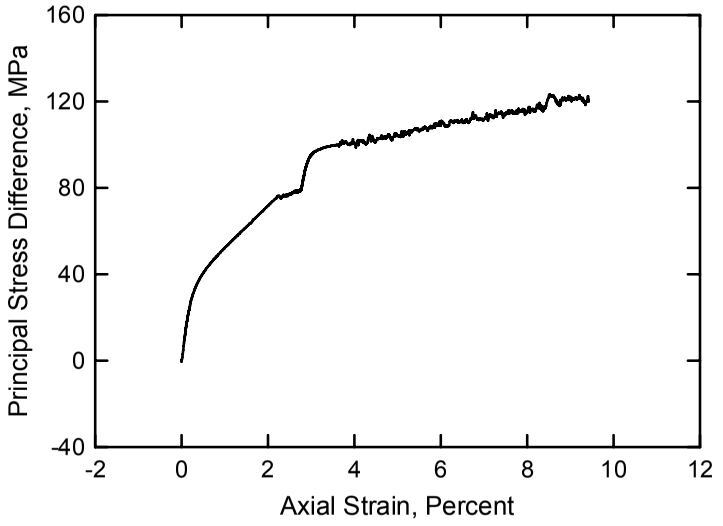

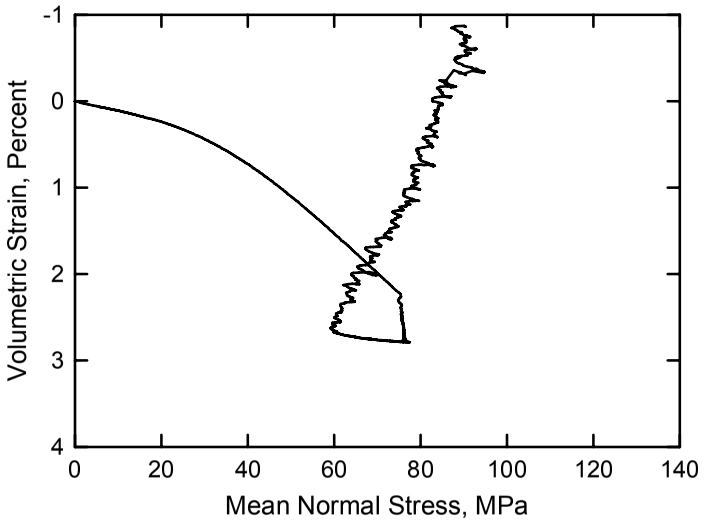

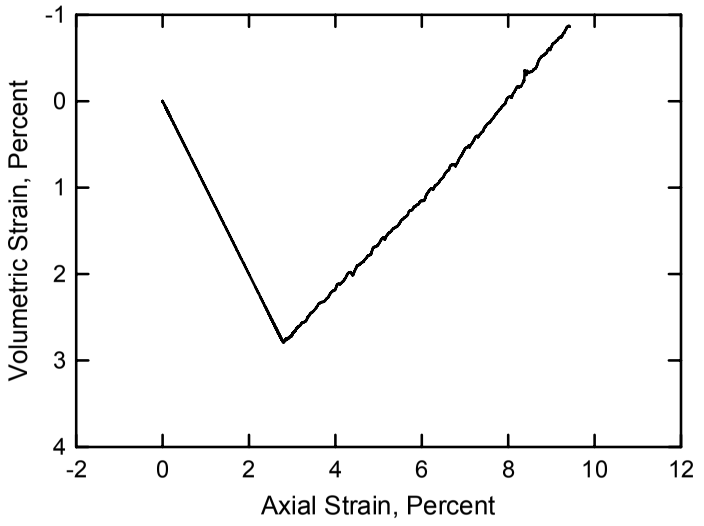

Plate 34

SAM-35 Concrete
Test No. 34

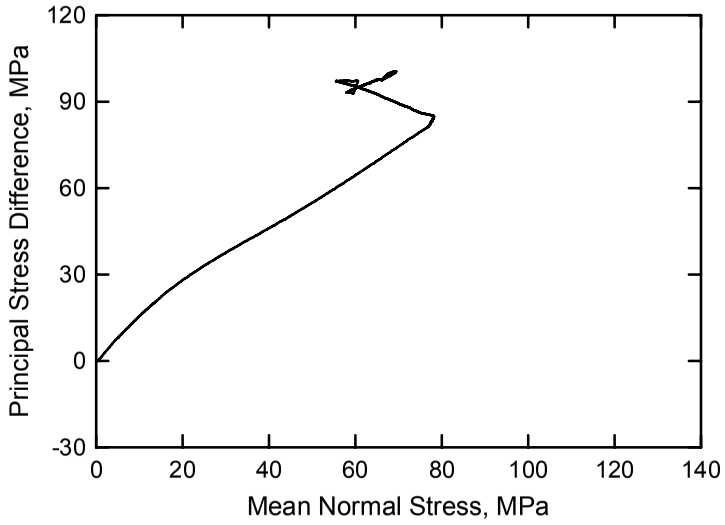

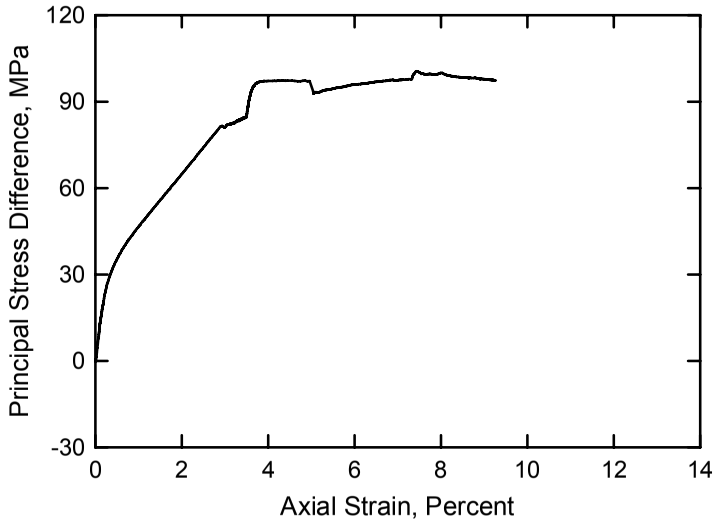

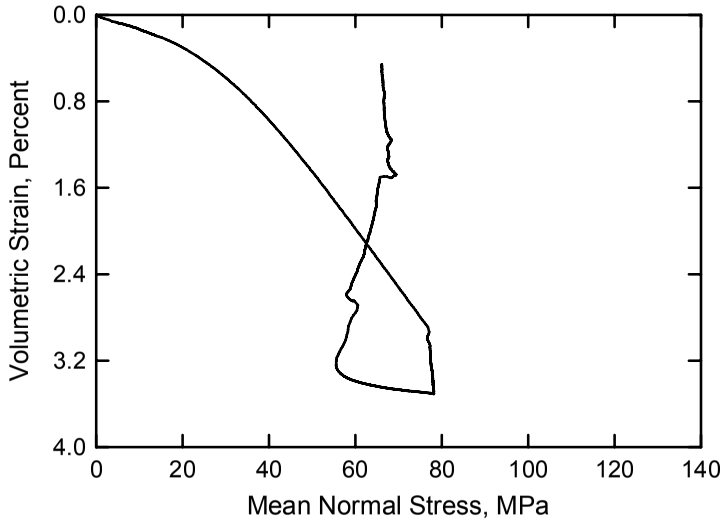

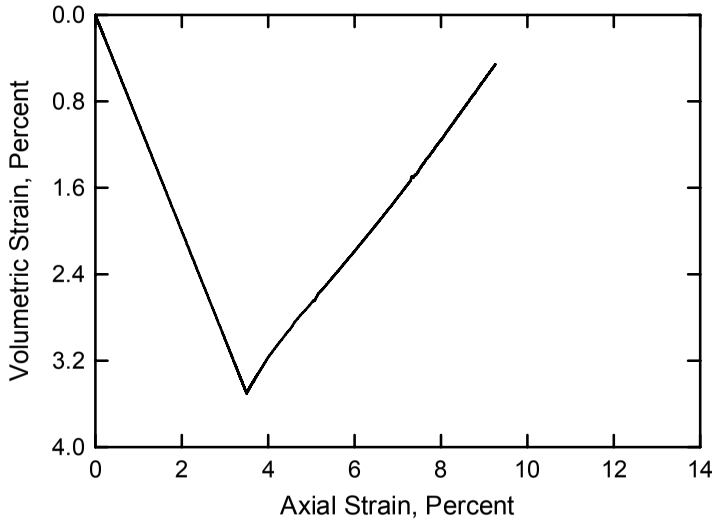

Plate 35

REPORT DOCUMENTATION PAGE

Form Approved
OMB No. 0704-0188

1. REPORT DATE *(DD-MM-YYYY)*	2. REPORT TYPE	3. DATES COVERED *(From - To)*
September 2006	Final report	

4. TITLE AND SUBTITLE

Laboratory Characterization of SAM-35 Concrete

5a. CONTRACT NUMBER

5b. GRANT NUMBER

5c. PROGRAM ELEMENT NUMBER

6. AUTHOR(S)

Erin M. Williams, Stephen A. Akers, and Paul A. Reed

5d. PROJECT NUMBER

5e. TASK NUMBER

5f. WORK UNIT NUMBER
AT40

7. PERFORMING ORGANIZATION NAME(S) AND ADDRESS(ES)

U.S. Army Engineer Research and Development Center
Geotechnical and Structures Laboratory
3909 Halls Ferry Road
Vicksburg, MS 39180-6199

8. PERFORMING ORGANIZATION REPORT NUMBER

ERDC/GSL TR-06-15

9. SPONSORING / MONITORING AGENCY NAME(S) AND ADDRESS(ES)

Headquarters, U.S. Army Corps of Engineers
Washington, DC 20314-1000

10. SPONSOR/MONITOR'S ACRONYM(S)

11. SPONSOR/MONITOR'S REPORT NUMBER(S)

12. DISTRIBUTION / AVAILABILITY STATEMENT

Approved for public release; distribution is unlimited.

13. SUPPLEMENTARY NOTES

14. ABSTRACT

Personnel of the Geotechnical and Structures Laboratory, U.S. Army Engineer Research and Development Center, conducted a laboratory investigation to characterize the strength and constitutive property behavior of a SAM-35 concrete. Forty-four mechanical property tests consisting of two hydrostatic compression tests, four unconfined compression (UC) tests, 18 triaxial compression (TXC) tests, two uniaxial strain tests, four uniaxial strain load/biaxial unload (UX/BX) tests, three uniaxial strain load/constant volume tests, two uniaxial strain load/constant strain ratio tests, five direct pull (DP) tests, and four reduced triaxial extension (RTE) tests were successfully completed. In addition to the mechanical property tests, nondestructive pulse-velocity measurements were performed on each specimen. The TXC tests exhibited a continuous increase in principal stress difference with increasing confining stress. A recommended compression failure surface was developed from the TXC and UC test results. Test data from the RTE and DP tests were used to develop a recommended extension failure surface for SAM-35. Results from the stress paths of the strain path tests and the recommended compression failure surface exhibited good agreement except for the UX/BX tests.

15. SUBJECT TERMS

Concrete
Compression tests
Extension tests
Material characterization
Material properties

16. SECURITY CLASSIFICATION OF:			17. LIMITATION OF ABSTRACT	18. NUMBER OF PAGES	19a. NAME OF RESPONSIBLE PERSON
a. REPORT	b. ABSTRACT	c. THIS PAGE			19b. TELEPHONE NUMBER *(include area code)*
UNCLASSIFED	UNCLASSIFED	UNCLASSIFED		90	